

$n + {}^3\text{H}$, $p + {}^3\text{He}$, $p + {}^3\text{H}$, and $n + {}^3\text{He}$ scattering with the hyperspherical harmonic methodM. Viviani ¹, L. Girlanda,^{2,3} A. Kievsky,¹ and L. E. Marcucci^{1,4}¹*Istituto Nazionale di Fisica Nucleare, Sezione di Pisa, I-56127 Pisa, Italy*²*Department of Mathematics and Physics, University of Salento, I-73100 Lecce, Italy*³*INFN-Lecce, I-73100 Lecce, Italy*⁴*Department of Physics “E. Fermi,” University of Pisa, I-56127 Pisa, Italy*

(Received 31 March 2020; accepted 17 August 2020; published 30 September 2020)

The $n + {}^3\text{H}$, $p + {}^3\text{He}$, $p + {}^3\text{H}$, and $n + {}^3\text{He}$ elastic and charge exchange reactions at low energies are studied by means of the hyperspherical harmonic method. The considered nuclear Hamiltonians include modern two- and three-nucleon interactions, and in particular results are reported in case of chiral two-nucleon potentials, with and without the inclusion of chiral three-nucleon (3N) interactions. A detailed study of the convergence and numerical stability of the method is presented. We have found that the effect the 3N force is in general tiny except for $p + {}^3\text{H}$ scattering below the opening of the $n + {}^3\text{He}$ channel. In such a case, the effect of 3N forces is appreciable and a clear dependence on the cutoff used to regularize the high-momentum tail of the interactions is observed. Such a dependence is related to the presence of the poorly known sharp 0^+ resonance, considered to be the first excited state of ${}^4\text{He}$.

DOI: [10.1103/PhysRevC.102.034007](https://doi.org/10.1103/PhysRevC.102.034007)**I. INTRODUCTION**

The four nucleon (4N) system has been object of intense studies in recent years. First, this system is particularly interesting as a “theoretical laboratory” to test the accuracy of our present knowledge of the nucleon-nucleon (NN) and three-nucleon (3N) interactions. In particular, the effects of the NN P waves and of the 3N forces are believed to be larger than in the $A = 2$ or 3 systems. Moreover, it is the simplest system where the 3N interaction can be studied in channels of total isospin $T = 3/2$. There is a number of reactions involving 4Ns which are of extreme importance for astrophysics, energy production, and studies of fundamental symmetries. As an example, the $p + {}^3\text{H} \rightarrow {}^4\text{He} + e^+ + e^-$ reaction is currently exploited as a tool for the discovery of an unknown particle [1].

Nowadays, the 4N bound-state problem can be numerically solved with good accuracy. For example, in Ref. [2] the binding energies and other properties of the α particle were studied using the AV8' [3] NN interaction; several different techniques produced results in very close agreement with each other (at the level of, or less than, 1%). More recently, the same agreement has also been obtained considering different realistic NN + 3N interactions [4–7].

In recent years, there has been a rapid advance in solving the 4N scattering problem with realistic Hamiltonians. Accurate calculations of four-body scattering observables have been achieved in the framework of the Faddeev-Yakubovsky (FY) equations [8–13], solved in momentum space, where the long-range Coulomb interaction is treated using the screening-renormalization method [14,15]. Solutions of the FY equations in configuration space [16–20] and several calculations using the resonating group model (RGM) [21–24]

were also reported. The application of the RGM together with the no-core shell model (NCSM) technique is being vigorously pursued [25,26], and the possibility of calculations of scattering observables using the Green-function Monte Carlo method has been explored, too [27].

In this contribution, the four-body scattering problem is solved using the Kohn variational principle and expanding the “core” part of the wave function (namely, the part which describes the system where the particles are close to each other) in terms of the hyperspherical harmonic (HH) functions (for a review, see Refs. [28,29]). Preliminary applications of this method were reported in Refs. [17,30,31] for local potentials, as the Argonne v_{18} (AV18) [32] NN potential, and in Refs. [33–35] for nonlocal potentials. Accurate benchmarks between FY (solved in momentum and configuration space) and HH results were reported in Ref. [36] for $n + {}^3\text{H}$ and $p + {}^3\text{He}$ elastic scattering and in Ref. [37] for $p + {}^3\text{H}$ and $n + {}^3\text{He}$ elastic scattering and charge-exchange reactions. These calculations were limited to energies below the threshold for three-body breakup. The good agreement found between the results obtained by the different methods attested the high accuracy reached in solving the 4N scattering problem.

In the present paper, the application of the HH method to study these reactions is presented in full detail, focusing in particular on the selection of the basis and the techniques used to evaluate the matrix elements. A discussion of the convergence of the calculated observables is also reported. Finally, we critically compare the results of this first campaign of calculations with the available experimental data.

The potentials used in this study are the chiral interactions derived at next-to-next-to-next-to-leading order (N³LO) by Entem and Machleidt [38,39], with cutoff $\Lambda = 500$ and

600 MeV. In some selected cases, we have also performed calculations using the new interactions derived at next-to-next-to-next-to-leading order (N4LO) in Ref. [40]. In this case, the adopted values of the cutoff parameter are $\Lambda = 450, 500, \text{ and } 550$ MeV. The calculations performed using one of these chiral potentials are labeled as N3LO500, and so on, i.e., specifying the value of the cutoff. We present the convergence of the calculated phase shifts for the case of the AV18 interaction, too.

We have also performed calculations including the chiral 3N interaction derived at next-to-next-to leading order (N2LO) in Refs. [41,42]. The two free parameters in this N2LO 3N potential, denoted usually as c_D and c_E , have been fixed in order to reproduce the experimental values of the $A = 3$ binding energies and the Gamow-Teller matrix element (GTME) of the tritium β decay [43,44]. Note that these parameters have been recently redetermined [45–47] after finding (and correcting) an inconsistency in the relation between the 3N parameter c_D and the axial current used so far [48].

The cutoff in the 3N interaction has been chosen to be consistent with the corresponding value of the NN interaction. The development of a 3N interaction including N3LO and N4LO contributions is still in progress [49–51]. In some cases, we have considered the Urbana IX (UIX) and Illinois 7 (IL7) 3N potentials [52,53], used with the AV18 potential. The calculation including both NN and 3N interactions have been labeled as N3LO500/N2LO500, AV18/IL7, and so on.

The four-body studies performed so far have highlighted several discrepancies between the theoretical predictions and experimental data. Let us consider first the $n + {}^3\text{H}$ elastic scattering. Calculations based on NN interactions disagree [8,16,17,22,30,54] rather sizably with the measured total cross section [55], both at zero energy and in the “peak” region ($E_n \approx 3.5$ MeV). Such an observable is found to be very sensitive to the NN interaction model [8]. At low energy, the discrepancy is removed by including a 3N force fixed to reproduce the triton binding energy [16,22,30], but it remains in the peak region. In Ref. [35], in a preliminary calculation, we observed that this disagreement is noticeably reduced using the N3LO500/N2LO500 interaction. In the present paper, we will report the results of more refined calculations performed with the N3LO500/N2LO500 and N3LO600/N2LO600 interactions, confirming the results of Ref. [35].

Regarding the $p + {}^3\text{He}$ elastic scattering, several accurate measurements of both the unpolarized cross section [56–58] and the proton analyzing power A_{y0} [31,58,59] can be found in the literature, allowing for a detailed study. The calculations performed so far with a variety of NN interactions have shown a glaring discrepancy between theory and experiment for A_{y0} [8,22,31,54,58]. This discrepancy is very similar to the well-known “ A_y puzzle” in $N + d$ scattering. This is a fairly old problem, already reported about 30 years ago [60,61] in the case of $n + d$ and later confirmed also in the $p + d$ case [62]. The inclusion of usual models of the 3N force has little effect on these $A = 3$ observables. To solve this puzzle, speculations about the deficiency of the NN potentials in 3P_J waves (where the spectroscopic notation ${}^{2S+1}L_J$ has been adopted) have been advanced. More recently, the effects of the contact

terms appearing at N4LO in the 3N force have been explored in order to explain this puzzle [63,64]. The situation of other $p + {}^3\text{He}$ observables (the ${}^3\text{He}$ analyzing power A_{0y} and some spin correlation observables as A_{yy}, A_{xx} , etc.) is less clear due to the lack of equally accurate measurements. In the early 2000s [65], at the Triangle University National Laboratory (TUNL), a new set of accurate measurements of various spin correlation coefficients were obtained at $E_p = 1.60, 2.25, 4, \text{ and } 5.54$ MeV, allowing for a phase-shift analysis (PSA). The aim of this paper is to compare the results of the theoretical calculations to these data. The effect of the inclusion of the chiral 3N force in $p + {}^3\text{He}$ has been already reported in Ref. [66], where we have shown that the inclusion of the chiral 3N interaction improves the agreement with the experimental data, in particular, for the proton vector analyzing power. This result is confirmed by the present study.

Regarding $p + {}^3\text{H}$ and $n + {}^3\text{He}$ below the $d + d$ threshold, only a few accurate calculations exist [8,9,12,18]. From the experimental point of view, for this range of energies there exist several measurements of the $p + {}^3\text{H}$ elastic differential cross section [67–74], $n + {}^3\text{He}$ elastic cross section [75,76] and total cross section [75–78], and various $n + {}^3\text{He}$ elastic polarization observables [79–83]. Regarding the $n + {}^3\text{He} \rightarrow p + {}^3\text{H}$ charge exchange reaction, there exist measurements of the total cross section [76,78,84–90], the differential cross section [91–94], and polarization observables [95–99]. Preliminary results obtained for these observables with the HH method were already presented in Ref. [37].

Here we complete those previous studies and, in particular, we study the effect of the inclusion of the 3N interaction in the low-energy 1S_0 phase shifts in order to extract the resonance energy and width of the first excited state of ${}^4\text{He}$. Such a state of ${}^4\text{He}$ is of particular interest. Its energy is slightly above the threshold for $p + {}^3\text{H}$ breakup but below that of $n + {}^3\text{He}$ [100]. For the description of this resonance, therefore, the Coulomb potential plays a very important role. The nature of such a resonance is still a puzzle after many years of studies. Electron scattering can give direct information on the transition form factor [100–102],

$$\mathcal{S}_{\mathcal{M}}(q, \omega) = \sum_n |\langle n | \mathcal{M}(q) | 0 \rangle|^2 \delta(\omega - E_n + E_0), \quad (1)$$

where $|0\rangle$, $|n\rangle$, E_0 , and E_n are eigenfunctions and eigenvalues of the 4N Hamiltonian H , respectively, $\mathcal{M}(q)$ is the isoscalar monopole operator, and ω and q the energy and three-momentum transferred by the external probe. At low values of ω , $\mathcal{S}_{\mathcal{M}}(q, \omega)$ is dominated by the contribution of the first 0^+ excited state of ${}^4\text{He}$, which therefore can be studied theoretically and experimentally. The interpretation of this excited state as a collective breathing mode or a particle-hole-like excitation is still to be clarified. Recently, two theoretical studies of $\mathcal{S}_{\mathcal{M}}(q, \omega)$ were performed. In Ref. [103], $\mathcal{S}_{\mathcal{M}}(q, \omega)$ was calculated using a bound-state technique, i.e., expanding the wave function over a Gaussian basis. In Refs. [104,105] a calculation using the Lorentz integral transform method to sum implicitly all the intermediate states was performed. The calculated transition form factors differ by a factor two and the origin of this discrepancy has not yet been clarified. In

this contribution, we estimate the position and width of the resonance directly from the calculated phase shifts.

This paper is organized as follows. In Sec. II, a description of the method is reported, while in Sec. III a detailed discussion of the convergence and numerical stability of the calculated phase shifts is presented. The results are reported in Sec. IV and compared with the available experimental data. The conclusions and the perspectives of this approach will be given in Sec. V. Some details regarding the regularization of the irregular Coulomb functions are given in the Appendix.

II. THE HH TECHNIQUE FOR SCATTERING STATES

This section is divided into five subsections. First, we discuss the asymptotic part of the wave function and then the HH expansion of the core part. In Secs. II C and II D, we discuss the application of the Kohn variational principle and then give some details of the calculations. Finally, in Sec. II E we discuss the choice of the subset of HH functions considered in the calculation.

A. Asymptotic functions

In this paper we limit ourselves to consider asymptotic states with two clusters in the initial/final states, denoted generally as $A + B$. For the sake of simplicity, a specific clusterization $A + B$ will be denoted by the index γ . More specifically, $\gamma = 1, \dots, 4$ will correspond to the following clusterizations: $n + {}^3\text{H}, p + {}^3\text{He}, p + {}^3\text{H}$, and $n + {}^3\text{He}$, respectively. Depending on the total charge (and on the energy), some of these asymptotic states may enter or not in the wave function.

Let us consider a scattering state with total angular momentum quantum number JJ_z and parity π (the dependence on the wave function and other quantities on $JJ_z\pi$ will be understood in the following). The wave function $\Psi^{\gamma LS}$ describing incoming clusters γ with relative orbital angular momentum L and channel spin S can be written as

$$\Psi^{\gamma LS} = \Psi_C^{\gamma LS} + \Psi_A^{\gamma LS}, \quad (2)$$

where the core part $\Psi_C^{\gamma LS}$ vanishes in the limit of large inter-cluster separations and hence describes the system where the particles are close to each other and their mutual interactions are strong. On the other hand, $\Psi_A^{\gamma LS}$ describes the relative motion of the two clusters in the asymptotic regions, where the mutual interaction is negligible (except for the long-range Coulomb interaction). In the asymptotic region the wave functions $\Psi^{\gamma LS}$ reduces to $\Psi_A^{\gamma LS}$, which must therefore be the appropriate asymptotic solution of the Schrödinger equation. $\Psi_A^{\gamma LS}$ can be decomposed as a linear combination of the following functions:

$$\Omega_{\gamma LS}^{\pm} = D_{\gamma} \mathcal{A} \left\{ [Y_L(\hat{y}_{\gamma}) \otimes [\phi_A \otimes \phi_B]_S]_{JJ_z} \times \left[\frac{\tilde{G}_L(\eta_{\gamma}, q_{\gamma} y_{\gamma})}{q_{\gamma} y_{\gamma}} \pm i \frac{F_L(\eta_{\gamma}, q_{\gamma} y_{\gamma})}{q_{\gamma} y_{\gamma}} \right] \right\}, \quad (3)$$

where D_{γ} are appropriate normalization factors (see below), y_{γ} is the distance between the center-of-mass (c.m.) of clusters A and B , q_{γ} is the magnitude of the relative momentum between the two clusters, and ϕ_A and ϕ_B bound-state wave functions. In the present work, the trinucleon bound-state wave functions (for both ${}^3\text{He}$ and ${}^3\text{H}$) are calculated very accurately by means of the HH method [4,33] using the corresponding $A = 3$ Hamiltonian. For a single nucleon, ϕ reduces to the spin-isospin state. The channel spin S is obtained coupling the angular momentum of the two clusters. In our case, clearly $S = 0, 1$. The symbol \mathcal{A} means that the expression between the curly braces has to be properly antisymmetrized.

The total energy of the scattering state in the center-of-mass system is

$$E = -B_A - B_B + T_r, \quad (4)$$

where

$$T_r = \frac{q_{\gamma}^2}{2\mu_{\gamma}}, \quad \frac{1}{\mu_{\gamma}} = \frac{1}{M_A} + \frac{1}{M_B}, \quad (5)$$

and M_X (B_X) is the mass (binding energy) of the cluster X . Clearly, in the case of a single nucleon $M_X = M_N$, where M_N is the nucleon mass and $B_X = 0$. In the following, we have disregarded the mass difference between protons and neutrons. The used M_N values will be specified in the subsequent pages. In Eq. (3), the functions F_L and \tilde{G}_L describe the asymptotic radial motion of the clusters A and B . If the two clusters are composed of Z_A and Z_B protons, respectively, then the parameter η_{γ} is defined as $\eta_{\gamma} = \mu_{\gamma} Z_A Z_B e^2 / q_{\gamma}$, where $e^2 = 1.43997 \text{ MeV fm}$. The function $F_L(\eta, qy)$ is the regular Coulomb function, while $\tilde{G}_L(\eta, qy)$ is a ‘‘regularized’’ version of the irregular Coulomb function $G_L(\eta, qy)$. In this work, we have used two different methods of regularization, namely

$$(1) \quad \frac{\tilde{G}_L(\eta, qy)}{qy} = \frac{G_L(\eta, qy)}{qy} - \frac{f_L(y)}{y^{L+1}} \exp(-\beta y), \quad (6)$$

$$(2) \quad \frac{\tilde{G}_L(\eta, qy)}{qy} = \frac{G_L(\eta, qy)}{qy} [1 - \exp(-\beta y)]^{2L+1}. \quad (7)$$

where $f_L(y)$ is chosen so that both functions $\tilde{G}_L(\eta, qy)/qy$ and

$$\bar{G}_L(\eta, qy) = \left[\frac{d^2}{dy^2} + \frac{2}{y} \frac{d}{dy} - \frac{L(L+1)}{y^2} - \frac{2\eta q}{y} + q^2 \right] \frac{\tilde{G}_L(\eta, qy)}{qy}, \quad (8)$$

be regular for $y \rightarrow 0$. The functions f_L are in general given as

$$f_L(y) = a_0 + a_1 y + a_2 y^2 + \dots + a_N y^N + (b_1 y + b_2 y^2 + \dots + b_M y^M) \log(2qy), \quad (9)$$

where N and M are positive integers and the coefficients a_i and b_i can be determined considering the analytic behavior of functions $\tilde{G}_L(\eta, qy)/qy$ and $\bar{G}_L(\eta, qy)$ for $y \rightarrow 0$. The expressions of the functions $f_L(y)$ are given in the Appendix. Method 1 is simpler. However, regularizing using method 2 has the following advantage: In computing $(H - E)\Omega_{\gamma LS}^{\pm}$, we are left (between others) with a term proportional to \bar{G}_L . Note that the Coulomb functions (both the regular and the irregular)

are the solution of the equation

$$\left[\frac{d^2}{dy^2} + \frac{2}{y} \frac{d}{dy} - \frac{L(L+1)}{y^2} - \frac{2\eta q}{y} + q^2 \right] \frac{X_L(\eta, qy)}{qy} = 0, \quad (10)$$

therefore, using method 1, we have

$$\begin{aligned} \bar{G}_L = - \left\{ f_L'' - \left(2\beta + \frac{2L}{y} \right) f_L' \right. \\ \left. + \left(\beta^2 + 2\frac{\beta L - \eta q}{y} + q^2 \right) f_L \right\} \frac{e^{-\beta y}}{y^{L+1}}, \end{aligned} \quad (11)$$

where $f' = df/dy$, and so on. As discussed in the Appendix, the functions $f_L(y)$ are constructed so that \bar{G}_L be regular at the origin. Therefore, the resulting function \bar{G}_L is a smooth function, not having the oscillatory behavior of G_L . For this reason, using method 1, the matrix elements $\langle \Psi | H - E | \Omega_{\gamma LS}^\pm \rangle$ are (slightly) less problematic from the numerical point of view than using method 2 of regularization.

Note that using both methods, the functions \bar{G}_L vanish exponentially as $y \rightarrow \infty$. Moreover, $\tilde{G}_L(\eta, qy) \rightarrow G_L(\eta, qy)$ when $y \gg 1/\beta$, thus not affecting the asymptotic behavior of $\Psi_A^{\gamma LS}$, namely

$$\tilde{G}_L(\eta, qy) \pm iF_L(\eta, qy) \rightarrow e^{\pm i(qy - L\pi/2 - \eta \ln(2qy) + \sigma_L)}, \quad (12)$$

where σ_L is the Coulomb phase shift. Therefore, $\Omega_{\gamma LS}^+$ ($\Omega_{\gamma LS}^-$) describes the outgoing (ingoing) relative motion of the clusters specified by γ .

If one of the clusters is a neutron (cases $\gamma = 1$ or 4), then $\eta = 0$ and the functions F_L and G_L reduce to

$$\frac{F_L(\eta, qy)}{qy} \rightarrow j_L(qy), \quad \frac{G_L(\eta, qy)}{qy} \rightarrow -y_L(qy), \quad (13)$$

where j_L and y_L are the regular and irregular spherical Bessel functions defined, for example, in Ref. [106]. The corresponding regularizing function $f_L(y)$ defined in Eq. (9) can be obtained by taking the expression of the coefficients a_i and b_i for $\eta \rightarrow 0$ (note that in this case all $b_i \rightarrow 0$, see the Appendix).

For example, the $p + {}^3\text{H}$ asymptotic states are (in our notation, this corresponds to the clusterization $\gamma = 3$)

$$\begin{aligned} \Omega_{3LS}^\pm = D_3 \sum_{l=1}^4 [Y_L(\hat{y}_l) \otimes [\phi_3^l(ijk) \otimes \chi_l \xi_l^p]_S]_{JJ_z} \\ \times \left[\frac{\tilde{G}_L(\eta_3, q_3 y_l)}{q_3 y_l} \pm i \frac{F_L(\eta_3, q_3 y_l)}{q_3 y_l} \right], \end{aligned} \quad (14)$$

where y_l is the distance between the proton (particle l) and ${}^3\text{H}$ (particles ijk), q_3 is defined via Eqs. (4) and (5), and

$$\eta_3 = \frac{\mu_3 e^2}{q_3}, \quad \mu_3 \approx \frac{3}{4} M_N. \quad (15)$$

Moreover, ϕ_3^l is the ${}^3\text{H}$ wave function (with the z component of isospin $T_z = -\frac{1}{2}$) and χ_l (ξ_l^p) the spin (isospin) state of the free proton. Note that we do not couple the isospin states. Therefore Ω_{3LS}^\pm are superpositions of states with total isospin $T = 0, 1$. The antisymmetry operator \mathcal{A} in this case reduces simply to the sum over the four possible $1 + 3$ partitions of the

particles, assuming $\phi_3^l(ijk)$ to be completely antisymmetric with respect to the exchange of particles i, j , and k .

In this paper, we consider only $1 + 3$ clusterizations, and the normalization factors D_γ can be conveniently chosen to be

$$D_\gamma = \sqrt{\frac{1}{4}} \sqrt{\frac{2\mu_\gamma q_\gamma}{(\kappa_\gamma)^3}}, \quad \kappa_\gamma = \sqrt{\frac{3}{2}}, \quad \gamma = 1, \dots, 4. \quad (16)$$

The parameter κ_γ is the coefficient of proportionality between the Jacobi vector \mathbf{x}_1 and the distance between the two clusters \mathbf{y} , namely $\mathbf{x}_1 = \kappa_\gamma \mathbf{y}$, see next subsection. Finally, the general expression of $\Psi_A^{\gamma LS}$ entering Eq. (2) is

$$\Psi_A^{\gamma LS} = \sum_{\gamma' L' S'} [\delta_{\gamma, \gamma'} \delta_{LL'} \delta_{SS'} \Omega_{\gamma' L' S'}^- - S_{LS, L' S'}^{\gamma, \gamma'}(E) \Omega_{\gamma' L' S'}^+], \quad (17)$$

where the parameters $S_{LS, L' S'}^{\gamma, \gamma'}(E)$ are S -matrix elements. Of course, the sum over L' and S' is over all values compatible with the given J and parity π . In particular, the sum over L' is limited to include either even or odd values such that $(-1)^{L'} = \pi$. The sum over γ' is over the possible final clusters compatible with the conservation of the total charge. Clearly, the parameters $S_{LS, L' S'}^{\gamma, \gamma'}(E)$ with $\gamma \neq \gamma'$ are related to the cross section of the reaction $\gamma \rightarrow \gamma'$, while $S_{LS, L' S'}^{\gamma, \gamma'}(E)$ to an elastic scattering process.

B. The hyperspherical harmonic functions

The core wave function $\Psi_C^{\gamma LS}$ has been here expanded using the HH basis. The superscript γLS means that $\Psi_C^{\gamma LS}$ is the core part of the wave function given in Eq. (2) describing a process where there are two incoming clusters specified by γ having a relative orbital angular momentum L and channel spin S . For four equal mass particles, a suitable choice of the Jacobi vectors is

$$\begin{aligned} \mathbf{x}_{1p} &= \sqrt{\frac{3}{2}} \left(\mathbf{r}_l - \frac{\mathbf{r}_i + \mathbf{r}_j + \mathbf{r}_k}{3} \right), \\ \mathbf{x}_{2p} &= \sqrt{\frac{4}{3}} \left(\mathbf{r}_k - \frac{\mathbf{r}_i + \mathbf{r}_j}{2} \right), \\ \mathbf{x}_{3p} &= \mathbf{r}_j - \mathbf{r}_i, \end{aligned} \quad (18)$$

where p specifies a given permutation corresponding to the order i, j, k , and l of the particles. By definition, the permutation $p = 1$ is chosen to correspond to the order 1, 2, 3, and 4. In terms of the Jacobi vectors, the kinetic energy T is written as

$$T = -\frac{1}{M_N} (\nabla_{\mathbf{x}_{1p}}^2 + \nabla_{\mathbf{x}_{2p}}^2 + \nabla_{\mathbf{x}_{3p}}^2). \quad (19)$$

The other possible choice of the Jacobi vectors is

$$\begin{aligned} \mathbf{y}_{1p} &= \mathbf{r}_l - \mathbf{r}_k, \\ \mathbf{y}_{2p} &= \frac{1}{\sqrt{2}} (\mathbf{r}_l + \mathbf{r}_k - \mathbf{r}_i - \mathbf{r}_j), \\ \mathbf{y}_{3p} &= \mathbf{r}_j - \mathbf{r}_i. \end{aligned} \quad (20)$$

In the following, we are going to use only the HH functions constructed with the Jacobi vectors given in Eq. (18). In fact,

the HH functions are essentially harmonics polynomials and those constructed with the Jacobi vectors given in Eq. (20) are just linear combinations of the HH functions constructed with the Jacobi vectors of Eq. (18). On the other hand, HH functions constructed for different choices of the particle permutation p are needed in order to construct wave functions with the correct permutational symmetry.

For a given choice of the Jacobi vectors, the hyperspherical coordinates are given by the so-called hyperradius ρ , defined by

$$\rho = \sqrt{x_{1p}^2 + x_{2p}^2 + x_{3p}^2}, \quad (\text{independent of } p), \quad (21)$$

and by a set of angular variables which in the Zernike and Brinkman [107,108] representation are (i) the polar angles $\hat{\mathbf{x}}_{ip} \equiv (\theta_{ip}, \phi_{ip})$ of each Jacobi vector and (ii) the two additional ‘‘hyperspherical’’ angles φ_{2p} and φ_{3p} defined as

$$\begin{aligned} \cos \varphi_{2p} &= \frac{x_{2p}}{\sqrt{x_{1p}^2 + x_{2p}^2}}, \\ \cos \varphi_{3p} &= \frac{x_{3p}}{\sqrt{x_{1p}^2 + x_{2p}^2 + x_{3p}^2}}, \end{aligned} \quad (22)$$

where x_{jp} is the modulus of the Jacobi vector \mathbf{x}_{jp} . The set of angular variables $\hat{\mathbf{x}}_{1p}, \hat{\mathbf{x}}_{2p}, \hat{\mathbf{x}}_{3p}, \varphi_{2p}$, and φ_{3p} is denoted hereafter as Ω_p . The expression of a generic HH function is

$$\begin{aligned} \mathcal{H}_{\ell_1, \ell_2, \ell_3, L_2, n_2, n_3}^{K, \Lambda, M}(\Omega_p) &= \mathcal{N}_{n_2, n_3}^{\ell_1, \ell_2, \ell_3} [(Y_{\ell_1}(\hat{\mathbf{x}}_{1p}) Y_{\ell_2}(\hat{\mathbf{x}}_{2p}))_{L_2} Y_{\ell_3}(\hat{\mathbf{x}}_{3p})]_{\Lambda M} \\ &\times (\sin \varphi_{2p})^{\ell_1} (\cos \varphi_{2p})^{\ell_2} (\sin \varphi_{3p})^{\ell_1 + \ell_2 + 2n_2} (\cos \varphi_{3p})^{\ell_3} \\ &\times P_{n_2}^{\ell_1 + \frac{1}{2}, \ell_2 + \frac{1}{2}}(\cos 2\varphi_{2p}) \\ &\times P_{n_3}^{\ell_1 + \ell_2 + 2n_2 + 2, \ell_3 + \frac{1}{2}}(\cos 2\varphi_{3p}), \end{aligned} \quad (23)$$

where $P_n^{a,b}$ are Jacobi polynomials and the coefficients $\mathcal{N}_{n_2, n_3}^{\ell_1, \ell_2, \ell_3}$ normalization factors. The quantity $K = \ell_1 + \ell_2 + \ell_3 + 2(n_2 + n_3)$ is the grand angular quantum number. The HH functions are the eigenfunctions of the hyperangular part of the kinetic energy operator. Furthermore, $\rho^K \mathcal{H}_{\ell_1, \ell_2, \ell_3, L_2, n_2, n_3}^{K, \Lambda, M}(\Omega_p)$ are homogeneous polynomials of the particle coordinates of degree K .

A set of antisymmetric hyperangular spin-isospin states of grand angular quantum number K , total orbital angular momentum Λ , total spin Σ , and total isospin T (for given values of total angular momentum J and parity π) can be constructed as follows:

$$\Psi_{\mu}^{K \Lambda \Sigma T} = \sum_{p=1}^{12} \Phi_{\mu}^{K \Lambda \Sigma T}(i, j, k, l), \quad (24)$$

where the sum is over the 12 even permutations $p \equiv i, j, k, l$, and

$$\begin{aligned} \Phi_{\mu}^{K \Lambda \Sigma T}(i, j, k, l) &= \{ \mathcal{H}_{\ell_1, \ell_2, \ell_3, L_2, n_2, n_3}^{K, \Lambda}(\Omega_p) [(s_i s_j)_{S_a} s_k]_{S_b} s_l]_{\Sigma} \}_{J J_z} \\ &\times [(t_i t_j)_{T_a} t_k]_{T_b} t_l]_{T T_z}. \end{aligned} \quad (25)$$

Here $\mathcal{H}_{\ell_1, \ell_2, \ell_3, L_2, n_2, n_3}^{K, \Lambda}(\Omega_p)$ is the HH state defined in Eq. (23), and s_i (t_i) denotes the spin (isospin) function of particle i .

The total orbital angular momentum Λ of the HH function is coupled to the total spin Σ to give the total angular momentum $J J_z$, whereas $\pi = (-1)^{\ell_1 + \ell_2 + \ell_3}$. The quantum number T specifies the total isospin of the state. The integer index μ labels the possible choices of hyperangular, spin, and isospin quantum numbers, namely

$$\mu \equiv \{ \ell_1, \ell_2, \ell_3, L_2, n_2, n_3, S_a, S_b, T_a, T_b \}, \quad (26)$$

compatibles with the given values of K, Λ, Σ, T, J , and π . Another important classification of the states is to group them in ‘‘channels’’: States belonging to the same channel have the same values of angular $\ell_1, \ell_2, \ell_3, L_2, \Lambda$; spin S_a, S_b, Σ ; and isospin T_a, T_b, T quantum numbers but different values of n_2, n_3 .

Each state $\Psi_{\mu}^{K \Lambda \Sigma T}$ entering the expansion of the 4N wave function must be antisymmetric under the exchange of any pair of particles. To this aim it is sufficient to consider states such that

$$\Phi_{\mu}^{K \Lambda \Sigma T}(i, j, k, l) = -\Phi_{\mu}^{K \Lambda \Sigma T}(j, i, k, l), \quad (27)$$

which is fulfilled when the condition

$$\ell_3 + S_a + T_a = \text{odd} \quad (28)$$

is satisfied.

The number $M_{K \Lambda \Sigma T}$ of antisymmetric functions $\Psi_{\mu}^{K \Lambda \Sigma T}$ having given values of K, Λ, Σ , and T but different combinations of quantum numbers μ [see Eq. (26)] is in general very large. In addition to the degeneracy of the HH basis, the four spins (isospins) can be coupled in different ways to Σ (T). However, many of the states $\Psi_{\mu}^{K \Lambda \Sigma T}, \mu = 1, \dots, M_{K \Lambda \Sigma T}$ are linearly dependent between themselves. In the expansion of $\Psi_C^{\gamma LS}$ it is necessary to include only the subset of linearly independent states, whose number is fortunately noticeably smaller than the corresponding value of $M_{K \Lambda \Sigma T}$.

The core part of the wave function can be finally written as

$$\Psi_C^{\gamma LS} = \sum_{K \Lambda \Sigma T} \sum_{\mu} u_{K \Lambda \Sigma T \mu}^{\gamma LS}(\rho) \Psi_{\mu}^{K \Lambda \Sigma T}, \quad (29)$$

where the sum is restricted only to the linearly independent states. We have found convenient to expand the ‘‘hyperradial’’ functions $u_{K \Lambda \Sigma T \mu}^{\gamma LS}(\rho)$ in a complete set of functions, namely

$$u_{K \Lambda \Sigma T \mu}^{\gamma LS}(\rho) = \sum_{m=0}^{M-1} c_{K \Lambda \Sigma T \mu m}^{\gamma LS} g_m(\rho), \quad (30)$$

and we have chosen

$$g_m(\rho) = \sqrt{b^9 \frac{m!}{(m+8)!}} L_m^{(8)}(b\rho) e^{-\frac{b}{2}\rho}, \quad (31)$$

where $L_l^{(8)}(b\rho)$ are Laguerre polynomials [106] and b is a parameter to be variationally optimized.

Using the expansion given in Eq. (30), finally the core part can be written as

$$\Psi_C^{\gamma LS} = \sum_{K \Lambda \Sigma T \mu} c_{K \Lambda \Sigma T \mu}^{\gamma LS} \Psi_{\mu}^{K \Lambda \Sigma T} g_m(\rho). \quad (32)$$

C. The Kohn variational principle

The S -matrix elements $\mathcal{S}_{LS,L'S'}^{\gamma,\gamma'}$ of Eq. (17) and the coefficients $c_{K\Lambda\Sigma T\mu,m}^{\gamma LS}$ occurring in the expansion of $\Psi_C^{\gamma LS}$ are determined using the Kohn variational principle (KVP). Recalling Eqs. (2), (17), and (32), the wave function can be written in a compact way as

$$\Psi^{\gamma LS} \equiv \Psi_\nu = \Omega_\nu^- - \sum_{\nu'} \mathcal{S}_{\nu,\nu'} \Omega_{\nu'}^+ + \sum_k c_{\nu k} \Psi_k, \quad (33)$$

where hereafter we use the notation $\nu \equiv \{\gamma LS\}$, $k \equiv \{K\Lambda\Sigma T\mu m\}$, and

$$\mathcal{S}_{\nu,\nu'} \equiv \mathcal{S}_{LS,L'S'}^{\gamma,\gamma'}, \quad c_{\nu k} \equiv c_{K\Lambda\Sigma T\mu m}^{\gamma LS}, \quad \Psi_k = \Psi_\mu^{K\Lambda\Sigma T} g_m(\rho). \quad (34)$$

In practice, the index ν specifies the possible asymptotic waves and the index k runs over all the terms used to expand the core part. To use the KVP for the S matrix, we need also the related wave function

$$\tilde{\Psi}_\nu = \Omega_\nu^+ - \sum_{\nu'} \mathcal{S}_{\nu',\nu}^* \Omega_{\nu'}^- + \sum_k c_{\nu k}^* \Psi_k, \quad (35)$$

where the asterisk denotes the complex conjugate. In particular, we can define $\tilde{\Psi}_\nu^{J,J_z} = (-)^{L+J+J_z} \mathcal{T} \Psi_\nu^{J,-J_z}$, where here we have shown explicitly the dependence on the total angular momentum and \mathcal{T} is the time-reversal operator. Since H commutes with \mathcal{T} , then both Ψ_ν^{J,J_z} and $\tilde{\Psi}_\nu^{J,J_z}$ are eigenstates of H with the same eigenvalue E . The KVP states that the coefficients $\mathcal{S}_{\nu,\nu'}$ and $c_{\nu k}$ are determined by making the functional $[\mathcal{S}_{\nu,\nu'}]$ defined as

$$[\mathcal{S}_{\nu,\nu'}] = \frac{\mathcal{S}_{\nu,\nu'} + \mathcal{S}_{\nu',\nu}}{2} - \frac{\langle \tilde{\Psi}_{\nu'} | H - E | \Psi_\nu \rangle + \langle \tilde{\Psi}_\nu | H - E | \Psi_{\nu'} \rangle}{4i}, \quad (36)$$

stationary with respect to variations of them [109–111]. The expression above is obtained when the normalization factors D_γ are chosen as in Eq. (16). After the variations of the functional, a linear set of equations for $\mathcal{S}_{\nu,\nu'}$ and $c_{\nu k}$ is obtained. For example, let us consider the functional for the diagonal case $\nu = \nu' = \nu_0$. Then

$$[\mathcal{S}_{\nu_0,\nu_0}] = \mathcal{S}_{\nu_0,\nu_0} - \frac{1}{2i} \left[A_{\nu_0,\nu_0}^{-,-} - \sum_\nu \mathcal{S}_{\nu_0,\nu} (A_{\nu,\nu_0}^{+,-} + A_{\nu_0,\nu}^{-,+}) + \sum_{\nu,\nu'} \mathcal{S}_{\nu_0,\nu} \mathcal{S}_{\nu_0,\nu'} A_{\nu,\nu'}^{+,+} + \sum_k c_{\nu_0,k} 2B_{k,\nu_0}^- - \sum_{k,\nu} c_{\nu_0,k} \mathcal{S}_{\nu_0,\nu} 2B_{k,\nu}^+ + \sum_{k,k'} c_{\nu_0,k} c_{\nu_0,k'} C_{k,k'} \right], \quad (37)$$

where

$$A_{\nu,\nu'}^{\lambda,\lambda'} = \langle \Omega_\nu^{-\lambda} | H - E | \Omega_{\nu'}^{\lambda'} \rangle, \quad (38)$$

$$B_{k,\nu}^\lambda = \langle \Psi_k | H - E | \Omega_\nu^\lambda \rangle, \quad (39)$$

$$C_{k,k'} = \langle \Psi_k | H - E | \Psi_{k'} \rangle, \quad (40)$$

and $\lambda, \lambda' \equiv \pm$. Note the definition of the matrix elements $A_{\nu,\nu'}^{\lambda,\lambda'}$ in Eq. (38) which takes into account that $(\Omega_\nu^\lambda)^\dagger = \Omega_\nu^{-\lambda}$. Moreover, $\langle \Psi_k | H - E | \Omega_\nu^\lambda \rangle = \langle \Omega_\nu^{-\lambda} | H - E | \Psi_k \rangle$ since the wave functions Ψ_k are square integrables. On the other hand, $A_{\nu,\nu'}^{\lambda,\lambda'} \neq A_{\nu',\nu}^{\lambda',\lambda}$. With the normalization factors D_γ chosen as in Eq. (16), it can be proved that

$$\frac{1}{2i} (A_{\nu,\nu}^{+,-} - A_{\nu,\nu}^{-,+}) = 1. \quad (41)$$

This relation can be used to test the numerical accuracy of the calculated matrix elements. From the variation of the expression given in Eq. (37), we can determine the S -matrix elements $\mathcal{S}_{\nu_0,\nu}$ and the coefficients $c_{\nu_0,k}$. In the following, we refer to $\mathcal{S}_{\nu_0,\nu}$ determined in this way as the “first-order” S -matrix elements. Explicitly, one obtains the following linear system:

$$\begin{bmatrix} C_{k,k'} & -B_{k,\nu'}^+ \\ -B_{k',\nu}^+ & \frac{1}{2} (A_{\nu,\nu'}^{+,+} + A_{\nu',\nu}^{+,+}) \end{bmatrix} \begin{pmatrix} c_{\nu_0,k'} \\ \mathcal{S}_{\nu_0,\nu'} \end{pmatrix} = \begin{bmatrix} -B_{k,\nu_0}^- \\ i\delta_{\nu_0,\nu} + \frac{1}{2} (A_{\nu,\nu_0}^{+,-} + A_{\nu_0,\nu}^{-,+}) \end{bmatrix}. \quad (42)$$

This linear system is solved using the Lanczos algorithm. A typical calculation involves the expansion of the core part with 10 000 HH functions and 16 functions $g_m(\rho)$. So the matrix elements $C_{k,k'}$ form a matrix of dimension 160 000 × 160 000. This part does not depend on the energy and can be calculated only once. The possible ν values are much less. In this work at maximum we can have four combinations for the $p + {}^3\text{H}$ and $n + {}^3\text{He}$ scattering in the $J > 0$ waves. For example, for this process and the wave $J^\pi = 1^-$, we may have the combinations $\nu \equiv \{\gamma LS\} = \{3 1 0\}$, $\{3 1 1\}$, $\{4 1 0\}$, $\{4 1 1\}$. Clearly the matrix elements $B_{k,\nu'}^\lambda$ and $A_{\nu,\nu'}^{\lambda,\lambda'}$ depend on the energy and have to be calculated every time from the beginning. However, their number is much less than that of the C -matrix elements. Moreover, the matrix on the left-hand side of Eq. (42) does not depend on ν_0 and therefore can be inverted only once for all ν_0 .

The calculation has to be performed for each values of J^π and for all the different types of interaction of interest. Finally, the procedure has to be repeated separately for the $T_z = -1$ ($n + {}^3\text{H}$ scattering), $T_z = +1$ ($p + {}^3\text{He}$ scattering), and $T_z = 0$ ($p + {}^3\text{H}$ and $n + {}^3\text{He}$ scattering) cases.

The KVP also states [109–111] that the quantities $[\mathcal{S}_{\nu,\nu'}]$ are a variational approximation to the exact S -matrix elements $\mathcal{S}_{\nu,\nu'}^{\text{exact}}$. To clarify better this assertion, let us write $\Psi_\nu = \Psi_\nu^{\text{exact}} + \epsilon_\nu$, where Ψ_ν are the wave functions determined as discussed above, Ψ_ν^{exact} the exact wave functions, and ϵ_ν the corresponding “error” functions. Then the KVP assures that $||[\mathcal{S}_{\nu,\nu'}] - \mathcal{S}_{\nu,\nu'}^{\text{exact}}|| \propto \epsilon^2$. Therefore, the convergence of the quantities $[\mathcal{S}_{\nu,\nu'}]$ to the exact S -matrix elements is quadratic in the error functions and consequently much faster than the convergence of the first-order estimates $\mathcal{S}_{\nu,\nu'}$. Usually, the quantities $[\mathcal{S}_{\nu,\nu'}]$ are called the “second-order” S -matrix elements. We note also that the quantities $[\mathcal{S}_{\nu,\nu'}]$ automatically verify the condition $[\mathcal{S}_{\nu,\nu'}] = [\mathcal{S}_{\nu',\nu}]$ (principle of detailed balance). On the other hand, for the S -matrix elements calculated

solving the linear system given in Eq. (42), this property is not guaranteed. Only after the inclusion of a sufficient number of terms in the expansion of the core part in Eq. (33) is the symmetry property for $\mathcal{S}_{v,v'}$ approximately verified.

D. Details of the calculation

Let us now consider the problem of the computation of the matrix elements of the Hamiltonian, and in particular of the NN and 3N interactions. First, let us consider the ‘‘core-core’’ matrix elements, which explicitly read

$$C_{k,k'} = \langle \Psi_{\mu}^{K\Lambda\Sigma T} g_m(\rho) | H - E | \Psi_{\mu'}^{K'\Lambda'\Sigma'T'} g_{m'}(\rho) \rangle, \quad (43)$$

where $\Psi_{\mu}^{K\Lambda\Sigma T}$ are given in Eqs. (24) and (25). This calculation is considerably simplified using the following property of the functions given in Eq. (25):

$$\Phi_{\mu}^{K\Lambda\Sigma T}(i, j, k, l) = \sum_{\mu'} a_{\mu,\mu'}^{K\Lambda\Sigma T}(p) \Phi_{\mu'}^{K\Lambda\Sigma T}(1, 2, 3, 4), \quad (44)$$

where the coefficients $a_{\mu,\mu'}^{K\Lambda\Sigma T}(p)$ have been obtained using the techniques described in Ref. [112]. In this way, we can write

$$\Psi_{\mu}^{K\Lambda\Sigma T} g_m(\rho) = g_m(\rho) \sum_{\mu'} \tilde{a}_{\mu,\mu'}^{K\Lambda\Sigma T} \Phi_{\mu'}^{K\Lambda\Sigma T}(1, 2, 3, 4), \quad (45)$$

where

$$\tilde{a}_{\mu,\mu'}^{K\Lambda\Sigma T} = \sum_{p=1}^{12} a_{\mu,\mu'}^{K\Lambda\Sigma T}(p). \quad (46)$$

The sum over the permutations enters only in the construction of the coefficients \tilde{a} , and it can be performed beforehand. With a wave function written in this way, most of the integrations needed to compute $C_{k,k'}$ can be performed analytically. The remaining low-dimensional integrations can therefore be easily calculated with sufficiently dense grids to obtain relative errors $\leq 10^{-6}$. The adopted procedure is the same as described in Ref. [28].

Second, let us consider the ‘‘core-asymptotic’’ and ‘‘asymptotic-asymptotic’’ matrix elements,

$$B_{k,v}^{\lambda} = \langle \Psi_{\mu}^{K\Lambda\Sigma T} g_m(\rho) | H - E | \Omega_{\gamma LS}^{\lambda} \rangle, \quad (47)$$

$$A_{v,v'}^{\lambda,\lambda'} = \langle \Omega_{\gamma LS}^{-\lambda} | H - E | \Omega_{\gamma' L'S'}^{\lambda'} \rangle. \quad (48)$$

The computation of $(H - E)\Omega_{\gamma LS}^{\lambda}$ can be simplified as follows. We refer specifically to the $p + {}^3\text{H}$ asymptotic state given in Eq. (14). Then

$$\begin{aligned} (H - E)\Omega_{3LS}^{\pm} &= D_3 \sum_{l=1}^4 \left[H_3(ijk) + V_{il} + V_{jl} + V_{kl} \right. \\ &\quad + W_{ijl} + W_{ikl} + W_{jkl} \\ &\quad + \left. \frac{e_{il}^2}{r_{il}} + \frac{e_{jl}^2}{r_{jl}} + \frac{e_{kl}^2}{r_{kl}} - \frac{\nabla_{\mathbf{x}_{1p}}^2}{M_N} + B_3 - \frac{q_3^2}{2\mu_3} \right] \\ &\quad \times [Y_L(\hat{\mathbf{y}}_l) \otimes [\phi_3^t(ijk) \otimes \chi_l \xi_l^p]_S]_{JJ_z} \\ &\quad \times \left[\frac{\tilde{G}_L(\eta_3, q_3 y_l)}{q_3 y_l} \pm i \frac{F_L(\eta_3, q_3 y_l)}{q_3 y_l} \right], \quad (49) \end{aligned}$$

where $H_3(ijk)$ is the Hamiltonian of the three-body subsystems formed by particles ijk , ϕ_3^t the ${}^3\text{H}$ bound-state wave function, B_3 the corresponding binding energy, V_{il} (W_{ijl}) the NN (3N) potential acting on the pair (triplet) of particles il (ijl), and

$$\frac{e_{il}^2}{r_{il}} \equiv \frac{e^2}{r_{il}} \frac{1 + \tau_z(i)}{2} \frac{1 + \tau_z(l)}{2}, \quad (50)$$

is the point-Coulomb potential between particles i and l including the isospin projection over the proton states (eventual additional electromagnetic interactions are lumped in V). Above $\tau_z(i)$ is the isospin Pauli matrix acting on particle i . Using $H_3(ijk)\phi_3^t(ijk) = -B_3\phi_3^t(ijk)$ and that $\mathbf{x}_{1p} = \kappa_3 \mathbf{y}_l$, see Eqs. (16) and (18), one obtains

$$(H - E)\Omega_{3LS}^{\pm} = \Omega_{3LS}^{\pm}(T) + \Omega_{3LS}^{\pm}(V), \quad (51)$$

$$\begin{aligned} \Omega_{3LS}^{\pm}(T) &= -\frac{D_3}{2\mu_3} \sum_{l=1}^4 [Y_L(\hat{\mathbf{y}}_l) \otimes [\phi_3^t(ijk) \otimes \chi_l \xi_l^p]_S]_{JJ_z} \\ &\quad \times \bar{G}_L(\eta_3, q_3 y_l), \quad (52) \end{aligned}$$

$$\begin{aligned} \Omega_{3LS}^{\pm}(V) &= D_3 \sum_{l=1}^4 \left(V_{il} + V_{jl} + V_{kl} \right. \\ &\quad + W_{ijl} + W_{ikl} + W_{jkl} \\ &\quad + \left. \frac{e_{il}^2}{r_{il}} + \frac{e_{jl}^2}{r_{jl}} + \frac{e_{kl}^2}{r_{kl}} - \frac{e^2}{y_l} \right) \\ &\quad \times [Y_L(\hat{\mathbf{y}}_l) \otimes [\phi_3^t(ijk) \otimes \chi_l \xi_l^p]_S]_{JJ_z} \\ &\quad \times \left[\frac{\tilde{G}_L(\eta_3, q_3 y_l)}{q_3 y_l} \pm i \frac{F_L(\eta_3, q_3 y_l)}{q_3 y_l} \right]. \quad (53) \end{aligned}$$

We have divided the expression of $(H - E)\Omega_{3LS}^{\pm}$ in a kinetic energy part plus a potential energy part. Note in the kinetic energy part the appearance of the function \bar{G}_L defined in Eq. (8). Moreover, $2\mu_3 = \kappa_3^2 M_N$, see Eq. (16), and $2\eta_3 q_3 = e^2 \kappa_3^2 M_N$, see Eq. (15). For the potential part, since ϕ_3^t is antisymmetric with respect to the exchange of the particles i, j , and k , in the matrix elements defined in Eqs. (47) and (48) one can also take $V_{il} + V_{jl} + V_{kl} \rightarrow 3V_{il}$, and so on.

We note that the functions $\Omega_{3LS}^{\pm}(T)$ and $\Omega_{3LS}^{\pm}(V)$ now vanish asymptotically at least as $1/(y_l)^2$. In fact, due to the presence of the bound-state wave function $\phi_3^t(ijk)$, the particles i, j , and k must be close. Then, we need only to discuss what happens for $y_l \rightarrow \infty$. In this limit, the function \bar{G}_L goes to zero exponentially as discussed in Sec. II A. For $\Omega_{3LS}^{\pm}(V)$, when $y_l \rightarrow \infty$, all distances r_{il} , r_{jl} , and r_{kl} go to ∞ and therefore all the NN and 3N potential terms V and W rapidly vanish. Regarding the Coulomb term, it can be rewritten as

$$\begin{aligned} &\left[\frac{e_{il}^2}{r_{il}} + \frac{e_{jl}^2}{r_{jl}} + \frac{e_{kl}^2}{r_{kl}} - \frac{e^2}{y_l} \right] \phi_3^t(ijk) \\ &= \left[e_{il}^2 \left(\frac{1}{r_{il}} - \frac{1}{y_l} \right) + e_{jl}^2 \left(\frac{1}{r_{jl}} - \frac{1}{y_l} \right) \right. \\ &\quad \left. + e_{kl}^2 \left(\frac{1}{r_{kl}} - \frac{1}{y_l} \right) \right] \phi_3^t(ijk), \quad (54) \end{aligned}$$

since in the ^3H wave function $\phi_3^l(ijk)$ only one of the particle is a proton and always $(e_{il}^2 + e_{jl}^2 + e_{kl}^2)\phi_3^l = e^2\phi_3^l$. Therefore, for $y_l \rightarrow \infty$ we have $\frac{1}{r_{il}} - \frac{1}{y_l} \sim O(1/y_l^2) \rightarrow 0$, and so on. A similar analysis can be performed for all the asymptotic states $\Omega_{\gamma LS}^\pm$ with the other values of γ ($\gamma = 1, 2$, and 4). Clearly, when the particle l is a neutron, the Coulomb term is missing. Therefore, also for the matrix elements $A_{v,v'}^{\lambda,\lambda'}$ given in Eq. (48), the integrands are always short ranged and their calculation does not present any singular behavior asymptotically.

As a final remark, we note that the relation $H_3(ijk)\phi_3^l(ijk) = -B_3\phi_3^l(ijk)$ is not exactly verified in our calculation, as we construct variationally ϕ_3^l in terms of an expansion over the three-body HH functions. However, as discussed in Ref. [110], this inaccuracy contributes at the end to increase the error function ϵ_v and the full procedure maintains its validity (for example, the quantities $[\mathcal{S}_{v,v'}]$ are still a variational approximation of the exact ones). As discussed later, we control this potential source of inaccuracy by increasing the number of terms included in the expansion of ϕ_3^l . We can anticipate that the error related to this approximation is well under control.

Let us now resume the discussion of the matrix elements given in Eqs. (47) and (48). Their calculations is simplified by “projecting” the states $\Omega_{\gamma LS}^\pm$ and also $\Omega_{\gamma LS}^\pm(T)$ over a complete set of angular-spin-isospin states, constructed in terms of the Jacobi vectors \mathbf{x}_i corresponding to the particle order 1,2,3,4. For example:

$$\Omega_{\gamma LS}^\pm = \sum_{\alpha} F_{\alpha}^{\gamma LS^\pm}(x_1, x_2, x_3) \mathcal{Y}_{\alpha}(\hat{\mathbf{x}}_1, \hat{\mathbf{x}}_2, \hat{\mathbf{x}}_3), \quad (55)$$

where

$$\mathcal{Y}_{\alpha}(\hat{\mathbf{x}}_1, \hat{\mathbf{x}}_2, \hat{\mathbf{x}}_3) = \{[(Y_{\ell_3}(\hat{\mathbf{x}}_3)_{s_1 s_2})_{j_3} (Y_{\ell_2}(\hat{\mathbf{x}}_2)_{s_3})_{j_2}]_{J_2} \times (Y_{\ell_1}(\hat{\mathbf{x}}_1)_{s_4})_{j_1}\}_{JJ_z} [[(t_1 t_2)_{T_2} t_3]_{T_3} t_4]_{TT_z}, \quad (56)$$

and $\alpha = \{\ell_1, \ell_2, \ell_3, j_1, j_2, j_3, J_2, S_2, T_2, T_3, T\}$. Note that due to the antisymmetry of the wave function, we must have $\ell_3 + S_2 + T_2 = \text{odd}$. We recall that the indices $LS\gamma$ specify the asymptotic states defined in Eq. (3). These quantities are expanded in terms of the states \mathcal{Y}_{α} constructed using the “ j ” coupling” for convenience, since with these states it is easier to compute the potential matrix elements (see below). This “partial wave expansion” is performed including all states α such that $\ell_i \leq \ell_{\max}$. The functions $F_{\alpha}^{\gamma LS^\pm}$ can be obtained very accurately by direct integration

$$F_{\alpha}^{\gamma LS^\pm}(x_1, x_2, x_3) = \int d\hat{\mathbf{x}}_1 d\hat{\mathbf{x}}_2 d\hat{\mathbf{x}}_3 [\mathcal{Y}_{\alpha}(\hat{\mathbf{x}}_1, \hat{\mathbf{x}}_2, \hat{\mathbf{x}}_3)]^\dagger \Omega_{\gamma LS}^\pm. \quad (57)$$

This six-dimensional integral can be reduced to a three-dimensional integral by performing the analytical integration over three Euler angles. Then we are left with the integration over the “internal” angles or, in other words, over the variables $\mu_{12} = \hat{\mathbf{x}}_1 \cdot \hat{\mathbf{x}}_2$, $\mu_{13} = \hat{\mathbf{x}}_1 \cdot \hat{\mathbf{x}}_3$, and $\mu_{23} = \hat{\mathbf{x}}_2 \cdot \hat{\mathbf{x}}_3$. This integration is performed using a Gauss-Legendre quadrature technique over n_{μ} points (see Sec. III C).

Finally, using the transformation given in Eq. (44) and the partial wave expansion given above, all these terms, Ψ_k , $\Omega_{\gamma LS}^\pm$,

and $\Omega_{\gamma LS}^\pm(T)$, can be rewritten as

$$\Psi^X = \sum_{\alpha} \mathcal{F}_{\alpha}^X(x_1, x_2, x_3) \mathcal{Y}_{\alpha}(\hat{\mathbf{x}}_1, \hat{\mathbf{x}}_2, \hat{\mathbf{x}}_3), \quad (58)$$

where Ψ^X stands for Ψ_k , $\Omega_{\gamma LS}^\pm$, or $\Omega_{\gamma LS}^\pm(T)$. Above, \mathcal{F} is either a combinations of Jacobi polynomials of the hyperangles and functions $g_m(\rho)$, see Eq. (45) for Ψ_k , or corresponds to a function $F_{\alpha}^{\gamma LS^\pm}$ for the asymptotic parts.

Then the matrix elements of a two-body potential can be evaluated as explained in the following. Permuting the particles in either the “bra” and in the “ket,” and using the antisymmetry properties of Ψ_k , $\Omega_{\gamma LS}^\pm$, $\phi_3^l(ijk)$, and so on, it is always possible to reduce these matrix elements to

$$\langle \Psi^X | V_{12} | \Psi^{X'} \rangle. \quad (59)$$

These integrals are easily calculated using the decomposition given in Eq. (58). Here we have developed two different procedures depending on whether the potential is local or nonlocal.

1. Local potentials

In this case Eq. (59) is given explicitly by

$$\langle \Psi^X | V_{12} | \Psi^{X'} \rangle = \int d^3\mathbf{x}_1 d^3\mathbf{x}_2 d^3\mathbf{x}_3 (\Psi^X(\mathbf{x}_1, \mathbf{x}_2, \mathbf{x}_3))^\dagger \times V(\mathbf{x}_3) \Psi^{X'}(\mathbf{x}_1, \mathbf{x}_2, \mathbf{x}_3). \quad (60)$$

The calculation of the above integral is performed in two steps. First, the spin-isospin-angular matrix elements

$$\int d\hat{\mathbf{x}}_1 d\hat{\mathbf{x}}_2 d\hat{\mathbf{x}}_3 \mathcal{Y}_{\alpha}(\hat{\mathbf{x}}_1, \hat{\mathbf{x}}_2, \hat{\mathbf{x}}_3)^\dagger V(\mathbf{x}_3) \mathcal{Y}_{\alpha'}(\hat{\mathbf{x}}_1, \hat{\mathbf{x}}_2, \hat{\mathbf{x}}_3) = v_{\ell_3, S_2, \ell'_3, S'_2}^{j_3, T_3, T, T'_3, T'}(x_3) \delta_{j_3, j'_3} \delta_{j_2, j'_2} \delta_{j_1, j'_1} \delta_{\ell_2, \ell'_2} \delta_{\ell_1, \ell'_1} \quad (61)$$

are computed analytically, and, second, the integration over the moduli of the Jacobi vectors,

$$\int_0^\infty dx_1 dx_2 dx_3 x_1^2 x_2^2 x_3^2 (\mathcal{F}_{\alpha}^X(x_1, x_2, x_3))^* \times v_{\ell_3, S_2, \ell'_3, S'_2}^{j_3, T_3, T, T'_3, T'}(x_3) \mathcal{F}_{\alpha'}^{X'}(x_1, x_2, x_3), \quad (62)$$

is obtained in the following way:

$$\int_0^\infty dx_1 dx_2 dx_3 x_1^2 x_2^2 x_3^2 = \int_0^\infty \rho^8 d\rho \int_0^{\frac{\pi}{2}} d\varphi_3 (\cos \varphi_3)^2 (\sin \varphi_3)^5 \times \int_0^{\frac{\pi}{2}} d\varphi_2 (\cos \varphi_2)^2 (\sin \varphi_2)^2, \quad (63)$$

where the hyperspherical angles φ_2 and φ_3 are defined in Eq. (22). The integration over ρ is performed on a “scaled” grid, using the new variable $0 \leq t \leq 1$,

$$\rho \equiv \rho(t) = h \frac{\alpha_s^{n_{\rho} t} - 1}{\alpha_s - 1}. \quad (64)$$

The parameters h , α_s , and n_ρ are chosen to optimize the integration. For example, most of the calculation performed in the present work have been performed with the choice $h = 0.04$ fm, $\alpha_s = 1.05$, and $n_\rho = 96$. Note that $\rho(t = 1) \approx 90$ fm in this case.

The integration over φ_2 is performed using the variable $x = \cos 2\varphi_2$ so that

$$\int_0^{\frac{\pi}{2}} d\varphi_2 (\cos \varphi_2)^2 (\sin \varphi_2)^2 = \frac{1}{8} \int_{-1}^{+1} dx \sqrt{1-x^2}, \quad (65)$$

and the integration over x is then performed using n_x Gauss-Chebyshev points [106]. Finally, the integration over φ_3 is performed in a similar way, namely using the variable $z = \cos 2\varphi_3$,

$$\int_0^{\frac{\pi}{2}} d\varphi_3 (\cos \varphi_3)^2 (\sin \varphi_3)^5 = \frac{1}{16\sqrt{2}} \int_{-1}^{+1} dz \sqrt{1+z}(1-z)^2, \quad (66)$$

using n_z Gauss-Legendre points related to the zeros of the P_{2n_z+1} Legendre polynomial [106].

In summary, for local potentials the accuracy of the matrix elements, and consequently of the phase shifts, depends on the following parameters:

- (i) ℓ_{\max} , the maximum value of the orbital angular momentum used to truncate the expansion of Eq. (55). Values $\ell_{\max} = 5$ or 6 have been found appropriate to obtain a sufficient numerical accuracy.
- (ii) The numbers n_x , n_z , and n_μ (the latter is used to perform the projection given in Eq. (57)) of Gauss-Chebyshev and Gauss-Legendre points used to perform the integrations of Eqs. (57), (65), and (66). Typical used values are $n_z = 50$, $n_x = 30$, and $n_\mu = 16$.
- (iii) The values of the parameters h , α_s , and n_ρ used to perform the integration over the hyperradius.
- (iv) The number N_3 of three-body HH functions used to construct the trinucleon bound-state wave function $\phi_3(ijk)$ entering the asymptotic functions $\Omega_{\nu LS}^\pm$, see Eq. (3).
- (v) The number M of Laguerre polynomials used to expand the hyperradial functions $u_{\kappa\Lambda\Sigma T\mu}^{\nu LS}(\rho)$, as given in Eqs. (30) and (31). This expansion depends also on the parameter b , and therefore one has also to check the dependence of the results on this (nonlinear) parameter.

In Sec. III C, we report a study of the dependence of the calculated phase shifts on these parameters.

2. Nonlocal NN potentials

In this case Eq. (59) is calculated in a slightly different way. Now we have

$$\begin{aligned} \langle \Psi^X | V_{12} | \Psi^{X'} \rangle &= \int d^3x_1 d^3x_2 d^3x_3 d^3x'_3 (\Psi^X(x_1, x_2, x_3))^\dagger \\ &\times V(x_3, x'_3) \Psi^{X'}(x_1, x_2, x'_3). \end{aligned} \quad (67)$$

The calculation of the above integral is performed in two steps. First, the spin-isospin-angular matrix elements

$$\begin{aligned} &\int d\hat{x}_1 d\hat{x}_2 d\hat{x}_3 d\hat{x}'_3 \mathcal{Y}_\alpha(\hat{x}_1, \hat{x}_2, \hat{x}_3)^\dagger V(x_3, x'_3) \mathcal{Y}_{\alpha'}(\hat{x}_1, \hat{x}_2, \hat{x}'_3) \\ &= v_{\ell_3, S_2, \ell'_3, S'_2}^{j_3, T_3, T, T', T'}(x_3, x'_3) \delta_{j_3, j'_3} \delta_{j_2, j'_2} \delta_{j_1, j'_1} \delta_{\ell_2, \ell'_2} \delta_{\ell_1, \ell'_1}, \end{aligned} \quad (68)$$

are computed analytically, and, second, the integration over the moduli of the Jacobi vectors,

$$\begin{aligned} &\int_0^\infty dx_1 dx_2 dx_3 dx'_3 x_1^2 x_2^2 x_3^2 x_3'^2 (\mathcal{F}_\alpha^X(x_1, x_2, x_3))^* \\ &\times v_{\ell_3, S_2, \ell'_3, S'_2}^{j_3, T_3, T, T', T'}(x_3, x'_3) \mathcal{F}_{\alpha'}^{X'}(x_1, x_2, x'_3), \end{aligned} \quad (69)$$

is obtained by using Gauss quadrature methods in the following way:

$$\begin{aligned} &\int_0^\infty dx_1 dx_2 dx_3 dx'_3 x_1^2 x_2^2 x_3^2 (x'_3)^2 \\ &= \int_0^\infty d\rho_2 dx_3 dx'_3 (\rho_2)^5 x_3^2 (x'_3)^2 \\ &\times \int_0^{\frac{\pi}{2}} d\phi_2 (\cos \phi_2)^2 (\sin \phi_2)^2, \end{aligned} \quad (70)$$

where $x_2 = \rho_2 \cos \phi_2$ and $x_1 = \rho_2 \sin \phi_2$. The integration over ϕ_2 is performed as specified in Eq. (65). Moreover,

$$\begin{aligned} &\int_0^\infty d\rho_2 (\rho_2)^5 F(\rho_2) = \int_0^\infty d\rho_2 (\rho_2)^5 e^{-a_y \rho_2} e^{a_y \rho_2} F(\rho_2) \\ &= \frac{1}{(a_y)^6} \int_0^\infty dy (y^5 e^{-y}) e^y F(y/a_y), \end{aligned} \quad (71)$$

where $y = a_y \rho_2$ and a_y is a parameter. The integration over y is performed using n_y Gauss points y_i generated from the weight function $y^5 e^{-y}$. The parameter a_y is then chosen in order to achieve accurate integrals with as-small-as-possible values of n_y . Finally, the integration of x_3 (and x'_3) is performed in a similar way, namely

$$\begin{aligned} &\int_0^\infty dx_3 (x_3)^2 F(x_3) = \int_0^\infty dx_3 (x_3)^2 e^{-a_z x_3} e^{a_z x_3} F(x_3) \\ &= \frac{1}{(a_z)^3} \int_0^\infty dz (z^2 e^{-z}) e^z F(z/a_z), \end{aligned} \quad (72)$$

where $z = a_z x_3$, with a_z being a free parameter. The integration over z is performed using n_z Gauss points z_i generated from the weight function $z^2 e^{-z}$. The parameter a_z is then chosen in order to achieve accurate integrals with as-small-as-possible values of n_z .

In this case, the accuracy of the matrix elements, and consequently also of the calculated phase shifts, depends on the following parameters:

- (i) ℓ_{\max} , the maximum value of the orbital angular momentum used to truncate the expansion of Eq. (55). Values $\ell_{\max} = 5$ or 6 have been found appropriate to obtain a sufficient numerical accuracy also in this case.
- (ii) The values of the number of points used to perform the integrations, namely n_z , n_y , n_x , and n_μ [as

before, n_x is used to perform the integration over ϕ_2 as specified in Eq. (65) and n_μ is used to perform the projection given in Eq. (57)]. Typical used values are $n_z = 30$, $n_y = 50$, $n_x = 20$, and $n_\mu = 16$. The precision of the integrals depends also on the parameters a_y and a_z . Note that, once large-enough values of n_y and n_z are used, the dependence on these two parameters is negligible. Usually, we have taken $a_y = a_z = 7 \text{ fm}^{-1}$.

- (iii) The number N_3 of three-body HH functions used to construct the trinucleon bound-state wave function $\phi_3(ijk)$.
- (iv) The number M of Laguerre polynomials used to expand the hyperradial functions $w_{K\Lambda\Sigma T\mu}^{\gamma LS}(\rho)$, as given in Eqs. (30) and (31). This expansion depends also on b , and therefore one has also to check the dependence of the results on this (nonlinear) parameter.

In Sec. III C, we will report a study of the dependence of the calculated phase shifts on these parameters.

3. Matrix elements of the 3N potential

The matrix elements of a three-body potential W_{ijk} can be evaluated in a similar way. In this work, we have taken into account only local 3N potentials. Consider the matrix element of W_{123} . This operator is completely symmetric under the exchange of particles 1, 2, and 3 and depends only on the Jacobi vectors \mathbf{x}_3 and \mathbf{x}_2 . By decomposing the wave function as in Eq. (58), we have explicitly

$$\langle \Psi^X | W_{123} | \Psi^{X'} \rangle = \int d^3\mathbf{x}_1 d^3\mathbf{x}_2 d^3\mathbf{x}_3 (\Psi^X(\mathbf{x}_1, \mathbf{x}_2, \mathbf{x}_3))^\dagger \times W(\mathbf{x}_2, \mathbf{x}_3) \Psi^{X'}(\mathbf{x}_1, \mathbf{x}_2, \mathbf{x}_3), \quad (73)$$

where the dependence of $W(\mathbf{x}_2, \mathbf{x}_3)$ on spin-isospin operators is understood. The calculation of the above integral is performed in two steps. First, the spin-isospin-angular matrix elements

$$\int d\hat{\mathbf{x}}_1 d\hat{\mathbf{x}}_2 d\hat{\mathbf{x}}_3 \mathcal{Y}_\alpha(\hat{\mathbf{x}}_1, \hat{\mathbf{x}}_2, \hat{\mathbf{x}}_3)^\dagger W(\mathbf{x}_2, \mathbf{x}_3) \mathcal{Y}_{\alpha'}(\hat{\mathbf{x}}_1, \hat{\mathbf{x}}_2, \hat{\mathbf{x}}_3) = w_{\ell_3 S_2 j_3 \ell_2 j_2, \ell'_3 S'_2 j'_3 \ell'_2 j'_2}^{J_2, T_3, T, T'_3, T'}(x_2, x_3) \delta_{j_1, j'_1} \delta_{\ell_1, \ell'_1} \delta_{J_2, J'_2} \quad (74)$$

are computed mostly analytically (we are left with a one-dimensional integration with respect to $\hat{\mathbf{x}}_2 \cdot \hat{\mathbf{x}}_3$, which can be readily obtained). We have prepared a code which for given values of x_2, x_3 computes efficiently those matrix elements for all forms of 3N potentials considered so far, namely Tucson-Melbourne, Brazil, Urbana, Illinois, and chiral N2LO. The

calculation is completed by the integration over the moduli of the Jacobi vectors,

$$\int_0^\infty dx_1 dx_2 dx_3 x_1^2 x_2^2 x_3^2 (\mathcal{F}_\alpha^X(x_1, x_2, x_3))^* \times w_{\ell_3 S_2 j_3 \ell_2 j_2, \ell'_3 S'_2 j'_3 \ell'_2 j'_2}^{J_2, T_3, T, T'_3, T'}(x_2, x_3) \mathcal{F}_{\alpha'}^{X'}(x_1, x_2, x_3), \quad (75)$$

again obtained by using Gauss quadrature method, as discussed previously. In order to speed up the calculation, we have imposed the following truncation to the 3N matrix elements:

$$w_{\ell_3 S_2 j_3 \ell_2 j_2, \ell'_3 S'_2 j'_3 \ell'_2 j'_2}^{J_2, T_3, T, T'_3, T'}(x_2, x_3) = 0 \quad \text{for} \\ \ell > \ell_{\max}^{3N}, \quad J_2 > J_{\max}^{3N}, \quad K > K_{\max}^{3N}, \quad (76)$$

where ℓ can be any of ℓ_3, ℓ_2, ℓ'_3 , and ℓ'_2 . In our calculation, w has been taken to vanish when acting on HH functions (either on the right or on the left) having a grand angular quantum number $K > K_{\max}^{3N}$. This truncation can be justified since the 3N potentials under consideration are rather smooth at short interparticle distances, and the contribution of components of large ℓ, J_2 , and K has been found to be very small. This has been verified numerically increasing the values of $\ell_{\max}^{3N}, J_{\max}^{3N}$, and K_{\max}^{3N} until the calculated phase shifts were found rather insensitive to further changes. Examples of the dependence of the results on these parameters will be discussed in Sec. III D.

4. Parameterization of the S matrix

The scattering observables can be obtained directly from the S-matrix elements. In the following, we present also the results for a selected set of S-matrix elements in order to check the convergence and compare with the results of the PSA of Ref. [65] for $p + {}^3\text{He}$ scattering. Always we calculate the S-matrix elements (and the observables) via Eq. (36), namely using the ‘‘second-order’’ estimates given by the quantities $[\mathcal{S}_{LS, L'S'}^{\gamma, \gamma'}]$ (we simply call them $\mathcal{S}_{LS, L'S'}^{\gamma, \gamma'}$ from now on). Moreover, these S-matrix elements are parameterized as follows.

For $n + {}^3\text{H}$, $p + {}^3\text{He}$, and $p + {}^3\text{H}$ scattering below the $n + {}^3\text{He}$ threshold ($T_r \lesssim 0.73 \text{ MeV}$), the number of open asymptotic clusterizations is 1. Then, for $J = 0$, there is only one LS combination in the sum over $L'S'$ of Eq. (17), namely $L' = 0, S' = 0$ ($L' = 1, S' = 1$) for the even- (odd-) parity state. Consequently, for these cases the S matrix reduces to one parameter which is parameterized as usual as $\mathcal{S}_{LS, LS}^{\gamma, \gamma'} = \eta_{J\pi} \exp(2i\delta_{J\pi})$. For $J > 0$, there are always two possible LS combinations, and correspondingly the S matrix has been parameterized as [113]

$$\mathcal{S}_{LS, L'S'}^{\gamma, \gamma'} = \begin{pmatrix} \cos \epsilon_{J\pi} & -\sin \epsilon_{J\pi} \\ \sin \epsilon_{J\pi} & \cos \epsilon_{J\pi} \end{pmatrix} \begin{bmatrix} \eta_1 \exp(2i\delta_{J\pi}^1) & 0 \\ 0 & \eta_2 \exp(2i\delta_{J\pi}^2) \end{bmatrix} \begin{pmatrix} \cos \epsilon_{J\pi} & \sin \epsilon_{J\pi} \\ -\sin \epsilon_{J\pi} & \cos \epsilon_{J\pi} \end{pmatrix}. \quad (77)$$

In this case we define $\eta_{J\pi} = \sqrt{(\eta_1^2 + \eta_2^2)/2}$. As is well known, the S matrix should be unitary. However, in the application of the Kohn principle given in Eq. (36), the value $\eta_{J\pi} = 1$ is not imposed: It is achieved only when the corresponding core part

$\Psi_C^{\gamma LS}$ is well described by the HH basis. We can use the value of $\eta_{J\pi}$ as a test of the convergence of the HH expansion. In cases of poor convergence, $\eta_{J\pi}$ is found to depend very much also on the choice of $f_L(y_i)$, the function used to regularize the

Coulomb function G_L . This function depends on the nonlinear parameter β , see Eqs. (6) and (7), and thus another test of the convergence is performed by analyzing the dependence of $\eta_{J\pi}$ vs. the parameter β . At the beginning of the calculation, when the number of HH functions is not enough to get convergence, $\eta_{J\pi}$ will be extremely dependent on the value of β (the phase shifts depend less critically on β). By increasing the number of HH components in the core wave function, we observe that $\eta_{J\pi} \rightarrow 1$ and the dependence on β becomes negligible. Note that the convergence rate has been found to depend on the value of β , and there exist some critical values of this parameter where the convergence can be very slow. However, it is not difficult to find regions of values of β where the convergence is fast and smooth and the final results are independent of β . Since we are here interested in the study of the convergence of the HH function, we have chosen β in one of the “favorable” region, where the convergence is achieved in a smooth and fast way. A detailed study on this subject is reported in Sec. III A.

For $p + {}^3\text{H}$ above the $n + {}^3\text{He}$ threshold ($T_r \gtrsim 0.73$ MeV) and $n + {}^3\text{He}$ scattering, there are two open asymptotic clusterizations, $\gamma = 3, 4$. Now the dimension of the S matrix is doubled with respect to the cases discussed above. Then it is more convenient to presents the results directly in terms of the matrix elements parameterized as

$$S_{LS,L'S'}^{\gamma,\gamma'} = \eta_{LS,L'S'}^{\gamma,\gamma'} \exp[2i\delta_{LS,L'S'}^{\gamma,\gamma'}]. \quad (78)$$

The parameters $\eta_{LS,L'S'}^{\gamma,\gamma'}$ are always ≤ 1 .

E. Choice of the basis

The main difficulty of the application of the HH technique is the slow convergence of the basis with respect to the grand angular quantum number K . This problem has been overcome by dividing the HH basis in *classes*, depending on the value of $\mathcal{L} = \ell_1 + \ell_2 + \ell_3$, total spin Σ , and n_2 and n_3 . The calculation is started by including in the expansion of the wave function the HH states of the first class (class “C1”) having grand angular quantum number $K \leq K_1$ and studying the convergence of a quantity of interest (for example, the phase shifts) increasing the value of K_1 . Once a satisfactory value of $K_1 = K_{1\text{max}}$ is reached, the states of the second class (class “C2”) with $K \leq K_2$ are added in the expansion, keeping all the states of the class C1 with $K_1 \leq K_{1\text{max}}$. Then K_2 is increased until the desired convergence is achieved, and so on.

Note that in the case of $p + {}^3\text{He}$ or $n + {}^3\text{H}$ scattering, the z component of the total isospin is $|T_z| = 1$, and therefore only channels with total isospin $T = 1$ or 2 have to be included in the expansion. The contribution of the $T = 2$ channels is expected to be quite tiny, and in this paper they have been disregarded. On the other hand, for $p + {}^3\text{H}$ and $n + {}^3\text{He}$ scattering, the z component of the total isospin is $T_z = 0$, and therefore we have to include in the HH expansion channels with total isospin $T = 0, 1$, and 2 . However, also in this case we have disregarded the contribution of the $T = 2$ channels.

Let us now discuss the choice of the classes of HH states for the various J^π cases (in the following, we will use also the spectroscopic notation). For example, for $J^\pi = 1^+$, both 3S_1 and 3D_1 components can be constructed by including a

rather small number of channels, since in this case the Pauli principle does not allow for the overlaps between the 4Ns. As a consequence, the core part is rather small and does not require a large number of channels to be well described. The same happens for $L \geq 2$ waves ($J^\pi = 2^+, 3^\pm, 4^\pm$ and so on), where the centrifugal barrier prevents the two clusters to come close to each other.

On the other hand, it is well known that there is a strong attraction in P waves [114]. In fact, various R -matrix analyses have shown the presence of resonances for the $J^\pi = 0^-, 1^-,$ and 2^- waves. As a consequence, the convergence of the HH expansion in these cases is much more problematic and, correspondingly, for these cases we have organized differently the HH expansion as explained below.

Regarding the $J^\pi = 0^+$ state, we have to distinguish between $T = 0$ and $T = 1$ states. For the $T = 1$ states, the only needed for the study of $n + {}^3\text{H}$ and $p + {}^3\text{He}$ processes, the Pauli principle prevents the overlaps between identical nucleons and, consequently, the core part does not require a large number of channels to be well described. On the other hand, in the $J^\pi = 0^+$ $T = 0$ wave, needed for the study of $p + {}^3\text{H}$ and $n + {}^3\text{He}$ processes, the potential is strongly attractive and the construction of the wave function turns out to be more difficult. In fact, in this wave there is the formation of the α particle with binding energy of 28.3 MeV. Moreover, just below the threshold of $n + {}^3\text{He}$ scattering, there is the first excited state of the α particle and therefore the S matrix in vicinity of this resonance will vary very fast with the energy. As a consequence, the convergence of the HH expansion for this state will require a large number of channels.

Let us now define in detail the choice of the classes in the various cases. For the less-critical cases ($J = 1^+, 2^+, 3^\pm, 4^\pm$, and so on), we have organized the HH expansion simply grouping the HH functions in classes depending on the value of $\mathcal{L} = \ell_1 + \ell_2 + \ell_3$. For example, for $J^\pi = 1^+$, the first class includes all HH functions with $\mathcal{L} = 0$, the second one all HH functions with $\mathcal{L} = 2$, and so on. So class C1 is composed of 3 $T = 0$ channels and 4 $T = 1$ channels with $\mathcal{L} = 0$, class C2 by 51 $T = 0$ channels and 76 $T = 1$ channels with $\mathcal{L} = 2$, class C3 by 159 $T = 0$ channels and 239 $T = 1$ channels with $\mathcal{L} = 4$, and so on. Clearly, in the study of $n + {}^3\text{H}$ and $p + {}^3\text{He}$ scattering, we need only to include the channels with $T = 1$. As will be shown below, the third class gives already a tiny contribution to the S matrix. A similar procedure has been used for the other “easy” waves $J^\pi = 2^+, 3^\pm$, and so on, and also for the $J^\pi = 0^+$ $T = 1$ wave in case of the study of $n + {}^3\text{H}$ and $p + {}^3\text{He}$ scattering. Clearly, for negative-parity states, class C1 includes all HH functions with $\mathcal{L} = 1$, class C2 all HH functions with $\mathcal{L} = 3$, and so on. For these cases, in general, the convergence is achieved, also with a strong repulsive potential like the AV18, with fairly small values of grand angular quantum number K ($K \lesssim 30$).

Regarding the expansion of the $J^\pi = 0^+$ state for $p + {}^3\text{H}$ and $n + {}^3\text{He}$ scattering, we have already discussed how the construction of the $T = 0$ component of the wave function is more critical. In this case, we need to include in the expansion HH functions with K up to 60 or more. We have followed the same subdivision adopted for the study of the ground state

TABLE I. Quantum numbers of the first channels considered in the expansion of the wave function of the 0^+ state. See the text for details.

α	ℓ_1	ℓ_2	ℓ_3	L_2	Λ	S_a	S_b	Σ	T_a	T_b	T
1	0	0	0	0	0	1	1/2	0	0	1/2	0
2	0	0	0	0	0	0	1/2	0	1	1/2	0
3	0	0	2	0	2	1	3/2	2	0	1/2	0

of the α particle [6]. First, we have seen that a very slow convergence is observed for the particular sets of HH functions which incorporate “two-body” correlations. It is therefore appropriate to group these HH functions in the first class and treat them with particular attention. In practice, in the first class we include the HH states with $n_2 = 0$ belonging to the channels listed in Table I. Note that the corresponding radial part of the HH functions depends only on $\cos \phi_{3p} = r_{ij}/\rho$ and thus these states take into account two-body correlations [see Eq. (23)]. This is the part of the wave function more difficult to construct due to the strong repulsions between the particles at short distances. In the second class, we have included the HH functions belonging to the channels listed in Table I but with $n_2 > 0$. These HH functions depend on $\cos \phi_{2p}$, which is proportional to the distance of particle k from the center of mass of the pair ij . Therefore, these states start to take into account three-body correlations. For the other classes, we have followed the procedure to group them depending on the values of \mathcal{L} and T . In practice, class C3 includes the (remaining) channels with $T = 0$ and $\mathcal{L} = 2$ and class C4 includes all $T = 1$ channels with $\mathcal{L} \leq 2$. Then class C5 (C6) includes both $T = 0$ and $T = 1$ channels with $\mathcal{L} = 4$ ($\mathcal{L} = 6$), and so on.

Let us consider now the $J^\pi = 0^-, 1^-,$ and 2^- waves. Note that, since the waves under consideration are of negative parity, only HH functions with odd values of $\mathcal{L} = \ell_1 + \ell_2 + \ell_3$ (and K) have to be considered. Also in these cases it is necessary to consider first the states that describe “two-body” correlations and group them in the first class. The second class will contain HH functions describing three-body correlations, and then we start to group them depending on the values of \mathcal{L} . However, for these states, we have observed a quite different rate of convergence with respect to the inclusion of HH functions belonging to channels with a given total spin Σ . In particular, the channels with $\Sigma = 1$ give a very important contribution to the structure of the scattering state for these values of J^π . On the contrary the channels with $\Sigma = 0$ and $\Sigma = 2$ are less important. The final choice of the classes for the cases $J^\pi = 0^-, 1^-,$ and 2^- is detailed below.

- (i) Class C1. In this class are included the HH states with $n_2 = 0$ belonging to the channels of Tables II–IV for the waves with $J^\pi = 0^-, 1^-,$ and 2^- , respectively, for both $T = 0$ and $T = 1$. As discussed above, these states take into account two-body correlations.
- (ii) Class C2. This class includes HH functions belonging (i) to the same channels as for class C1 but with $n_2 > 0$ and (ii) to the rest of channels with $\ell_1 + \ell_2 + \ell_3 = 1$.

TABLE II. Quantum numbers of the first channels considered in the expansion of the wave function of the 0^- state. See the text for details.

α	ℓ_1	ℓ_2	ℓ_3	L_2	Λ	S_a	S_b	Σ	T_a	T_b	T
1	1	0	0	1	1	1	1/2	1	0	1/2	0
2	1	0	0	1	1	1	3/2	1	0	1/2	0
3	1	0	0	1	1	0	1/2	1	1	1/2	0
4	1	0	2	1	1	1	1/2	1	0	1/2	0
5	1	0	2	1	1	1	3/2	1	0	1/2	0
6	1	0	2	1	1	0	1/2	1	1	1/2	0
1	1	0	0	1	1	1	1/2	1	0	1/2	1
2	1	0	0	1	1	1	3/2	1	0	1/2	1
3	1	0	0	1	1	0	1/2	1	1	1/2	1
4	1	0	0	1	1	0	1/2	1	1	3/2	1
5	1	0	2	1	1	1	1/2	1	0	1/2	1
6	1	0	2	1	1	1	3/2	1	0	1/2	1
7	1	0	2	1	1	0	1/2	1	1	1/2	1
8	1	0	2	1	1	0	1/2	1	1	3/2	1

The HH functions of type (i) take into account the three-body correlations.

- (iii) Class C3. This class includes the HH functions belonging to the remaining channels with $\ell_1 + \ell_2 + \ell_3 = 3$ and $\Sigma = 1$.

TABLE III. Quantum numbers of the first channels considered in the expansion of the wave function of the 1^- state. See the text for details.

α	ℓ_1	ℓ_2	ℓ_3	L_2	Λ	S_a	S_b	Σ	T_a	T_b	T
1	1	0	0	1	1	1	1/2	0	0	1/2	0
2	1	0	0	1	1	0	1/2	0	1	1/2	0
3	1	0	0	1	1	1	1/2	1	0	1/2	0
4	1	0	0	1	1	1	3/2	1	0	1/2	0
5	1	0	0	1	1	0	1/2	1	1	1/2	0
6	1	0	2	1	1	1	1/2	0	0	1/2	0
7	1	0	2	1	1	0	1/2	0	1	1/2	0
8	1	0	2	1	1	1	1/2	1	0	1/2	0
9	1	0	2	1	2	1	1/2	1	0	1/2	0
10	1	0	2	1	1	1	3/2	1	0	1/2	0
11	1	0	2	1	2	1	3/2	1	0	1/2	0
1	1	0	0	1	1	1	1/2	0	0	1/2	1
2	1	0	0	1	1	0	1/2	0	1	1/2	1
3	1	0	0	1	1	0	1/2	0	1	3/2	1
4	1	0	0	1	1	1	1/2	1	0	1/2	1
5	1	0	0	1	1	1	3/2	1	0	1/2	1
6	1	0	0	1	1	0	1/2	1	1	1/2	1
7	1	0	0	1	1	0	1/2	1	1	3/2	1
8	1	0	2	1	1	1	1/2	0	0	1/2	1
9	1	0	2	1	1	0	1/2	0	1	1/2	1
10	1	0	2	1	1	0	1/2	0	1	3/2	1
11	1	0	2	1	1	1	1/2	1	0	1/2	1
12	1	0	2	1	2	1	1/2	1	0	1/2	1
13	1	0	2	1	1	1	3/2	1	0	1/2	1
14	1	0	2	1	2	1	3/2	1	0	1/2	1

TABLE IV. Quantum numbers of the first channels considered in the expansion of the wave function of the 2^- state. See the text for details.

α	ℓ_1	ℓ_2	ℓ_3	L_2	Λ	S_a	S_b	Σ	T_a	T_b	T
1	1	0	0	1	1	1	1/2	1	0	1/2	0
2	1	0	0	1	1	1	3/2	1	0	1/2	0
3	1	0	0	1	1	0	1/2	1	1	1/2	0
4	1	0	2	1	1	1	1/2	1	0	1/2	0
5	1	0	2	1	2	1	1/2	1	0	1/2	0
6	1	0	2	1	3	1	1/2	1	0	1/2	0
7	1	0	2	1	1	1	3/2	1	0	1/2	0
8	1	0	2	1	2	1	3/2	1	0	1/2	0
9	1	0	2	1	3	1	3/2	1	0	1/2	0
1	1	0	0	1	1	1	1/2	1	0	1/2	1
2	1	0	0	1	1	1	3/2	1	0	1/2	1
3	1	0	0	1	1	0	1/2	1	1	1/2	1
4	1	0	0	1	1	0	1/2	1	1	3/2	1
5	1	0	2	1	1	1	1/2	1	0	1/2	1
6	1	0	2	1	2	1	1/2	1	0	1/2	1
7	1	0	2	1	3	1	1/2	1	0	1/2	1
8	1	0	2	1	1	1	3/2	1	0	1/2	1
9	1	0	2	1	2	1	3/2	1	0	1/2	1
10	1	0	2	1	3	1	3/2	1	0	1/2	1

- (iv) Class C4. This class includes the HH functions belonging to the channels with $\ell_1 + \ell_2 + \ell_3 = 3$ and $\Sigma = 0$ and 2.
- (v) Class C5. This class includes the HH functions belonging to the channels with $\ell_1 + \ell_2 + \ell_3 = 5$.

We remark again that the classification related to the total spin is important since we have observed that the component with $\Sigma = 1$ requires more states to be well accounted for, while the $\Sigma = 2$ and $\Sigma = 0$ components give only a tiny contribution to the phase shift (however, they are important for achieving $\eta_{J^\pi} = 1$). Some examples of convergence for the phase shifts, mixing angles, and “elasticity parameter” η_{J^π} will be given in the next section.

III. CONVERGENCE AND NUMERICAL STABILITY

In this section, an analysis of the convergence and numerical stability of the results will be discussed.

A. Study of the convergence for $n + {}^3\text{H}$ and $p + {}^3\text{He}$ scattering

Let us first concentrate on $n + {}^3\text{H}$ and $p + {}^3\text{He}$ scattering. At the energies considered here only one asymptotic state is open, and the S matrix can be conveniently decomposed in terms of a single phase shift (for the $J^\pi = 0^\pm$ waves) or in terms of two phase shifts and one mixing parameter, as discussed in Sec. IID 4. We recall that for these processes we need to include only $T = 1$ channels in the HH expansion.

Here we have considered the AV18 and N3LO500 potential models. Both potentials represent the NN interaction in its full richness, with short-range repulsion, tensor, and other non-central components and charge symmetry-breaking terms, and both reproduce the NN scattering data with a χ^2/datum very

close to 1. The main difference is that the AV18 interaction is local and has a strong repulsive part at short interparticle distances, while the N3LO500 potential is nonlocal and has a somewhat less repulsive core. In both cases, the electromagnetic interaction has been limited to just the point-Coulomb potential. Moreover, we have taken $1/M_N = 41.47108 \text{ MeV fm}^2$ with the AV18 potential and $1/M_N = 41.47 \text{ MeV fm}^2$ with the N3LO500 potential. The function G_L has been regularized with method 1 corresponding to two values of β as reported in the tables.

Since the convergence is similar for both $n + {}^3\text{H}$ and $p + {}^3\text{He}$ phase shifts, we will concentrate on the charged case, where the presence of the long-range Coulomb potential can complicate the calculation. Moreover, the convergence has been found to be slower as the proton energy $E_p = (4/3)T_r$ increases, so the tests have been performed for $E_p = 5.54 \text{ MeV}$, the larger $p + {}^3\text{He}$ energy considered in this paper. In this subsection, the matrix elements have been computed using $\ell_{\text{max}} = 5$, $n_z = 30$, $n_y = 50$, $n_x = 20$, and $n_\mu = 16$. We have in all cases used $M = 16$ and $b = 4.0 \text{ fm}^{-1}$ in the expansion of the hyperradial functions $u_{K\Lambda\Sigma T\mu}^{\gamma LS}(\rho)$.

Let us discuss first the convergence for the “easy” cases, namely for $J^\pi = 0^+, 1^+, 2^+, 3^\pm$ and so on. As an example, we consider here only the $J^\pi = 0^+$ case. As discussed previously, for $n + {}^3\text{H}$ and $p + {}^3\text{He}$ scattering we have only one possible clusterization and for $J^\pi = 0^+$, $L, S = 0, 0$, the S matrix is one-dimensional, parameterized as $\eta_{0^+} \exp[2i\delta(^1S_0)]$. The results obtained for the $p + {}^3\text{He}$ η_{0^+} and $\delta(^1S_0)$ at $E_p = 5.54 \text{ MeV}$ (corresponding to $T_r = 4.15 \text{ MeV}$) are reported in Table V. As can be seen from the table, the convergence is similar for both potentials, since in this wave the interaction between p and ${}^3\text{He}$ clusters is dominated by the Pauli repulsion. The differences between the phase shifts obtained by the two potentials are related to the different ${}^3\text{He}$ binding energy (and radius). Including an appropriate 3N interaction, the phase shifts calculated with the different models becomes quite close to each other. The inclusion of the first class (channels with $\mathcal{L} = 0$) already produces a very good estimate for the phase shift. The inclusion of the second class (channels with $\mathcal{L} = 2$) decreases the phases shift by about 0.3° (0.7°) for the N3LO500 (AV18) case. Finally, the inclusion of the third class (channels with $\mathcal{L} = 4$) produces only tiny changes in the result, showing the rapid convergence with respect to \mathcal{L} .

From the table, we can also observe the dependence of η and δ with respect to the chosen value of β . As it can be seen, δ practically does not depend on β . On the contrary, the inelasticity parameter is quite sensitive to β when the number of HH functions included in the expansion is small. However, including the second class with HH states up to $K_2 \approx 28$, the dependence on β is noticeably reduced and $\eta \rightarrow 1$. Note that the inclusion of the third class has only a tiny effect on η . For N3LO500, including the three classes, η becomes 1 with nearly five digits. For AV18, although the phase shift has reached a good convergence, η is slightly different from unity. It appears necessary in this case to include more states of the first and second classes to reach an accuracy similar to the N3LO500 case. An analogous behavior is observed using method 2 of regularization, and for the other “easy” states $1^+, 2^+, 3^\pm$, and so on.

TABLE V. Convergence of the $J^\pi = 0^+$ $p + {}^3\text{He}$ inelasticity parameter η_{0+} and phase shift $\delta({}^1S_0)$ ($^\circ$) at $E_p = 5.54$ MeV corresponding to the inclusion in the core part of the wave function of three different classes in which the HH basis has been subdivided. See the main text for more details. The N3LO500 and AV18 potentials are considered here with the inclusion of the point-Coulomb interaction. The function G_L has been regularized with method 1, using the two values of β .

K_1	K_2	K_3	$\beta = 0.80 \text{ fm}^{-1}$		$\beta = 0.90 \text{ fm}^{-1}$	
			η_{0+}	$\delta({}^1S_0)$	η_{0+}	$\delta({}^1S_0)$
N3LO500						
32			1.00495	-68.914	1.00027	-68.909
36			1.00501	-68.911	1.00029	-68.906
40			1.00505	-68.909	1.00029	-68.904
44			1.00507	-68.909	1.00030	-68.903
44	16		1.00025	-68.581	1.00055	-68.568
44	20		1.00005	-68.564	1.00026	-68.558
44	24		1.00001	-68.557	1.00009	-68.553
44	28		1.00000	-68.555	1.00002	-68.549
44	28	10	1.00000	-68.547	1.00002	-68.544
44	28	12	1.00000	-68.545	1.00002	-68.540
44	28	14	1.00000	-68.544	1.00001	-68.538
AV18						
32			1.00229	-70.041	1.00415	-70.511
36			1.00219	-70.018	1.00421	-70.488
40			1.00212	-70.001	1.00429	-70.472
44			1.00207	-69.989	1.00436	-70.459
44	16		1.00251	-69.318	1.00093	-69.318
44	20		1.00199	-69.280	1.00083	-69.271
44	24		1.00151	-69.254	1.00076	-69.246
44	28		1.00113	-69.236	1.00070	-69.231
44	28	10	1.00114	-69.224	1.00068	-69.217
44	28	12	1.00114	-69.216	1.00067	-69.206
44	28	14	1.00114	-69.210	1.00065	-69.198

Let us now concentrate on the “difficult” cases, namely on the waves $J^\pi = 0^-$, 1^- , and 2^- . As an example, let us show the results for the state $J^\pi = 1^-$. In this case we can have $L, S = 1, 0$ and $1, 1$ and the S matrix has been decomposed as in Eq. (77), in terms of the parameters $\delta({}^1P_1)$, $\delta({}^3P_1)$, ϵ_{1-} and two inelasticity parameters η_{1P_1} and η_{3P_1} . The convergence for the various quantities obtained using the N3LO500 potential is reported in Table VI, where, for the sake of simplicity, we have reported only the combination $\eta_{1-} = \sqrt{[(\eta_{1P_1})^2 + (\eta_{3P_1})^2]}/2$. First, we notice the different rate of convergence for the two phase shifts, $\delta({}^1P_1)$ and $\delta({}^3P_1)$ (this is true also for the AV18 potential). For both potentials, the convergence of the class C1 is rather slow and a fairly large values of K_1 have to be used. The inclusion of the second and third classes increases $\delta({}^1P_1)$ by about 1.5° . The increase of $\delta({}^3P_1)$ is more sizable, almost 6° , and also the effect on ϵ_{1-} is noticeable. Including the states with $\Sigma = 0$ and 2 , first appearing when the class C4 is considered, has the same effect on both $\delta({}^1P_1)$ and $\delta({}^3P_1)$, about 1° , and its contribution is very important to obtain $\eta_{1-} \rightarrow 1$. The contribution of class C5 (including the channels with $\mathcal{L} = 5$) is very small, and

TABLE VI. Convergence of $1^- p + {}^3\text{He}$ inelasticity parameter η_{1-} , phase shifts $\delta({}^1P_1)$ and $\delta({}^3P_1)$ ($^\circ$), and mixing angle ϵ_{1-} ($^\circ$) at $E_p = 5.54$ MeV corresponding to the inclusion in the core part of the wave function of the different classes C1–C5 in which the HH basis has been subdivided. The N3LO500 is considered here with the inclusion of the point-Coulomb interaction. The function G_L has been regularized with method 1, using $\beta = 0.70 \text{ fm}^{-1}$. In the last row, the results with $\beta = 0.80 \text{ fm}^{-1}$ are also given.

K_1	K_2	K_3	K_4	K_5	η_{1-}	$\delta({}^1P_1)$	$\delta({}^3P_1)$	ϵ_{1-}
29					1.00502	20.506	37.192	11.130
33					1.00502	20.516	37.243	11.102
37					1.00502	20.520	37.268	11.088
41					1.00502	20.522	37.279	11.081
41	19				1.00525	21.774	42.115	10.104
41	23				1.00534	21.799	42.173	10.090
41	27				1.00541	21.814	42.201	10.083
41	31				1.00548	21.824	42.213	10.080
41	31	17			1.00541	21.886	42.848	9.824
41	31	21			1.00541	21.888	42.906	9.800
41	31	25			1.00541	21.889	42.936	9.787
41	31	25	13		1.00075	22.755	43.859	9.393
41	31	25	17		1.00035	22.843	43.917	9.393
41	31	25	21		1.00023	22.883	43.928	9.399
41	31	25	21	11	1.00026	22.884	43.929	9.396
41	31	25	21	13	1.00026	22.898	43.939	9.392
41	31	25	21	15	1.00026	22.902	43.945	9.388
$\beta = 0.80 \text{ fm}^{-1}$								
41	31	25	21	15	1.00006	22.887	43.951	9.378

therefore we expect that the contribution of the remaining HH states having $\mathcal{L} > 5$ be negligible.

The convergence of the $J^\pi = 0^-$ and 2^- waves is similar to that observed for the $J^\pi = 1^-$ wave. In particular, the convergence of the 3P_0 (3P_2) phase shift follows a similar pattern as the 1P_1 (3P_1) phase shift. The convergence with the AV18 potential of all these parameters is slower, see below.

In order to obtain a quantitative estimate of the “missing” phase shift due to the truncation of the HH expansion of the various classes, let us introduce $\delta(K_1, K_2, \dots)$ as the phase shift obtained by including in the expansion all the HH states of the class C1 with $K \leq K_1$, all the HH states of the class C2 having $K \leq K_2$, and so on. Let us then consider $\bar{K}_1, \bar{K}_2, \dots$ a given convenient choice of the grand angular quantum number K_i for each class i and define

$$\Delta_n(\bar{K}_1, \bar{K}_2, \dots) = \delta(\bar{K}_1 + 2n, \bar{K}_2 + 2n, \dots) - \delta(\bar{K}_1 + 2n - 2, \bar{K}_2 + 2n - 2, \dots). \quad (79)$$

Namely Δ_n is the difference of the phase shift computed by increasing each K_i by two units. The values of $\Delta_n(\bar{K}_1, \bar{K}_2, \dots)$ obtained for the N3LO500 and AV18 potentials and for the 1S_0 , 3S_1 , 3P_0 , 1P_1 , 3P_1 , and 3P_2 phase shifts are shown in Fig. 1.

Some explicit values of calculated $\delta(K_1, K_2, K_3, \dots)$ are reported in Tables VII and VIII. In Table VII, we report the $p + {}^3\text{He}$ phase shifts calculated using the N3LO500 potential at $E_p = 5.54$ MeV, and also at lower energy $E_p = 2.25$ MeV,

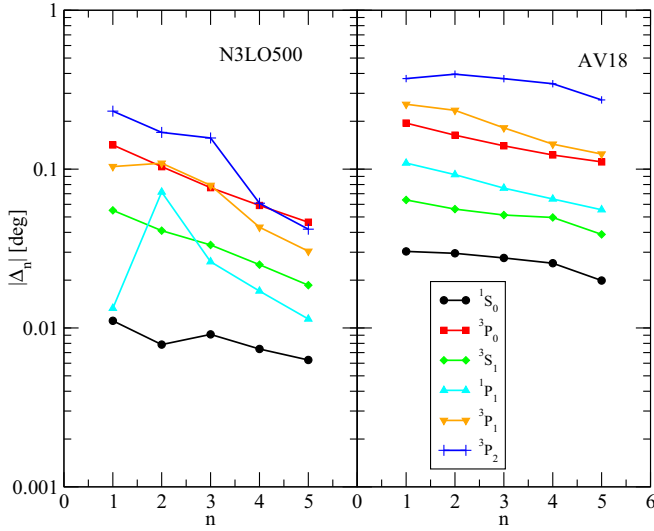


FIG. 1. The values of $|\Delta_n(\bar{K}_1, \bar{K}_2, \dots)|$ obtained for the N3LO500 (left panel) and AV18 (right panel) potentials and the 1S_0 , 3S_1 , 3P_0 , 1P_1 , 3P_1 , and 3P_2 phase shifts. The quantity n is defined in Eq. (79), i.e., $2n$ is the increase of the grand angular quantum number for each class starting from a given set $\bar{K}_1, \bar{K}_2, \dots$. See the main text for more details.

for the “simple” state 1S_0 , while the corresponding phase shifts for the “difficult” states 1P_1 and 3P_1 are reported in Table VIII. The values of the quantities K_i reported in the rows corresponding to the value “ $n = 0$ ” are just the \bar{K}_i selected in these cases. By inspecting these tables and Fig. 1, it is possible to observe in some cases an increase of $|\Delta_n|$. This is due to the following fact. Since many HH states are linearly dependent and have to be excluded from the expansion, sometimes states describing important configurations appear only for some $K \geq K_{\min}$. When the K_i ’s are increased and reach the value K_{\min} , such configurations start to be included in the expansion, and the corresponding phase shift has an abrupt change. For larger values of K_i , all important configurations are already included and the values of Δ_n vary smoothly. In particular, as

it can be seen for $n \geq 3$, the differences Δ_n start to decrease approximately linearly in a logarithmic scale. Therefore we can extrapolate the behavior $\Delta_n \propto x^n$, with $x \leq 1$. From this simple behavior, we can readily estimate the missing phase shift due to the truncation of the expansion to finite values of n . Suppose we have calculated $\delta(\bar{K}_1 + 2n, \bar{K}_2 + 2n, \dots)$ up to a given n_{\max} ; then $\Delta_{n_{\max}+1} = x\Delta_{n_{\max}}$, and so on. Then the missing phase shift can be estimated as

$$\begin{aligned} \Delta_M &= \sum_{n=n_{\max}+1}^{\infty} \Delta_n = x\Delta_{n_{\max}} + x^2\Delta_{n_{\max}} + \dots \\ &= \frac{x}{1-x} \Delta_{n_{\max}}. \end{aligned} \quad (80)$$

Typical values for x are ≈ 0.8 . The calculated missing phase shifts with Eq. (80) are reported in Tables VII and VIII in the rows labeled “ Δ_M ,” while in the rows denoted “EXT” we list the extrapolated phase shifts computed as

$$\delta_{\text{EXT}} = \delta(\bar{K}_1 + 2n_{\max}, \bar{K}_2 + 2n_{\max}, \dots) + \Delta_M. \quad (81)$$

As it can be seen from Table VII, the values of Δ_M are estimated to be rather small in all cases. For the “difficult” cases reported in Table VIII, the convergence seems to be under control for N3LO500. On the contrary, for AV18 and specifically at the largest energy, the values of Δ_M are estimated to be sizable. In this case, higher values of K_1/K_5 should be employed. We can see that the missing phase shift is less than 2%. In any case, the extrapolation procedure affects mainly the third digit of the phase shifts, and this has no practical consequences for the $p + {}^3\text{He}$ observables.

The extrapolation of other phase shifts is performed analogously. Therefore, we can conclude saying that the convergence for the N3LO500 potential is usually good. In this case, the extrapolation factor $x \approx 0.8$. The same is found with all other interactions derived within chiral EFT. On the other hand, for the AV18 potential the convergence is usually a bit slower. For this case, usually an extrapolation factor $x \approx 0.85$ is found to be more appropriate.

TABLE VII. Convergence of 1S_0 $p + {}^3\text{He}$ phase shift ($^\circ$) at $E_p = 2.25$ and 5.54 MeV corresponding to the inclusion in the core part of the wave function of the different subsets of HH basis. The N3LO500 and AV18 potentials are considered here with the inclusion of the point-Coulomb interaction. The corresponding values of the missing phase shifts, as calculated with Eq. (80), are given by the quantity Δ_M . In the rows labeled “EXT,” the extrapolated phase shifts computed as described in text have been reported (in all cases $x \approx 0.8$).

n	K_1	K_2	K_3	$E_p = 2.25$ MeV		$E_p = 5.54$ MeV	
				N3LO500	AV18	N3LO500	AV18
0	34	18	4	-41.259	-41.792	-68.580	-69.308
1	36	20	6	-41.255	-41.767	-68.572	-69.278
2	38	22	8	-41.251	-41.744	-68.563	-69.248
3	40	24	10	-41.248	-41.722	-68.555	-69.220
4	42	26	12	-41.245	-41.703	-68.549	-69.195
5	44	28	14	-41.243	-41.687	-68.544	-69.175
		Δ_M		-0.009	-0.064	-0.021	-0.080
		EXT		-41.234	-41.623	-68.523	-69.095
		x		0.8	0.8	0.8	0.8

TABLE VIII. The same as in Table VII but for the 1P_1 and 3P_1 phase shifts.

n	K_1	K_2	K_3	K_4	K_5	$\delta(^1P_1) (^\circ)$		$\delta(^3P_1) (^\circ)$	
						2.25 MeV	5.54 MeV	2.25 MeV	5.54 MeV
N3LO500									
0	31	21	15	13	5	10.301	22.771	16.800	43.609
1	33	23	17	15	7	10.306	22.785	16.843	43.713
2	35	25	19	17	9	10.334	22.857	16.891	43.823
3	37	27	21	19	11	10.343	22.884	16.925	43.903
4	39	29	23	21	13	10.350	22.901	16.944	43.947
5	41	31	25	23	15	10.354	22.913	16.958	43.979
			Δ_M			0.016	0.048	0.055	0.124
			EXT			10.370	22.961	17.013	44.103
			x			0.8	0.8	0.8	0.8
AV18									
0	51	25	21	15	1	9.965	22.070	15.721	40.871
1	53	27	23	17	3	9.999	22.179	15.809	41.127
2	55	29	25	19	5	10.029	22.272	15.882	41.362
3	57	31	27	21	7	10.055	22.347	15.945	41.544
4	59	33	29	23	9	10.077	22.412	15.998	41.687
5	61	35	31	25	11	10.098	22.468	16.055	41.812
			Δ_M			0.119	0.417	0.323	0.708
			EXT			10.206	22.785	16.378	42.520
			x			0.85	0.85	0.85	0.85

Finally, we mention that the convergence rate when including any type of 3N interactions has been found similar to the cases when only the NN interaction is considered. In fact, in general the 3N interactions are rather soft at short interparticle distances, and therefore the convergence rate of the various classes does not change appreciably.

B. Convergence for $p + ^3\text{H}$ and $n + ^3\text{He}$ scattering

Let us now consider the convergence of the HH expansion for $p + ^3\text{H}$ and $n + ^3\text{He}$ scattering. Now channels with $T = 0$ and 1 have to be included in the expansion of the core part. In general, we have observed similar convergence patterns as already discussed, except for the $J^\pi = 0^+$ state. In fact, it is well known that ^4He has a narrow resonance in the $J^\pi = 0^+$, $T = 0$ wave just above the $p + ^3\text{H}$ threshold. Therefore, this wave has to be considered a “difficult” case, as the description of the core part requires the inclusion of a large number of HH states, those necessary to describe the $J^\pi = 0^+$ resonance. In fact, for this case, the classes have been organized in a slightly different method as discussed in Sec. II E.

Here we discuss only the convergence for the $J^\pi = 0^+$ wave. For other J^π waves, the convergence has a similar behavior as discussed in the previous subsection. Clearly, for $p + ^3\text{H}$ scattering below the $n + ^3\text{He}$ threshold ($T_r \lesssim 0.73$ MeV) there is only one open asymptotic clusterization and the S matrix is one dimensional. Above that threshold, and for $n + ^3\text{He}$ scattering, there are two open asymptotic clusterizations. For the $J = 0^+$ wave, we have again $LS = 00$. The S matrix is parameterized as in Eq. (78) $S_{00,00}^{\gamma,\gamma'} = \eta_{00,00}^{\gamma,\gamma'} \exp(2i\delta_{00,00}^{\gamma,\gamma'})$ and we recall that $\gamma = 3$ (4) corresponds

to the $p + ^3\text{H}$ ($n + ^3\text{He}$) clusterization. The results obtained for $\eta_{00,00}^{3,3}$ and $\delta_{00,00}^{3,3}$ at $E_p = 0.60$ MeV (corresponding to $T_r = 0.45$ MeV) and $E_p = 2.0$ MeV (corresponding to $T_r = 1.50$ MeV) are reported in Table IX.

From the table, we can observe the large effect of class 2 (the triplet basis). We observe also that for $E_p = 0.60$ MeV, the inclusion of the fourth class (states with isospin $T = 1$) has a large effect, in particular on the parameter $\eta_{00,00}^{3,3}$. Only after including this class does this parameter starts to approach the value 1. At $E_p = 2.0$ MeV, the effect of the fourth class is less important. The inclusion of the fifth class, including both $T = 0$ and 1 HH states with $\ell_{\max} = 4$ is still important, while the inclusion of HH states with $\ell_{\max} = 6$ (sixth class) is much less sizable.

Also for this case we can apply the extrapolation procedure discussed previously and the results are reported in Table X. We note that, also for the N3LO500 potential, the convergence is not well achieved and the values of Δ_M are sizable, in particular at $E_p = 0.60$ MeV, close to the energy of the first excited state of ^4He . Note that at this energy, the $n + ^3\text{He}$ channel is closed and therefore one should find $\eta_{00,00}^{3,3} = 1$. At $E_p = 2.0$ MeV, the convergence is less problematic and we estimate $(\eta_{00,00}^{3,3})^2 \approx 0.06$. This means that at this energy the elastic process $p + ^3\text{H} \rightarrow p + ^3\text{H}$ will have a 6% probability.

For the present case, the uncertainties connected to the extrapolation formula given in Eq. (80) are more significant, especially below the $n + ^3\text{He}$ threshold. Assuming to have an uncertainty $\Delta x \approx 0.04$ for the factor x (a rather conservative estimate), the corresponding “error” in Δ_M is given by $\frac{\Delta x}{(1-x)^2} |\Delta_{n_{\max}}| \approx |\Delta_{n_{\max}}|$ assuming $x \approx 0.8$. For example, for

TABLE IX. Convergence of $0^+ p + {}^3\text{H}$ parameters $\eta_{00,00}^{3,3}$ and $\delta_{00,00}^{3,3}$ ($^\circ$) defined in Eq. (78) at $E_p = 0.60$ and 2.0 MeV corresponding to the inclusion in the core part of the wave function of the different classes C1–C6 in which the HH basis has been subdivided. The N3LO500 potential is considered here with the inclusion of the point-Coulomb interaction. The function G_L has been regularized with method 1, using $\beta = 0.80 \text{ fm}^{-1}$.

K_1	K_2	K_3	K_4	K_5	K_6	$E_p = 0.60 \text{ MeV}$		$E_p = 2.0 \text{ MeV}$	
						$\eta_{00,00}^{3,3}$	$\delta_{00,00}^{3,3}$	$\eta_{00,00}^{3,3}$	$\delta_{00,00}^{3,3}$
38						1.0588	2.89	0.3549	9.20
42						1.0595	2.94	0.3553	9.27
46						1.0598	2.97	0.3556	9.30
50						1.0599	2.98	0.3556	9.32
50	40					1.2895	14.26	0.1209	36.86
50	42					1.3074	14.71	0.1204	36.73
50	44					1.3239	15.11	0.1199	36.61
50	46					1.3384	15.44	0.1194	36.51
50	46	32				1.7115	26.90	0.2102	77.89
50	46	34				1.7240	27.09	0.2104	77.91
50	46	36				1.7325	27.21	0.2105	77.93
50	46	36	40			1.0117	44.84	0.2002	75.99
50	46	36	42			1.0060	45.61	0.2002	75.99
50	46	36	44			1.0025	46.30	0.2002	75.98
50	46	36	44	18		1.0030	51.79	0.2325	80.23
50	46	36	44	20		1.0032	51.89	0.2351	80.47
50	46	36	44	22		1.0016	52.08	0.2354	80.50
50	46	36	44	22	14	1.0011	52.08	0.2354	80.56
50	46	36	44	22	16	1.0010	52.16	0.2360	80.64

$E_p = 0.60 \text{ MeV}$, we obtain $\delta_{00,00}^{3,3}(\text{EXT}) = 57.60 \pm 1.35^\circ$, approximately a 2% uncertainty. This uncertainty will not spoil the comparison with the experimental data, since the latter quantities are known with larger error bars.

Again, the convergence for other chiral interactions with or without the inclusion of the 3N forces are similar. Regarding the AV18 potential, the convergence of the 0^+ , $T = 0$ phase shift would require the inclusion of HH functions with larger K values. We have not pursued such a calculation any longer in the present study.

C. Numerical stability

In this subsection, we want to discuss the dependence of the results on the grids used for the calculation of the matrix elements, the number of three-body HH functions used to construct $\phi_3(i, j, k)$, and on the parameters M and b entering the expansion of the hyperradial functions [see Eq. (31)]. We limit ourselves only to consider the calculation of the 1S_0 , 3S_1 , 3P_0 , 1P_1 , 3P_1 , and 3P_2 $p + {}^3\text{He}$ phase shifts at $E_p = 5.54 \text{ MeV}$ with the N3LO500 potential. Similar results were obtained for all the other cases considered in this paper.

TABLE X. Convergence of the parameters $\eta_{00,00}^{3,3}$ and $\delta_{00,00}^{3,3}$ ($^\circ$) at $E_p = 0.60$ and 2.00 MeV corresponding to the inclusion in the core part of the wave function of the different classes of HH basis. The N3LO500 potential is considered here with the inclusion of the point-Coulomb interaction. The corresponding values of the missing phase shifts, as calculated with Eq. (80), are given by Δ_M . In the rows labeled “EXT”, the extrapolated phase shifts computed as described in text have been reported (in all cases $x \approx 0.8$).

n	K_1	K_2	K_3	K_4	K_5	K_6	$E_p = 0.60 \text{ MeV}$		$E_p = 2.0 \text{ MeV}$	
							$\eta_{00,00}^{3,3}$	$\delta_{00,00}^{3,3}$	$\eta_{00,00}^{3,3}$	$\delta_{00,00}^{3,3}$
0	40	36	26	34	12	6	1.0068	40.90	0.2156	78.11
1	42	38	28	36	14	8	1.0054	44.06	0.2219	78.93
2	44	40	30	38	16	10	1.0040	46.78	0.2269	79.56
3	46	42	32	40	18	12	1.0028	49.03	0.2309	80.03
4	48	44	34	42	20	14	1.0017	50.81	0.2337	80.37
5	50	46	36	44	22	16	1.0010	52.16	0.2360	80.64
				Δ_M			-0.0028	5.44	0.0092	1.08
				EXT			0.9982	57.60	0.2452	81.72
				x			0.8	0.8	0.8	0.8

TABLE XI. $p + {}^3\text{He}$ phase shifts ($^\circ$) at $E_p = 5.54$ MeV calculated for different values of the parameters used in the calculation. The parameter ℓ_{\max} is the maximum value of orbital angular momenta used to expand the asymptotic states, see Eq. (55). The number of grids points n_z , n_y , n_x , and n_μ are used in the numerical integration of the potential matrix elements. N_3 is the number of three-body HH functions used to construct the ${}^3\text{He}$ wave function. Finally, the parameters b (fm^{-1}) and M are used in the expansion of the hyperradial functions in terms of Laguerre polynomials, see Eqs. (30) and (31). The N3LO500 potential is considered here with the inclusion of the point-Coulomb interaction. The ${}^3\text{He}$ binding energy obtained with $N_3 = 390$ ($N_3 = 480$) three-body HH functions is 7.12869 (7.12871) MeV. See Sec. IID for more details. The changed parameters with respect to “case a” are highlighted in bold.

Case	ℓ_{\max}	n_z	n_y	n_x	n_μ	N_3	b	M	$\delta({}^1S_0)$	$\delta({}^3S_1)$	$\delta({}^3P_0)$	$\delta({}^1P_1)$	$\delta({}^3P_1)$	$\delta({}^3P_2)$
a	5	30	50	20	16	365	4.0	16	-68.518	-60.104	25.065	22.955	44.091	47.811
b	5	40	60	30	18	365	4.0	16	-68.533	-60.111	25.042	22.960	44.102	47.815
c	6	30	50	20	16	365	4.0	16	-68.524	-60.105	25.057	22.991	44.191	47.927
d	5	30	50	20	16	480	4.0	16	-68.514	-60.104	25.070	22.938	44.081	47.805
e	5	30	50	20	16	365	3.5	16	-68.524	-60.109	25.081	22.969	44.102	47.819
f	5	30	50	20	16	365	3.5	18	-68.523	-60.108	25.081	22.961	44.104	47.825

The values of the “extrapolated” (as discussed in the previous subsection) phase shifts obtained for different values of the parameters in case of the potential N3LO500 are reported in Table XI. In the “case a” row, we have reported the phase shifts calculated using the “standard” values of ℓ_{\max} , number of grids points, number of three-body HH functions, and values of M and b used so far. Increasing the values of grids points n_z , n_y , n_x , n_μ used to compute the matrix elements (case b), the calculated phase shifts change only by approximately 0.1%. The effect of increasing ℓ_{\max} (case c) has a slightly larger effect, in particular for the 3P_1 and 3P_2 phase shifts. The increasing of the number of three-body HH functions (case d) to describe the ${}^3\text{He}$ bound state produces negligible effects. The same using a different value of b (case e). Finally, the phase shifts are rather insensitive to the increase of the number M of Laguerre polynomials. In addition to the cases discussed in Table XI, the calculation of the matrix elements depends also on the parameters a_y and a_z used to define the grids in the integrals given in Eqs. (71) and (72). We have found that once large-enough values for n_y and n_z are used, the dependence on these two parameters is completely negligible. Therefore, we can conclude that the calculated phase shifts are almost insensitive to the choice of the various parameters.

A similar analysis has been performed also for other potentials, in particular for AV18, which has a stronger repulsion at short interparticle distances. In this case, the calculations depend on the parameters discussed in Sec. IID 1, and in

particular on h , α_s , and n_ρ defining the ρ grid, see Eq. (64). For example, the 3P_2 phase shift calculated using the “standard grid” ($h = 0.04$ fm, $\alpha_s = 1.05$, and $n_\rho = 96$) is 46.704° , while using a denser grid ($h = 0.03$ fm, $\alpha_s = 1.04$, and $n_\rho = 127$) results in 46.726° . In summary, we have found that the calculated phase shifts are almost insensitive to the changes of the various parameters also in this case. The greatest sensitivity is found again for the parameter ℓ_{\max} . Increasing it by one unit, however, causes at most 0.5% changes in the phase shifts.

D. Numerical stability with the inclusion of the 3N potential

In this subsection, the numerical stability of the results when the 3N potential is included is studied. The method now involves the calculation of the 3N potential matrix elements discussed in Sec. IID 3. Here we report the results of the inclusion of the N2LO500 3N interaction together with the N3LO500 NN potential.

In Table XII, the dependence of the usual $p + {}^3\text{He}$ phase shifts at $E_p = 5.54$ MeV on several parameters is studied. Some of these quantities also enter the calculation of the matrix elements of the NN potential, namely ℓ_{\max} , n_z , n_y , n_x , n_μ , N_3 , b , and M . In the cases reported below, we have used the same values of the grid points n_z , n_y , and n_x to calculate both NN and 3N matrix elements, given in Eqs. (67) and (75), respectively. Moreover, adding the 3N force, the calculations also depend on the values of the parameters ℓ_{\max}^{3N} , J_{\max}^{3N} , and

TABLE XII. $p + {}^3\text{He}$ phase shifts ($^\circ$) at $E_p = 5.54$ MeV calculated for different values of the parameters when a 3N interaction is included. The parameters ℓ_{\max} , n_z , n_y , n_x , n_μ , N_3 , b , and M have the same meanings as in Table XI. The dimension of parameter b is fm^{-1} . The parameters ℓ_{\max}^{3N} , J_{\max}^{3N} , and K_{\max}^{3N} are used in the truncation of the spin-isospin-angular matrix elements of the 3N force, see Sec. IID 3 for more details. The calculation are performed using the N3LO500/N2LO500 interaction with the inclusion of the point-Coulomb potential. The ${}^3\text{He}$ binding energy obtained with $N_3 = 390$ ($N_3 = 480$) three-body HH functions is 7.72988 (7.72991) MeV. The changed parameters with respect to the “case a” are highlighted in bold.

Case	ℓ_{\max}	n_z	n_y	n_x	n_μ	N_3	b	M	ℓ_{\max}^{3N}	J_{\max}^{3N}	K_{\max}^{3N}	$\delta({}^1S_0)$	$\delta({}^3S_1)$	$\delta({}^3P_0)$	$\delta({}^1P_1)$	$\delta({}^3P_1)$	$\delta({}^3P_2)$
a	5	30	50	20	16	365	4.0	16	5	15/2	16	-66.554	-58.523	24.188	22.579	44.990	49.732
b	5	30	50	20	16	365	4.0	16	6	17/2	16	-66.554	-58.524	24.188	22.580	44.993	49.734
c	5	30	50	20	16	365	4.0	16	5	15/2	18	-66.554	-58.520	24.205	22.584	45.015	49.749
d	6	40	60	30	18	480	3.5	18	5	15/2	16	-66.533	-58.518	24.209	22.613	45.101	49.869

TABLE XIII. NN+3N interaction models used in this work. In columns 2–4 the values of the cutoff parameter Λ and the coefficients c_D and c_E entering the chiral 3N force are reported (the coefficients are adimensional). In the last columns we have reported the corresponding ${}^3\text{H}$, ${}^3\text{He}$, and ${}^4\text{He}$ binding energies. The experimental values of the latter quantities are reported in the last line.

Model	Λ (MeV)	c_D	c_E	$B({}^3\text{H})$ (MeV)	$B({}^3\text{He})$ (MeV)	$B({}^4\text{He})$ (MeV)
N3LO500/N2LO500	500	+0.945	−0.0410	8.471	7.729	28.34
N3LO600/N2LO600	600	+1.145	−0.6095	8.467	7.733	28.59
N4LO450/N2LO450	450	+0.560	+0.460	8.482	7.714	28.53
N4LO500/N2LO500	500	−0.745	−0.150	8.473	7.728	28.15
N4LO550/N2LO550	550	−1.030	−0.570	8.470	7.731	28.07
Expt.				8.480	7.718	28.30

K_{max}^{3N} used to truncate the spin-isospin-angular matrix elements w of the 3N force, given in Eq. (76).

As it can be seen from the table, the effect of the truncation of the spin-isospin-angular matrix elements w of the 3N force (cases b and c) is rather well under control, since we observe only very tiny differences between the phase shifts. The use of denser grids, more accurate ${}^3\text{He}$ wave functions, and a larger number of Laguerre polynomials (case d) produces at most changes of the order of 0.2%. Therefore, we can conclude that the numerical aspect of the inclusion of the 3N interaction in the calculation of the $p + {}^3\text{He}$ phase shifts is well under control. A similar degree of accuracy has been reached also for other 3N interactions.

IV. RESULTS

In this section we report the results obtained for various scattering observables. In the first subsection, a study of $n + {}^3\text{H}$ and $p + {}^3\text{He}$ elastic scattering is presented, while the second subsection is dedicated to the study of the resonant states of ${}^4\text{He}$ as extracted from the $p + {}^3\text{H}$ phase shifts. Finally, in the last subsection we present an analysis of the $p + {}^3\text{H} \rightarrow p + {}^3\text{H}$, $p + {}^3\text{H} \rightarrow n + {}^3\text{He}$, and $n + {}^3\text{He} \rightarrow n + {}^3\text{He}$ processes.

As stated before, in this section we report the results obtained mainly using the N3LO interaction derived by Entem and Machleidt [38,39], corresponding to two different cutoff values ($\Lambda = 500$ MeV and $\Lambda = 600$ MeV). These NN interactions are labeled, respectively, N3LO500 and N3LO600. In this way we can explore the dependence on the cutoff value Λ of the 4N observables. The 3N force considered here has been derived at N2LO in Ref. [41] (the 3N force at N3LO and N4LO are still under construction but we plan in future to include them in the 4N calculations). With the N3LO500 (N3LO600) NN interaction, we have considered the 3N N2LO force labeled N2LO500 (N2LO600) with the parameters c_D and c_E fixed to reproduce the 3N binding energy and the tritium GTME. These values were recently redetermined in Ref. [46] after finding and correcting an inconsistency between the 3N force and the axial current used so far [48].

In some cases, we have also considered the new potentials developed at successive order (N4LO) in Ref. [40] for three different cutoff values ($\Lambda = 450$, 500, and 550 MeV). With such NN interaction, we have used the same N2LO 3N force. In this case, however, the values for the πN parameters c_i entering the 3N N2LO force have been chosen as in the last

column of Table IX of Ref. [40], taking into account in an effective way part of the missing N3LO and N4LO 3N forces (the two-pion-exchange contribution). In such a way, these N2LO 3N force may be seen as effective N4LO 3N forces [40]. The corresponding values for c_D and c_E have been fixed again by reproducing the 3N binding energy and the tritium GTME [47].

For the sake of clarity, the adopted values of all employed parameters c_D and c_E are summarized in Table XIII, where we have also reported the corresponding ${}^3\text{H}$, ${}^3\text{He}$, and ${}^4\text{He}$ binding energies. Note that in the following we have used $1/M_N = 41.47$ MeV fm² with the N3LO potentials defined in Refs. [38,39] and $1/M_N = 41.47107$ MeV fm² with the new N4LO potentials of Ref. [40]. As it can be seen, the calculated ${}^4\text{He}$ binding energies are rather close to the experimental value. Therefore, eventual 4N forces should be rather tiny and their effect in $A = 4$ scattering at low energy can be safely neglected.

For this study we have focused our attention to the effect of the 3N interaction. For this reason we have restricted the electromagnetic interaction between the nucleons to just the point-Coulomb interaction between the protons. Note that with the N3LO500 and N3LO600 NN interactions, one should include only the effect of the two-photon exchange, Darwin-Foldy term, and vacuum polarization interactions in the 1S_0 partial wave [39]. We have disregarded them in this work. The effect of these additional electromagnetic interactions is the subject of a forthcoming paper [115].

A. $p + {}^3\text{He}$ and $n + {}^3\text{H}$ scattering

The $p + {}^3\text{He}$ and $n + {}^3\text{H}$ observables are calculated at specific values of the kinetic energy E_N of the incident nucleon, related to T_r by

$$E_N = \frac{4}{3}T_r. \quad (82)$$

In the energy range considered here ($E_N \leq 6$ MeV), the various $n + {}^3\text{H}$ and $p + {}^3\text{He}$ observables are dominated by S -wave and P -wave phase shifts (D -wave phase shifts give only a marginal contribution, and more peripheral phase shifts are negligible).

Let us first discuss the results for $n + {}^3\text{H}$ zero-energy scattering. The relevant quantities are the singlet a_s and triplet a_t scattering lengths, the zero-energy total cross section σ_T , and the coherent scattering length a_c , related as follows:

$$\sigma_T = \pi(|a_s|^2 + 3|a_t|^2), \quad a_c = \frac{1}{4}a_s + \frac{3}{4}a_t. \quad (83)$$

TABLE XIV. Total cross section σ_T (b) and coherent scattering length a_c (fm) for $n + {}^3\text{H}$ zero energy scattering calculated with different interactions. The last rows report the experimental values.

Interaction	σ_T	a_c
AV18	1.85	3.83
AV18/UIX	1.73	3.71
N3LO500	1.802	3.780
N3LO600	1.797	3.775
N3LO500/N2LO500	1.687	3.658
N3LO600/N2LO600	1.693	3.663
Expt.	1.70 ± 0.03 [55]	3.82 ± 0.07 [116]
		3.59 ± 0.02 [117]
		3.607 ± 0.017 [118]

The experimental accessible quantities are σ_T and a_c . The $n + {}^3\text{H}$ cross section has been accurately measured over a wide energy range and the extrapolation to zero energy does not present any problems. The value obtained is $\sigma_T = 1.70 \pm 0.03$ b [55]. The coherent scattering length has been measured by neutron interferometry techniques. The most recent values reported in the literature have been obtained by the same group; they are $a_c = 3.82 \pm 0.07$ fm [116] and $a_c = 3.59 \pm 0.02$ fm [117], the latter value being obtained with a more advanced experimental arrangement. Finally, the value $a_c = 3.607 \pm 0.017$ fm has been obtained from $p - {}^3\text{He}$ data by using an approximate Coulomb-corrected R -matrix theory [118].

The total cross section and coherent scattering length calculated with the considered interactions are compared with the experimental values in Table XIV. Since in the a_s - a_t plane, the ellipse corresponding to the experimental value of the total cross section σ_T and the straight line corresponding to the coherent scattering length a_c are almost tangent [30], the extraction of the experimental scattering lengths suffers of large uncertainties (in particular for a_s). Therefore, we prefer to compare directly the results of the calculations with σ_T and a_c . It is well known that the $n + {}^3\text{H}$ singlet and triplet scattering lengths are linearly correlated with the ${}^3\text{H}$ binding energy B_3 [30]. Therefore, only with the interactions including the 3N force (which well reproduce B_3) the calculated σ_T and a_c are close to the experimental values. From inspection of Table XIV, it can be concluded that there is a satisfactory agreement between the calculated and the measured value of σ_T . However, the calculated coherent scattering lengths differ slightly from the experimental value, in particular from the more accurate one, $a_c = 3.607 \pm 0.017$. Interestingly, the a_c calculated using the χEFT interactions differ less from the experimental value than the value calculated with AV18/UIX. It would be interesting to study this observables with the most recent chiral interactions of Ref. [40]. Work in this direction is in progress.

The $n + {}^3\text{H}$ total cross section as function of the incoming neutron energy E_n is shown in Fig. 2. The light cyan (darker blue) band shown in the figure collects the results obtained using the N3LO500 and N3LO600 (N3LO500/N2LO500 and N3LO600/N2LO600) interactions. Therefore the width of the

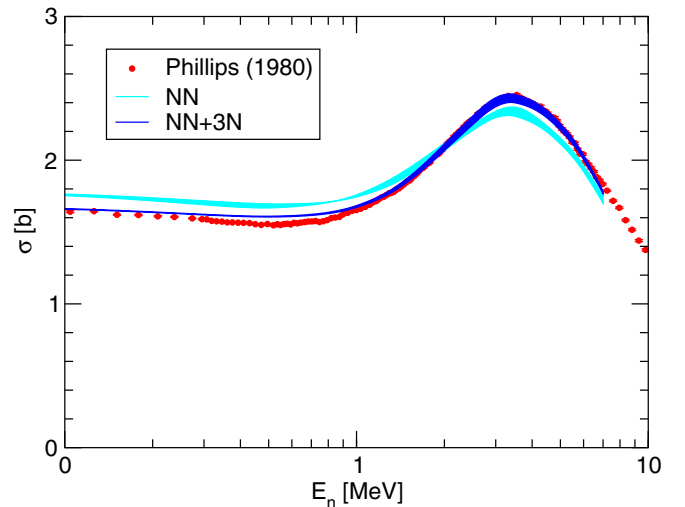


FIG. 2. $n + {}^3\text{H}$ total cross section as function of the incoming neutron energy E_n calculated with the NN N3LO interaction of Refs. [38,39] (light cyan band) or including also the 3N N2LO interaction discussed in the text (darker blue band). The width of the bands reflects the spread of theoretical results using $\Lambda = 500$ or 600 MeV cutoff values. See the main text for more details. The experimental values are taken from Ref. [55].

bands reflects the theoretical “uncertainty” connected to the use of interactions with two different cutoff values. As it can be seen by inspecting the figure, the width of the bands is very tiny, and a very good agreement with the experiment is observed, in particular for the results obtained including the 3N force.

Let us discuss now $p + {}^3\text{He}$ scattering. In this case, there exists an accurate PSA which has allowed for the extraction of phase shifts and mixing parameters from the available experimental data [65]. A comparison of a selected set of calculated phase shifts with those obtained by this PSA is shown in Fig. 3. Again, the light cyan (darker blue) bands shown in the figure collect the results obtained using the N3LO500 and N3LO600 (N3LO500/N2LO500 and N3LO600/N2LO600) interactions and the width of the bands reflects the use of the two different cutoff values. The inspection of the figure reveals that, using the interaction models with only a NN potential, both S - and P -wave phase shifts result to be at variance with the PSA. Including the 3N force, we observe a general improvement of the description of the phase shifts. The decreasing (in absolute value) of the S phase shifts when the 3N force is added is mainly due to the smaller dimension of the ${}^3\text{He}$ nucleus following the increase of binding energy. These phase shifts are negative since the Pauli principle does not allow us to have three protons in S wave. The P waves are attractive. In particular, for the 3P_1 and 3P_2 waves, the 3N interaction provides an extra attraction; the resulting phase shifts are in nice agreement with the PSA. Regarding the 1P_1 and 3P_0 phase shifts, the 3N interaction reduces a little bit the disagreement with the experimental ones, but the calculated values still overpredict the experimental values at the largest energy.

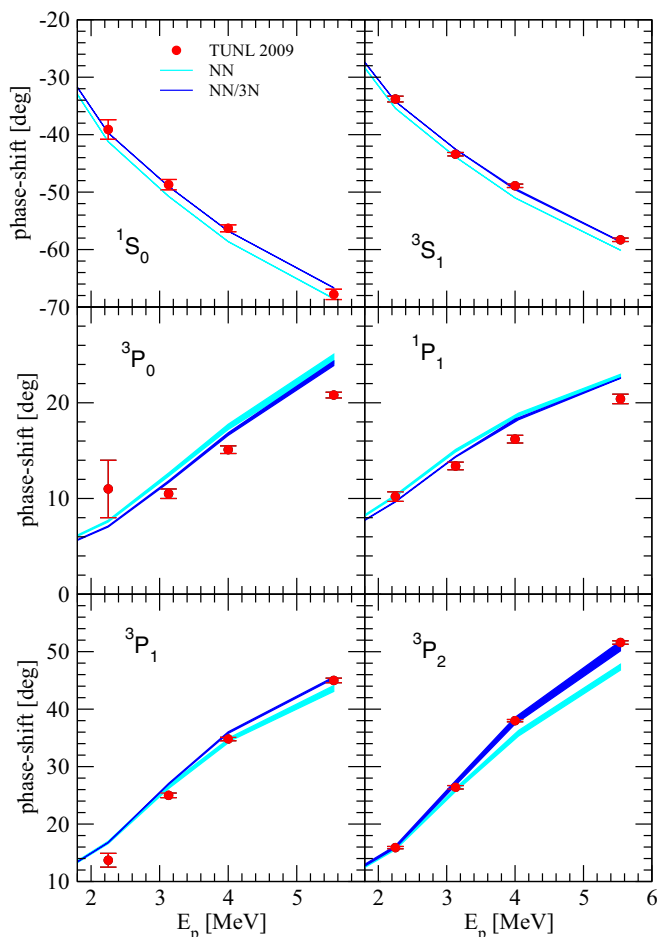


FIG. 3. $p + {}^3\text{He}$ phase shifts as function of the incoming proton energy E_p calculated with the NN N3LO interaction of Refs. [38,39] (light cyan band) or including also the 3N N2LO interaction discussed in the text (darker blue band). The results of the PSA performed at TUNL have been also reported [65].

Let us now compare the theoretical results directly with a selected set of observables for which there are accurate experimental data. We have reported the results for the $p + {}^3\text{He}$ unpolarized differential cross section in Fig. 4 for various energies of the incident proton. As usual, the results obtained with the NN (NN + 3N) potentials are shown as a light cyan (darker blue) band. As it can be seen by inspecting the figure, the widths of the bands in this case are very tiny; they can be appreciated only at energy $E_p = 5.54$ MeV for $\theta_{c.m.} \approx 30^\circ$. Furthermore, we observe a very good agreement with the experimental values, in particular for the results obtained including the 3N force.

On the contrary, for the proton analyzing power A_{y0} , shown in Fig. 5, we note a large sensitivity to the inclusion of the 3N interaction. The calculations performed using N3LO500 and N3LO600, in fact, largely underpredict the experimental data, a fact already observed before also using other interactions [31,36,58]. A sizable improvement is found by including the N2LO 3N interaction, as already found in Ref. [66] and recently confirmed by Ref. [20]. The underprediction of the experimental data is now around 6–10%.

For the ${}^3\text{He}$ analyzing power A_{0y} , shown in Fig. 6, we note a smaller sensitivity to the inclusion of the 3N interaction. However, the results obtained with the 3N force show a slightly larger dependence on the cutoff. Here the experimental values have larger errors, and therefore it is not possible to arrive to a definite answer about the performance of the different interactions.

To better point out the sensitivity to the particular interaction model, in Fig. 7 an enlargement of A_{y0} and A_{0y} at $E_p = 5.54$ MeV in the peak region is shown. From the inspection of the figure, we note that the observables are sensitive to the choice of the cutoff Λ , in particular A_{y0} calculated with the $\Lambda = 600$ MeV interaction model is slightly closer to the experimental data. Here we have reported also the results obtained using the AV18/IL7 phenomenological interaction. We

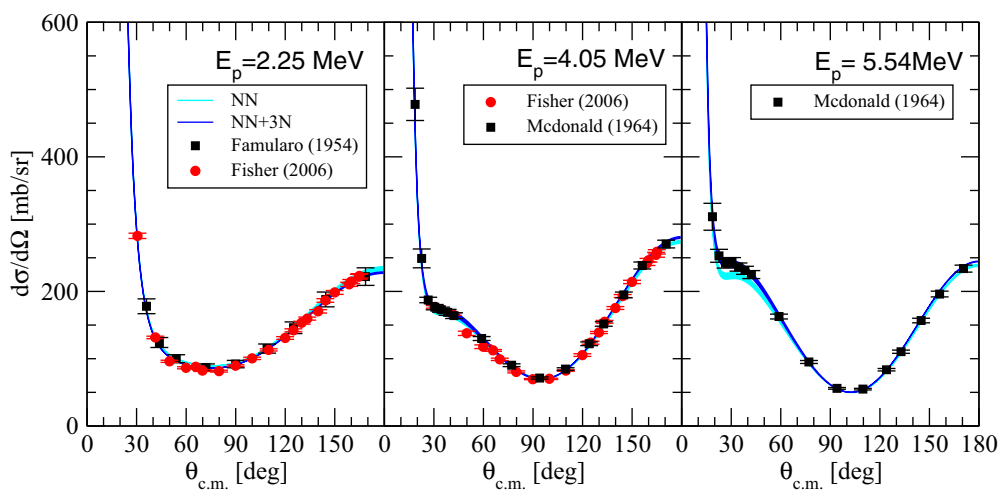


FIG. 4. $p + {}^3\text{He}$ differential cross section as function of the center-of-mass scattering angle for three different proton energies E_p calculated with the NN N3LO interactions of Refs. [38,39] (light cyan band) or including also the 3N N2LO interactions (darker blue band). The width of the bands reflects the use of two different cutoff values, $\Lambda = 500$ and 600 MeV. The experimental data are from Refs. [56–58].

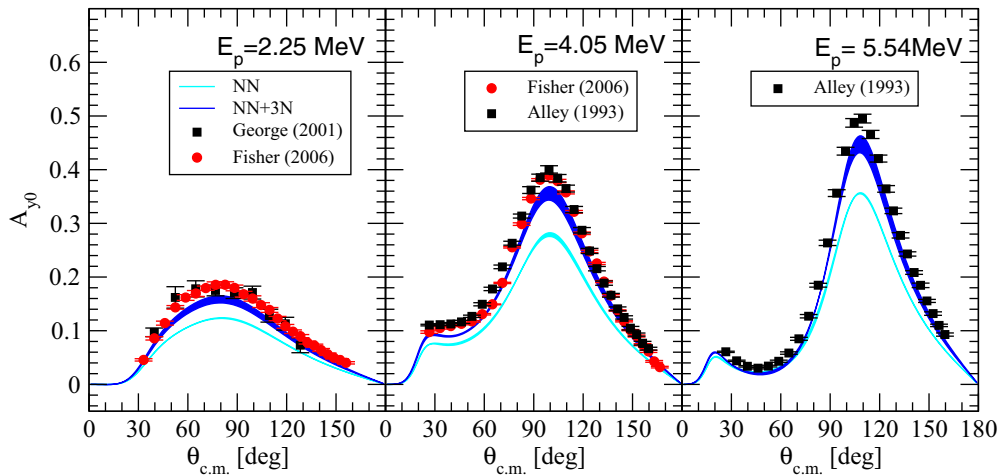


FIG. 5. Same as in Fig. 4 but for the $p + {}^3\text{He}$ analyzing power A_{y0} . The experimental data are from Refs. [31,58,59].

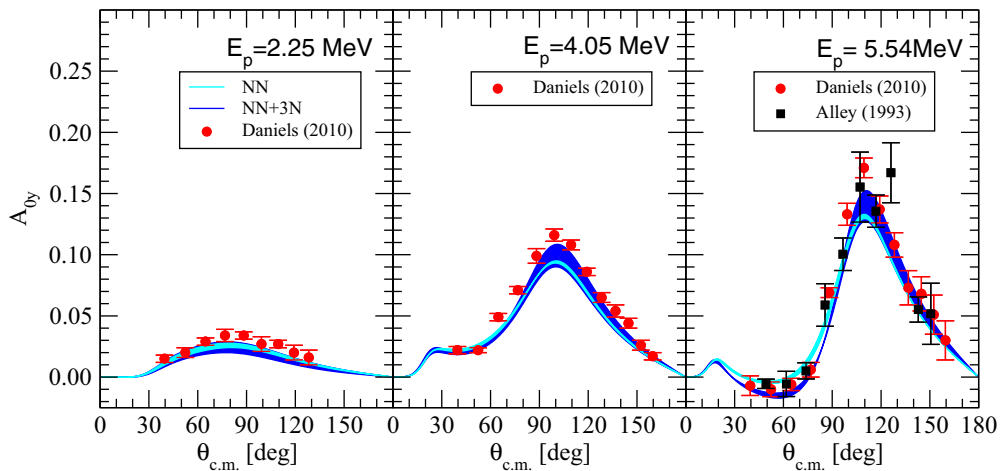


FIG. 6. Same as in Fig. 4, but for the $p + {}^3\text{He}$ analyzing power A_{0y} . The experimental data are from Refs. [59,65].

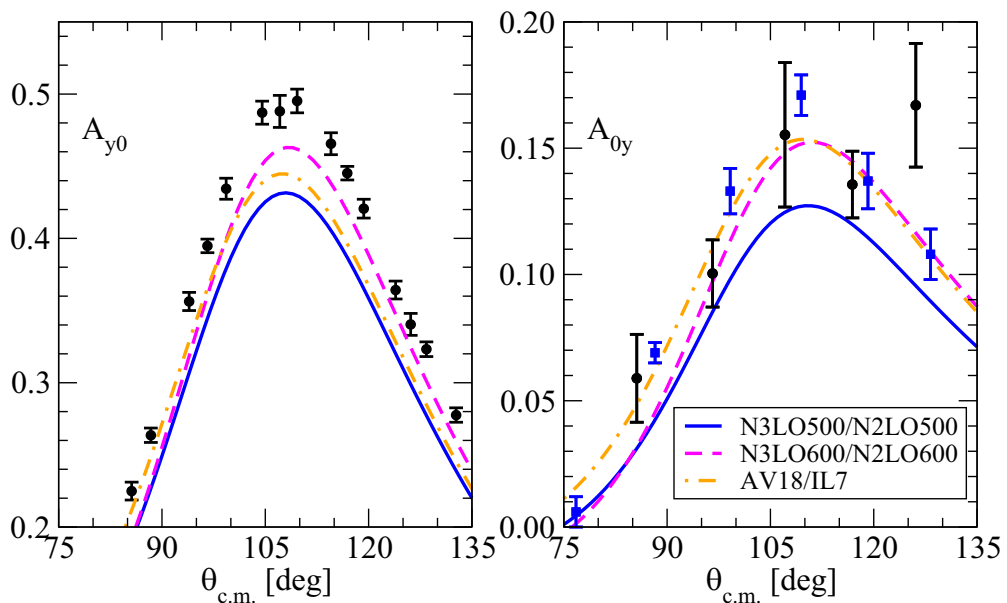


FIG. 7. $p + {}^3\text{He}$ analyzing powers at $E_p = 5.54$ MeV calculated with the N3LO500/N2LO500 (blue solid lines), N3LO600/N2LO600 (dashed magenta lines), and AV18/IL7 (dot-dashed red lines) interaction models. The experimental data are from Refs. [31,58,59].

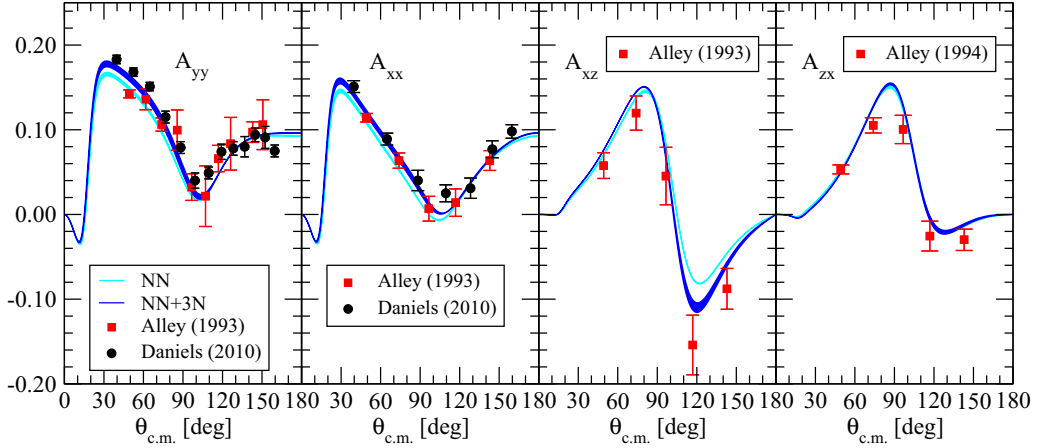


FIG. 8. Same as in Fig. 4 but for the $p + {}^3\text{He}$ A_{yy} , A_{xx} , A_{xz} , and A_{zx} spin polarization coefficients at $E_p = 5.54$ MeV. The experimental data are from Refs. [59,65].

note that A_{y0} calculated with AV18/IL7 is very similar to the results obtained with the chiral models, while A_{0y} is in better agreement with the data than with N3LO500/N2LO500.

The previously observed large underprediction of the $p + {}^3\text{He}$ A_{y0} observable, when only NN forces were taken into account [31,36,54,58], was considered to be due to some deficiencies of the interaction in P waves, as, for example, due to the appearance of a unconventional “spin-orbit” interaction in $A > 2$ systems [119]. The IL7 model has been fitted to reproduce the P -shell nuclei spectra and, in particular, the two low-lying states in ${}^7\text{Li}$. This may explain the improvement in the description of the $p + {}^3\text{He}$ analyzing powers obtained with this interaction model. Regarding the N2LO 3N force models, its two parameters have been fitted to 3N observables (the 3N binding energy and the tritium GTME), quantities which are more sensitive to S waves. Therefore, its capability to improve the description of the $p + {}^3\text{He}$ analyzing powers is not imposed but it is somewhat built in.

In the literature, there are also measurements of spin polarization coefficients. Unfortunately, these measurements have not the same precision as for the unpolarized cross section and the proton analyzing power. As an example, we report in Fig. 8 A_{yy} , A_{xx} , A_{xz} , and A_{zx} calculated at $E_p = 5.54$ MeV compared with the available experimental data. As can be seen, the sensitivity to Λ is small reflecting in the small widths of the two bands. Also the effect of 3N force is tiny, and we observe a good agreement between calculations and data.

B. Resonances of ${}^4\text{He}$

Let us now consider the $p + {}^3\text{H}$ scattering. The incident energy of the proton beam in the laboratory system is related to the center-of-mass kinetic energy as $E_p = \frac{4}{3}T_r$. We remember that for $T_r > B({}^3\text{H}) - B({}^3\text{He}) \equiv \Delta_3 \approx 0.72$ MeV, the channel $n + {}^3\text{He}$ is open. In this subsection, however, we focus on the results obtained for the parameters $\delta_{LS,L'S'}^{3,3}$ and $\eta_{LS,L'S'}^{3,3}$ describing the elastic process $p + {}^3\text{H} \rightarrow p + {}^3\text{H}$. As usual, they are related to the S matrix as given in Eq. (78). For the sake of simplicity, here we denote $\delta_{LS,L'S'}^{3,3} \equiv \delta_{p+{}^3\text{H}}$ and we refer to it as the $p + {}^3\text{H}$ phase shift.

Let us present first a calculation performed for the 0^+ wave with the Minnesota (central) potential [120] in order to compare our results with the accurate calculations performed in Refs. [121,122]. We have reported the calculated values of 0^+ phase shift $\delta_{p+{}^3\text{H}}$ (corresponding to the 1S_0 wave in spectroscopic notation) in Fig. 9, together with the results of Ref. [121]. For the Minnesota potential, the $n + {}^3\text{He}$ threshold is at $E = 0.675$ MeV, shown in the figure by an arrow. For that energy the phase shift has a discontinuity. Probably, at energies just below the opening of the $n + {}^3\text{He}$ channel, it should be convenient to include in the wave function also an asymptotic “closed” component like

$$\Omega_{4LS}^c = \sum_{l=1}^4 [Y_L(\hat{y}_l) \otimes [\phi_3^h \otimes \chi_l \xi_l^n]_{JJ_z}] \frac{\exp(-\beta_4 y_l)}{y_l}, \quad (84)$$

where ϕ_3^h is the ${}^3\text{He}$ wave function, ξ_l^n the isospin state of the neutron (particle l), and y_l the distance between the

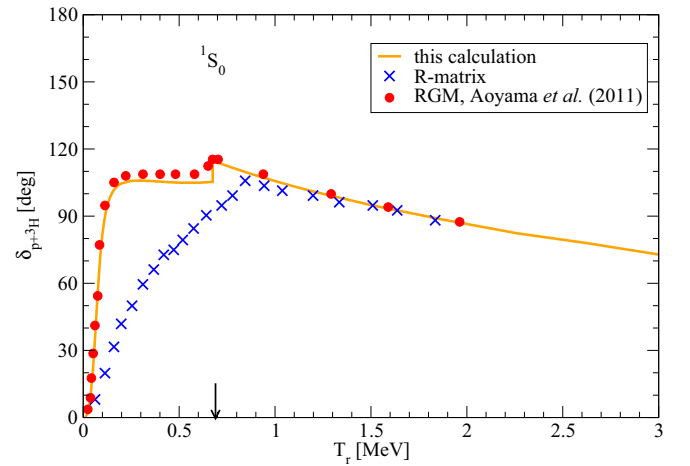


FIG. 9. $p + {}^3\text{H}$ 1S_0 phase shift calculated with the Minnesota potential as function of the center-of-mass kinetic energy T_r . Solid line: present calculation; red dots: RGM calculation of Ref. [121]; crosses: phase shift extracted from the R -matrix analysis [24]. The arrow denotes the energy of the $n + {}^3\text{He}$ threshold.

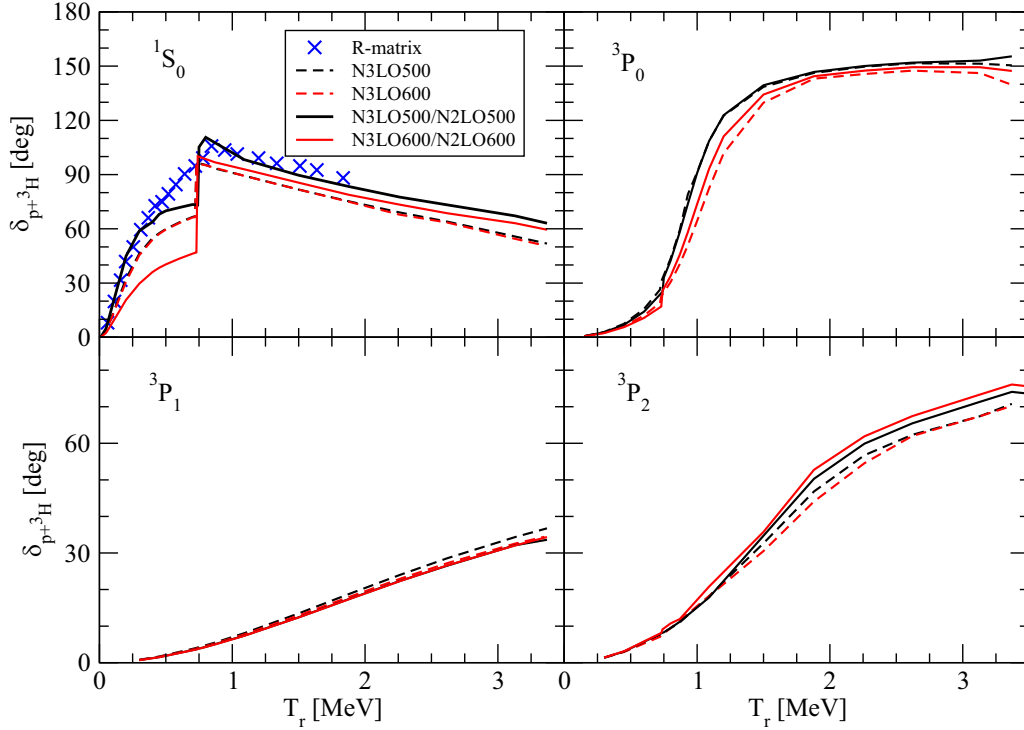


FIG. 10. $p + {}^3\text{H}$ phase shifts as function of the center-of-mass kinetic energy T_r calculated with the N3LO500 (red dashed curves), N3LO600 (red dotted curves), N3LO500/N2LO500 (black solid curves), and N3LO600/N2LO600 (red dot-dashed curves) interactions. The experimental phase shifts have been extracted by an R -matrix analysis in Ref. [24].

center-of-mass of ${}^3\text{He}$ and the neutron. Above, we have specified that $\gamma = 4$ and $\beta_4 = \sqrt{2\mu_4(\Delta_3 - T_r)}$, where $\Delta_3 \approx 0.72$ MeV is the difference between the ${}^3\text{H}$ and ${}^3\text{He}$ binding energies. When $T_r \rightarrow \Delta_3$, β_4 becomes rather small and the component Ω_{4LS}^c will have a long-range tail. Configurations of this type are rather difficult to be constructed in terms of the HH expansion, whence the utility of explicitly including them in the variational wave function. Work in this direction is currently in progress.

Returning to Fig. 9, we note that the results of our calculation and that of Ref. [121] are very close. The phase shift has a “resonant” behavior, with a very sharp increase followed by a plateau. In particular, $\delta_{p+{}^3\text{H}}$ reaches the value of 90° for $E \approx 0.12$ MeV.

Now let us try to extract the energy E_R and width Γ of the resonance using two methods. In the first method, one can just estimate E_R as the value of T_r for which the first derivative $\delta'_{p+{}^3\text{H}}$ has a maximum and $\Gamma = 2/\delta'_{p+{}^3\text{H}}(E_R)$ [123]. Using the phase shifts reported in Fig. 9, we obtain $E_R = 0.064$ MeV and $\Gamma = 0.088$ MeV.

Another method to determine E_R and Γ has been taken from Ref. [124]. The idea is to fit the calculated S matrix for various energies using a Padé approximation, namely

$$S(k) = \frac{1 + \sum_{n=1}^N a_n k^n}{1 + \sum_{n=1}^N (-)^n a_n k^n}, \quad (85)$$

where $k = \sqrt{2\mu T_r}$ and μ is the $p + {}^3\text{H}$ reduced mass. This form is suggested by the general properties of the S matrix, in particular that $S(-k) = S(k)^{-1}$ and that $S(k \rightarrow 0) \rightarrow 1$.

Given a number N of values $S(k_i)$, $i = 1, \dots, N$, the coefficients a_n can be simply obtained solving the linear system

$$\sum_{n=1}^N [1 + (-)^{n+1} S(k_i)] k_i^n a_n = S(k_i) - 1. \quad (86)$$

The resonances are then calculated as the poles of the S matrix, namely the zeros of the denominator of Eq. (85). The problem thus reduces to find the zeros of the polynomial $1 + \sum_{n=1}^N (-)^n a_n k^n$, which can be readily obtained using the method described in Ref. [125]. However, since the S matrix is extracted using only a finite number of energies, the procedure finds a number of spurious poles, in addition to the “true” poles. To recognize the true poles, in Ref. [124] it is suggested to vary N and to observe the position of the poles in the plane $\text{Re}(k)$, $\text{Im}(k)$: The position of the “true” poles should be independent on N , while the spurious pole positions will vary considerably with N .

We have used this procedure using the phase shifts calculated with the Minnesota potential and selecting increasing values of $N = 4, 6, \dots$. We have found one stable pole, from which the values $E = E_R = 0.067$ MeV and $\Gamma = 0.070$ MeV are extracted, in reasonable agreement with the values determined using the first method. We note that in Ref. [121], the resonance energy is determined, by a bound-state approximation, to be $E_R = 0.12$ MeV, which corresponds to the energy T_r for which $\delta = 90^\circ$. In Ref. [122], the resonance is obtained by a complex scaling method at $E_R = 0.07$ MeV and $\Gamma = 0.06$ MeV (with a numerical error estimated to be several tens of keV), in good agreement with our results.

TABLE XV. Energy of the 0^+ resonance and its width as extracted from the phase shifts reported in Fig. 11. The experimental values are extracted from the R -matrix analysis reported in Ref. [114].

Interaction	E_R (MeV)	Γ (MeV)
N3LO500	0.126	0.556
N3LO600	0.134	0.588
N3LO500/N2LO500	0.118	0.484
N3LO600/N2LO600	0.130	0.989
N4LO450/N2LO450	0.126	0.400
N4LO500/N2LO500	0.118	0.490
N4LO550/N2LO550	0.130	0.740
Expt.	0.39	0.50

We now present the results for some $p + {}^3\text{H}$ phase shifts calculated with the N3LO500, N3LO600, N3LO500/N2LO500, and N3LO600/N2LO600 interactions in Fig. 10. We note rather large differences for the 1S_0 phase shift when the 3N force is added, while for the P -wave phase shifts the results with and without the 3N force are rather close. Again, below the threshold of the $n + {}^3\text{He}$ channel, the inclusion of the ‘‘closed’’ component as given in Eq. (84) could improve the convergence, in particular for the 1S_0 case. Work in this direction is in progress. In any case, for the 1S_0 phase shift, below the opening of the $n + {}^3\text{He}$ channel, the results obtained using the N3LO500/N2LO500 and N3LO600/N2LO600 differ considerably. In order to explore this result, we have performed additional calculations using the N4LO450/N2LO450, N4LO500/N2LO500, and N4LO550/N2LO550 interactions. The results obtained for the 1S_0 phase shift at low energies are reported in Fig. 11.

We note that the results obtained with the N3LO500/N2LO500 and N4LO500/N2LO500 interactions are very close (we remember that the values of c_1 , c_3 , c_4 , c_D , and c_E in these two 3N force interactions are different).

TABLE XVI. Energies E_R and widths Γ of the resonances in the different waves obtained using the chiral interactions. The experimental values are taken from Ref. [114] and obtained from an R -matrix analysis.

Interaction	3P_0		1P_1	
	E_R (MeV)	Γ (MeV)	E_R (MeV)	Γ (MeV)
N3LO500	0.89	0.46	1.7	8.2
N3LO600	1.05	0.57	1.7	8.6
N3LO500/N2LO500	0.90	0.46	1.8	8.6
N3LO500/N2LO500	0.98	0.54	1.8	8.7
R matrix	1.20	0.84	6.13	12.7
Interaction	3P_1		3P_2	
	E_R (MeV)	Γ (MeV)	E_R (MeV)	Γ (MeV)
N3LO500	1.0	4.7	1.4	3.1
N3LO600	1.0	4.8	1.5	3.3
N3LO500/N2LO500	1.3	4.7	1.4	2.7
N3LO600/N2LO600	1.3	4.4	1.7	2.9
R matrix	4.43	6.10	2.02	2.01

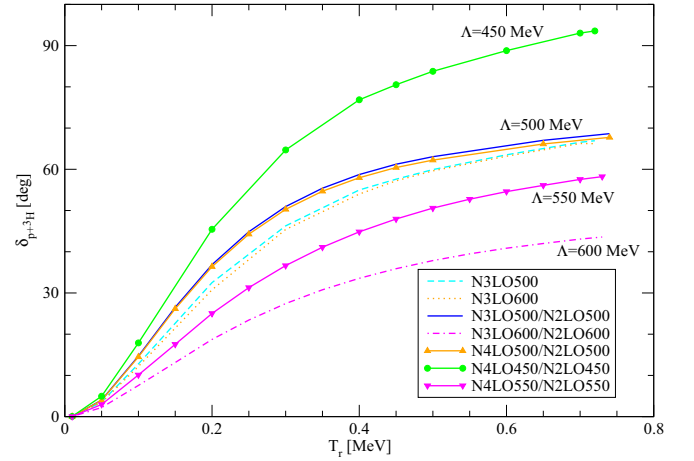


FIG. 11. 1S_0 $p + {}^3\text{H}$ phase shift as function of the center-of-mass kinetic energy T_r calculated with several interactions.

On the other hand, we observe again a strong dependence on the cutoff values. The interactions with the softer cutoff corresponds to larger values of the $p + {}^3\text{H}$ phase shift. Note that the differences between the phase shifts calculated with the various Λ are significantly larger than the theoretical uncertainties connected to the extrapolation procedure discussed in the previous section, which at $E_p = 0.60$ MeV (corresponding to $T_r = 0.45$ MeV) was estimated to be around 1.4° . Therefore, these differences cannot be ascribed to the uncertainties in the extrapolation of the phase shifts.

From these phase shifts it is possible to extract the resonance parameters as discussed previously. We report in Table XV the values obtained using method 1. The values of E_R are somewhat independent on the inclusion of the 3N force and the value of the cutoff and are around 0.1 MeV, somewhat at variance with respect to the experimental datum. On the contrary, the width is very sensitive to the cutoff. The potentials with cutoff $\Lambda > 500$ MeV predict a too-large width when compared to the experimental value.

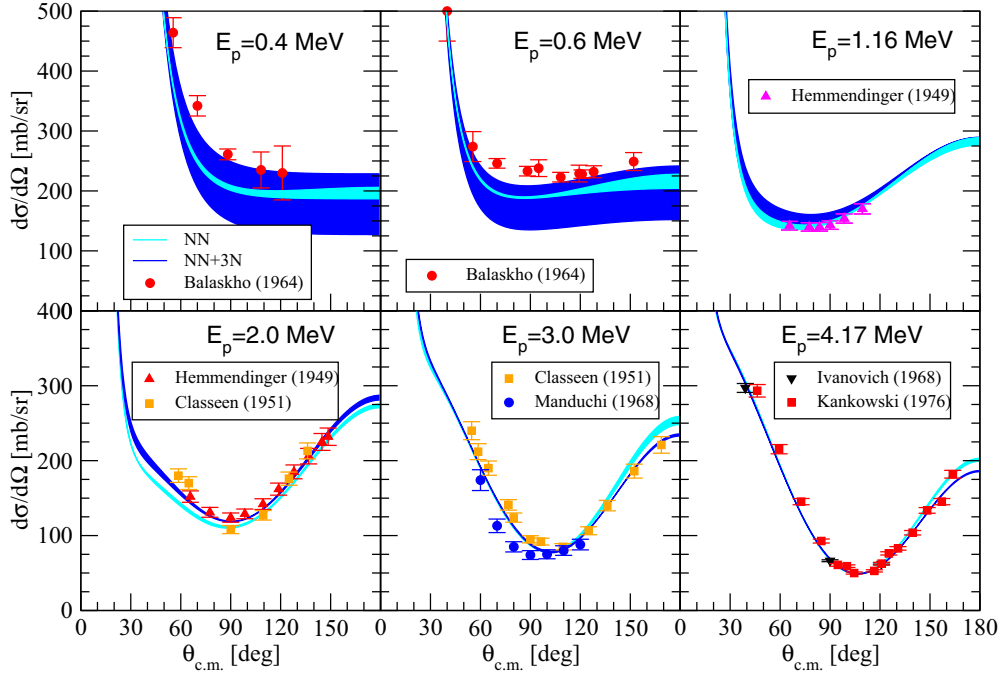


FIG. 12. Same as in Fig. 4 but for the $p + {}^3\text{H}$ differential cross section. The experimental data are from Refs. [67–69,72–74].

We have also extracted the resonance parameters from the 3P_0 , 1P_1 , 3P_1 , and 3P_2 phase shifts (some of them are reported in Fig. 10). The results are listed in Table XVI. The experimental information is obtained using an R -matrix method as discussed in Ref. [114], so it is not clear whether the two methods would give consistent results. Work to clarify this issue is still in progress. From inspection of the table, we can see that the values of E_R are consistently smaller than the experimental ones. The width of the resonance in the 0^- wave is predicted to be smaller than that reported by the R -matrix analysis. From the calculation, this resonance is found to have approximately the same width as the 0^+ resonance studied earlier. The dependence on the cutoff and on the inclusion of the 3N interaction is not critical. The width of the resonances

found in the 1^- wave are noticeably large. Very likely in this case the extracted values of E_R and Γ are not significant. On the other hand, the resonance in the 2^- wave is well established, and the energy and width are in reasonable agreement with the values extracted from the R -matrix analysis.

C. $p + {}^3\text{H}$ and $n + {}^3\text{He}$ scattering

Let us now consider the results obtained for the $p + {}^3\text{H}$ and $n + {}^3\text{He}$ observables. We have reported the results for the $p + {}^3\text{H}$ unpolarized differential cross section in Fig. 12 at various energies of the incident proton. Again, the results obtained with N3LO500 and N3LO600 (N3LO500/N2LO500 and N3LO600/N2LO600) potentials are collected in the light

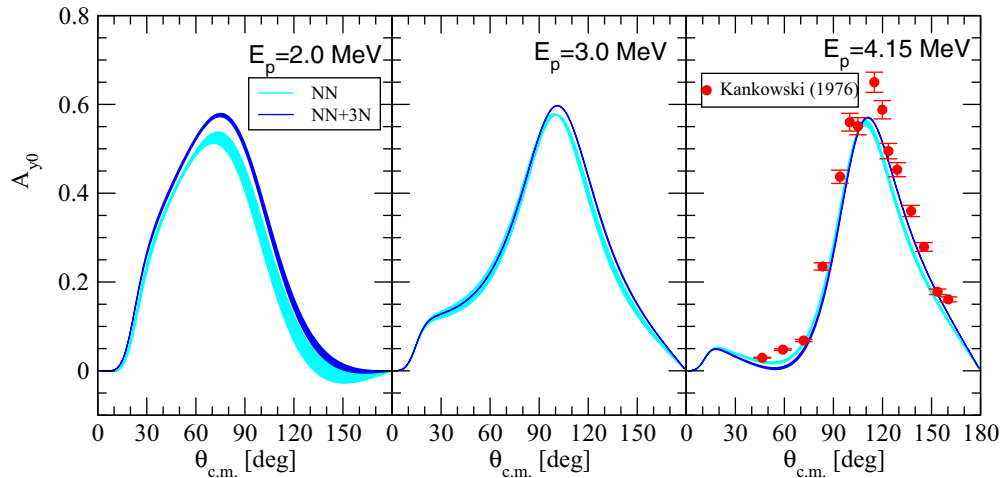


FIG. 13. Same as in Fig. 4 but for the $p + {}^3\text{H}$ proton analyzing power. The experimental data are from Refs. [59,65].

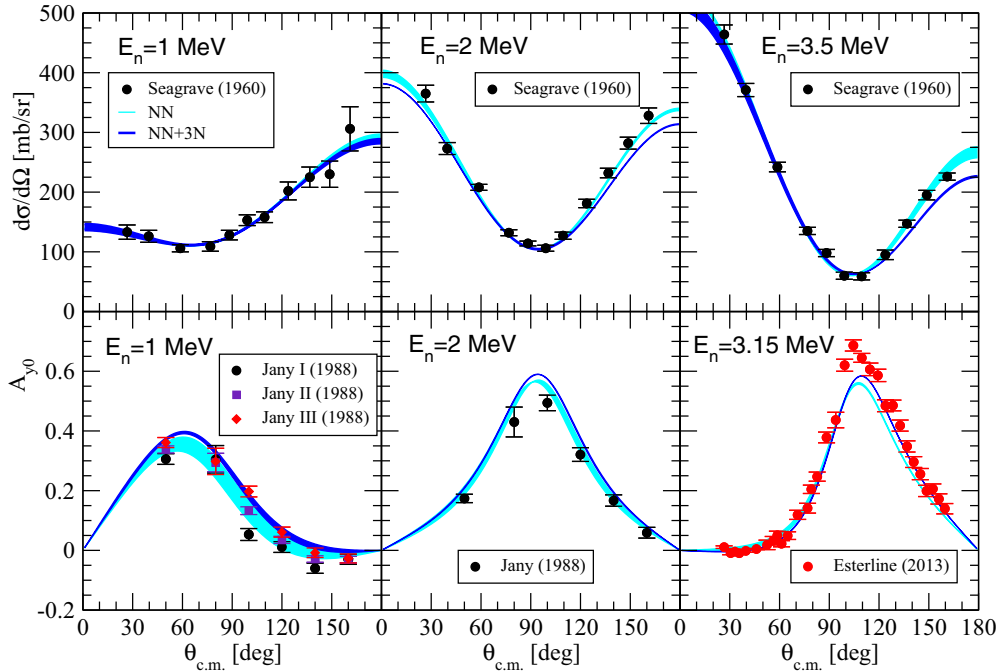


FIG. 14. The same as Fig. 4 but for the $n + {}^3\text{He}$ differential cross section and neutron analyzing power. The experimental data are from Refs. [75,82,83].

cyan (darker blue) bands. By inspecting the figure, at the two lowest energies the effect of 3N force is sizable. We also note that, at the two lowest energies, the observable becomes very cutoff dependent when including the 3N force. For those energies the $n + {}^3\text{He}$ channel is closed, and the cross section considerably depends on the position of the first excited state of ${}^4\text{He}$. In fact, the differences in the cross section originate

mainly from the 1S_0 phase shift. Above the $n + {}^3\text{He}$ threshold, the width of the band is small, as observed before for $p + {}^3\text{He}$. In this case, we find that the contribution of the 3N force is small. The $p + {}^3\text{H}$ analyzing powers are reported in Fig. 13, where we show only the results obtained at energies larger than the $n + {}^3\text{He}$ threshold (below it this observable is tiny). For these energies, the effect of 3N force is not very

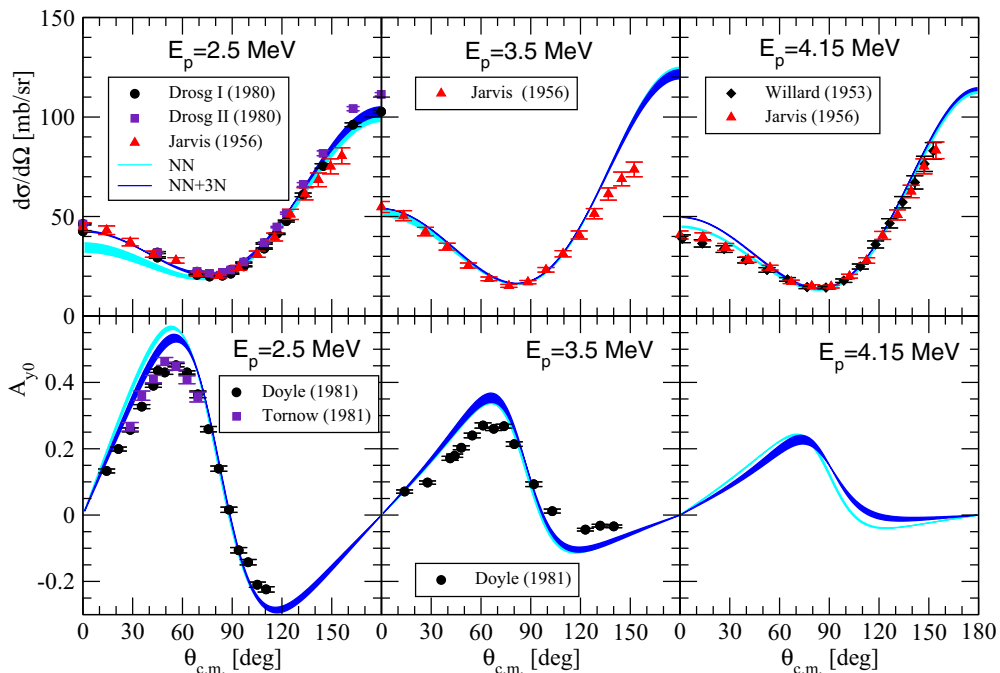


FIG. 15. The same as in Fig. 4 but for the $p + {}^3\text{He} \rightarrow n + {}^3\text{He}$ differential cross section and proton analyzing power. The experimental data are from Refs. [92–94,96,97].

important. We find that the height of the peaks is only slightly increased when the 3N force are included, but this does not significantly help in reducing the disagreement observed with the experimental data at $E_p = 4.15$ MeV, as can be seen in Fig. 13.

Some of the results obtained for $n + {}^3\text{He}$ elastic scattering are reported in Fig. 14. The results obtained using NN interaction only or including also the 3N force are as usual shown by bands. As it can be seen inspecting the figure, the widths of the bands are always small, showing that the dependence on Λ is not critical. Also the effects of the inclusion of the 3N forces are small.

The results for some $p + {}^3\text{H} \rightarrow n + {}^3\text{He}$ charge exchange reaction observables are reported in Fig. 15, together with the available experimental data. We see that the contribution of the 3N force is small for these observables. Again, the dependence on the cutoff is not critical.

V. CONCLUSIONS AND PERSPECTIVES

We have discussed in detail the application of the HH method to the 4N scattering problem, limiting our study to processes with only two clusters in the asymptotic regions (but below the energies for which the channel $d + d$ is open). We have discussed the issues of convergence and numerical stability, showing that they are under control. The convergence of the HH expansion is usually well achieved for chiral potentials, except for the $p + {}^3\text{H}$ $J^\pi = 0^+$ phase shift, where large extrapolations are needed in order to take into account the contribution of HH states of large K . However, we have also discussed the procedure used to estimate the “missing” phase shift, believed to be reliable.

In the paper we have also included the results of a first campaign of calculations of various low-energy elastic and charge-exchange processes. In particular, we have studied the effect of including the N2LO 3N forces, constrained to reproduce the ${}^3\text{H}$ binding energy and the GTME in tritium β decay. For $n + {}^3\text{H}$ elastic scattering, the inclusion of the 3N forces is very helpful in reproducing the scattering lengths and the total cross section, in particular in the resonance region. For $p + {}^3\text{He}$ the main effect of the inclusion of 3N force is to reduce the disagreement between theory and experiment in the observable A_{y0} , which is present when only NN forces are taken into account.

For $n + {}^3\text{He}$ elastic scattering and the charge exchange reaction $p + {}^3\text{H} \rightarrow n + {}^3\text{He}$, the inclusion of the 3N forces is tiny, although in general it helps to obtain a slightly better description of the data. On the other hand, for the $p + {}^3\text{H}$ elastic scattering (at energies below the opening of the $n + {}^3\text{He}$ channel) sizable effects of the 3N force are observed mainly in the 1S_0 wave. In particular, a rather strong dependence on the cutoff used to regularize the chiral potential is found when the 3N force is included in the calculations. We have speculated that this effect might be related to a critical dependence on the 3N force of the position and width of the resonance representing the first excited state of ${}^4\text{He}$. Further studies of this resonance are currently in progress. Moreover, it would

be rather important to have new and more accurate measurements of $p + {}^3\text{H}$ elastic scattering at these low energies, as the available experimental data are rather old and of limited angular range.

More refined calculations of the same processes with the new generation of chiral potentials up to N4LO [40] are currently in progress. First, we would like to improve the calculations of the $p + {}^3\text{H}$ phase shifts just below the opening of the $n + {}^3\text{He}$ channel including explicitly in the wave functions the “closed” component given in Eq. (84). Moreover, calculations with larger sets of HH functions will be undertaken. From the observables calculated using the interactions at different chiral orders, we plan also to estimate the “theoretical uncertainties” due to our incomplete knowledge of the nuclear dynamics, following the procedure proposed in Ref. [126]. Further calculations performed with the local EFT interactions developed in Refs. [46,127,128] are planned. These latter interactions take into account also the Δ -particle degrees of freedom. Finally, we propose also to explore the effect of the 3N force contact terms appearing at N4LO [63,64]. These terms are currently studied in the $A = 3$ system in order to solve the A_y puzzle found in $N + d$ scattering. It would be very interesting to see whether these terms can help in solving also the various disagreements discussed in this paper for $A = 4$ scattering.

The availability of the $n + {}^3\text{H}$, $p + {}^3\text{He}$, $p + {}^3\text{H}$, and $n + {}^3\text{He}$ scattering wave functions will allow for the study of various radiative capture reactions, as $p + {}^3\text{H} \rightarrow {}^4\text{He} + \gamma$ and $n + {}^3\text{He} \rightarrow {}^4\text{He} + \gamma$, of electron scattering elastic and transition form factors, as for the ${}^4\text{He}(e, e'){}^4\text{He}^*$ process, of reactions of astrophysical interest, as the “hep” reaction ${}^3\text{He}(p, e^- \nu_e){}^4\text{He}$, and of the process ${}^3\text{H}(p, e^+ e^-){}^4\text{He}$, recently exploited experimentally in order to demonstrate the existence of a new kind of particle [1].

In the near future, we plan also to extend the formalism to $d + d$ scattering and to energies above the threshold for the breakup in three or more clusters in the final state. Work in this direction has been already undertaken.

ACKNOWLEDGMENT

The authors acknowledge the National Supercomputing Consortium CINECA where part of the calculations presented in this paper were performed.

APPENDIX: THE REGULARIZATION OF THE FUNCTION G_L

In this Appendix, we describe the functions $f_L(y)$ used to regularize the irregular Coulomb functions using method 1, namely

$$\frac{\tilde{G}_L(\eta, qy)}{qy} = \frac{G_L(\eta, qy)}{qy} - \frac{f_L(y)}{y^{L+1}} \exp(-\beta y), \quad (\text{A1})$$

where, in general,

$$f_L(y) = a_0 + a_1y + a_2y^2 + \dots + a_Ny^N + (b_1y + b_2y^2 + \dots + b_My^M) \log(2qy). \quad (\text{A2})$$

An important aspect of this method is that the function

$$\bar{G}_L = - \left\{ f_L'' - \left(2\beta + \frac{2L}{y} \right) f_L' + \left(\beta^2 + 2\frac{\beta L - \eta q}{y} + q^2 \right) f_L \right\} \frac{e^{-\beta y}}{y^{L+1}}, \quad (\text{A3})$$

where $f' = df/dy$, and so on, becomes a smooth function, without any oscillatory behavior. The function f_L is chosen (as discussed below) so that both \tilde{G}_L/qy and \bar{G}_L are regular at the origin. Let us first discuss the cases $L = 0$ and $L = 1$ separately, and then we give the general expression for $L > 1$.

1. Case $L = 0$

Let us start from the small- y behavior of the irregular Coulomb function G_0 , which reads [106]

$$\frac{G_0(\eta, qy)}{qy} \rightarrow \frac{1}{C_0(\eta)q} \left\{ [2\eta q + 2\eta^2 q^2 y + O(y^2)] \log(2qy) + \left[\frac{1}{y} + O(y) \right] \right\}. \quad (\text{A4})$$

The quantities $C_L(\eta)$ are defined as [106]

$$C_0(\eta) = \sqrt{\frac{2\pi\eta}{e^{2\pi\eta} - 1}}, \quad C_L(\eta) = \frac{\sqrt{L^2 + \eta^2}}{L(2L + 1)} C_{L-1}(\eta). \quad (\text{A5})$$

Note that $C_L(0) = 1/(2L + 1)!$. Let us look for a function $f_0(y)$ expressed as

$$f_0(y) = a_0 + a_1y + (b_1y + b_2y^2 + b_3y^3) \log(2qy). \quad (\text{A6})$$

For $y \rightarrow 0$

$$\frac{f_0(y)e^{-\beta y}}{y} \rightarrow \frac{a_0}{y} + a_1 - a_0\beta + O(y) + [b_1 + (b_2 - \beta b_1)y + O(y^2)] \log(2qy). \quad (\text{A7})$$

In order to have $\tilde{G}_0/qy = G_0/qy - f_0(y)e^{-\beta y}/y$ regular at the origin (together with its first derivative), we have to make vanish the coefficients of the terms $1/y$, $\log(2qy)$, and $y \log(2qy)$, namely

$$a_0 = \frac{1}{C_0(\eta)q}, \quad b_1 = 2\eta qa_0, \quad b_2 = 2\eta q(\eta q + \beta)a_0. \quad (\text{A8})$$

The other two coefficients a_1 and b_3 are determined so that \bar{G}_0 is regular at the origin. From Eq. (A3), and using the expressions for the coefficients a_0 , b_1 , and b_2 given above, we find for $y \rightarrow 0$

$$\bar{G}_0 = \left\{ \frac{3b_2 - 2\beta(a_1 + b_1) + (\beta^2 + q^2)a_0 - 2\eta qa_1}{y} + O(y^0) + [6b_3 - (4\beta + 2\eta q)b_2 + (\beta^2 + q^2)b_1 + O(y)] \log(2qy) \right\} e^{-\beta y}. \quad (\text{A9})$$

Therefore, we choose

$$a_1 = \frac{\beta^2 + q^2 + 2\eta q(\beta + 3\eta q)}{2(\beta + \eta q)} a_0, \quad (\text{A10})$$

$$b_3 = \frac{1}{3}(2\beta + \eta q)b_2 - \frac{\beta^2 + q^2}{6} b_1. \quad (\text{A11})$$

In this way \bar{G}_0 is regular at the origin.

2. Case $L = 1$

As before, we start from the small- y behavior of G_1 , which reads [106]

$$\frac{G_1(\eta, qy)}{qy} \rightarrow \frac{1}{3C_1(\eta)q^2} \left\{ \frac{2}{3}q^2\eta(1 + \eta^2) \left[qy + \frac{\eta}{2}(qy)^2 + O(y^3) \right] \log(2qy) + \left[\frac{1}{y^2} - \frac{\eta q}{y} + \frac{1 + 2\eta^2}{2}q^2 + O(y) \right] \right\}. \quad (\text{A12})$$

Let us look for a function $f_1(y)$ expressed as

$$f_1(y) = a_0 + a_1y + a_2y^2 + (b_3y^3 + b_4y^4) \log(2qy). \quad (\text{A13})$$

For $y \rightarrow 0$

$$\frac{f_1(y)e^{-\beta y}}{y^2} \rightarrow \frac{a_0}{y^2} + \frac{a_1 - a_0\beta}{y} + \left(a_2 - a_1\beta + a_0 \frac{\beta^2}{2} \right) + O(y) + [b_3y + (b_4 - b_3\beta)y^2 + O(y^3)] \log(2qy). \quad (\text{A14})$$

In order to have $\tilde{G}_1/qy = G_1/qy - f_1(y)e^{-\beta y}/y^2$ regular at the origin (together with its first derivative), we have to make vanish the coefficients of the terms $1/y^2$, $1/y$, and $y \log(2qy)$, namely

$$a_0 = \frac{1}{3C_1(\eta)q^2}, \quad a_1 = (\beta - \eta q)a_0, \quad b_3 = \frac{2}{3}q^3\eta(1 + \eta^2)a_0. \quad (\text{A15})$$

The other two coefficients a_2 and b_4 are determined so that \bar{G}_1 is regular at the origin. From Eq. (A3), and using the expressions for the coefficients a_0 , a_1 , and b_3 given above, we find for $y \rightarrow 0$

$$\bar{G}_1 = \left\{ \frac{2a_2 - [\beta^2 + q^2 + 2\eta q(\beta - \eta q)]a_0}{y^2} + \frac{[2q^3\eta(1 + \eta^2) + (\beta^2 + q^2)(\beta - \eta q)]a_0}{y} - \frac{2(\beta + \eta q)a_2}{y} + O(y^0) + [4b_4 - (4\beta + 2\eta q)b_3 + O(y)] \log(2qy) \right\} e^{-\beta y}. \quad (\text{A16})$$

Therefore, we choose

$$a_2 = \left[\frac{\beta^2 + q^2}{2} - \eta q(\beta - \eta q) \right] a_0, \quad b_4 = \frac{2\beta + \eta q}{2} b_3. \quad (\text{A17})$$

With this choice also the coefficient of the term $1/y$ automatically vanishes. In this way \bar{G}_1 is regular at the origin.

3. Cases $L \geq 2$

Now for $y \rightarrow 0$ the logarithmic term in the expression of G_L/qy does not present any singular behavior (it is multiplied by a factor y^{L+1}). Therefore, we can retain all coefficients $b = 0$ in Eq. (A2). The coefficients a 's are then fixed using the same procedure as described above. Now we define $f_L(y)$ as

$$f_L(y) = a_0 + a_1y + a_2y^2 + \dots + a_{L+2}y^{L+2}, \quad L \geq 2, \quad (\text{A18})$$

and we introduce

$$\tilde{f}_L(y) = f_L(y)e^{-\beta y}, \quad \tilde{f}_L(y) = \sum_{k=0}^{\infty} \tilde{a}_k y^k, \quad (\text{A19})$$

where

$$\tilde{a}_k = \sum_{k'=0}^{L+2} \frac{a_{k'}(-\beta)^{k-k'}}{(k-k')!}, \quad k = 0, \dots, \infty. \quad (\text{A20})$$

The coefficients \tilde{a}_k , $k = 0, \dots, L+2$ can be fixed by requiring that \tilde{G}_L/qy and \bar{G}_L be regular at the origin, with the result that

$$\begin{aligned} k=0 \quad \tilde{a}_0 &= \frac{1}{(2L+1)C_L(\eta)q^{L+1}}, & k=1 \quad \tilde{a}_1 &= -\frac{\eta q}{L}\tilde{a}_0, \\ k=2, \dots, L+2 \quad \tilde{a}_k &= -\frac{2\eta q\tilde{a}_{k-1} - q^2\tilde{a}_{k-2}}{k(k-2L-1)}. \end{aligned} \quad (\text{A21})$$

The parameters a_k , $k = 0, \dots, L+2$, can be readily obtained from \tilde{a}_k by recurrence, using Eq. (A20). In fact

$$a_0 = \tilde{a}_0 = \frac{1}{(2L+1)C_L(\eta)q^{L+1}}, \quad (\text{A22})$$

$$a_k = \tilde{a}_k - \sum_{k'=0}^{k-1} \frac{a_{k'}(-\beta)^{k-k'}}{(k-k')!}, \quad k = 1, \dots, L+2. \quad (\text{A23})$$

Since we need to fix \tilde{a}_k , $k = 0, \dots, L+2$, we need to have at least $L+3$ parameters a_0, \dots, a_{L+2} in the expansion for $f_{L \geq 2}$ given in Eq. (A18), i.e., we can set $a_{k \geq L+3} = 0$.

- [1] A. J. Krasznahorkay *et al.*, [arXiv:1910.10459](#) (2019).
- [2] H. Kamada, A. Nogga, W. Glockle, E. Hiyama, M. Kamimura, K. Varga *et al.*, *Phys. Rev. C* **64**, 044001 (2001).
- [3] B. S. Pudliner, V. R. Pandharipande, J. Carlson, S. C. Pieper, and R. B. Wiringa, *Phys. Rev. C* **56**, 1720 (1997).
- [4] A. Nogga, A. Kievsky, H. Kamada, W. Glockle, L. E. Marcucci, S. Rosati, and M. Viviani, *Phys. Rev. C* **67**, 034004 (2003).
- [5] R. Lazauskas and J. Carbonell, *Phys. Rev. C* **70**, 044002 (2004).
- [6] M. Viviani, A. Kievsky, and S. Rosati, *Phys. Rev. C* **71**, 024006 (2005).
- [7] R. B. Wiringa, S. C. Pieper, J. Carlson, and V. R. Pandharipande, *Phys. Rev. C* **62**, 014001 (2000).
- [8] A. Deltuva and A. C. Fonseca, *Phys. Rev. C* **75**, 014005 (2007); *Phys. Rev. Lett.* **98**, 162502 (2007); *Phys. Rev. C* **76**, 021001(R) (2007).
- [9] A. Deltuva, A. C. Fonseca, and P. U. Sauer, *Phys. Lett. B* **660**, 471 (2008).
- [10] A. Deltuva and A. C. Fonseca, *Phys. Rev. C* **86**, 011001(R) (2012); **87**, 054002 (2013).
- [11] A. Deltuva and A. C. Fonseca, *Phys. Rev. Lett.* **113**, 102502 (2014); *Phys. Rev. C* **90**, 044002 (2014).
- [12] A. Deltuva and A. C. Fonseca, *Phys. Lett. B* **742**, 285 (2015); *Phys. Rev. C* **91**, 034001 (2015); **92**, 024001 (2015).
- [13] A. Deltuva and A. C. Fonseca, *Phys. Rev. C* **95**, 024003 (2017).
- [14] E. O. Alt, W. Sandhas, and H. Ziegelmann, *Phys. Rev. C* **17**, 1981 (1978); **21**, 1733 (1980).
- [15] A. Deltuva, A. C. Fonseca, and P. U. Sauer, *Phys. Rev. C* **71**, 054005 (2005); **72**, 054004 (2005).
- [16] F. Ciesielski and J. Carbonell, *Phys. Rev. C* **58**, 58 (1998); F. Ciesielski, J. Carbonell, and C. Gignoux, *Phys. Lett. B* **447**, 199 (1999).
- [17] R. Lazauskas, J. Carbonell, A. C. Fonseca, M. Viviani, A. Kievsky, and S. Rosati, *Phys. Rev. C* **71**, 034004 (2005).
- [18] R. Lazauskas, *Phys. Rev. C* **79**, 054007 (2009).
- [19] R. Lazauskas, *Phys. Rev. C* **86**, 044002 (2012).
- [20] R. Lazauskas and J. Carbonell, *Front. Phys.* **7**, 251 (2020).
- [21] H. M. Hofmann and G. M. Hale, *Nucl. Phys. A* **613**, 69 (1997).
- [22] B. Pfitzinger, H. M. Hofmann, and G. M. Hale, *Phys. Rev. C* **64**, 044003 (2001).
- [23] H. M. Hofmann and G. M. Hale, *Phys. Rev. C* **68**, 021002(R) (2003).
- [24] H. M. Hofmann and G. M. Hale, *Phys. Rev. C* **77**, 044002 (2008).
- [25] S. Quaglioni and P. Navrátil, *Phys. Rev. Lett.* **101**, 092501 (2008).
- [26] P. Navrátil, R. Roth, and S. Quaglioni, *Phys. Rev. C* **82**, 034609 (2010).
- [27] R. Wiringa (private communication).
- [28] A. Kievsky *et al.*, *J. Phys. G: Nucl. Part. Phys.* **35**, 063101 (2008).
- [29] L. E. Marcucci *et al.*, [arXiv:1912.09751](#).
- [30] M. Viviani, S. Rosati, and A. Kievsky, *Phys. Rev. Lett.* **81**, 1580 (1998).
- [31] M. Viviani, A. Kievsky, S. Rosati, E. A. George, and L. D. Knutson, *Phys. Rev. Lett.* **86**, 3739 (2001).
- [32] R. B. Wiringa, V. G. J. Stoks, and R. Schiavilla, *Phys. Rev. C* **51**, 38 (1995).
- [33] M. Viviani *et al.*, *Few-Body Syst.* **39**, 159 (2006).
- [34] L. E. Marcucci, A. Kievsky, L. Girlanda, S. Rosati, and M. Viviani, *Phys. Rev. C* **80**, 034003 (2009).
- [35] M. Viviani *et al.*, *Few-Body Syst.* **45**, 119 (2009).
- [36] M. Viviani, A. Deltuva, R. Lazauskas, J. Carbonell, A. C. Fonseca, A. Kievsky, L. E. Marcucci, and S. Rosati, *Phys. Rev. C* **84**, 054010 (2011).
- [37] M. Viviani, A. Deltuva, R. Lazauskas, A. C. Fonseca, A. Kievsky, and L. E. Marcucci, *Phys. Rev. C* **95**, 034003 (2017).
- [38] D. R. Entem and R. Machleidt, *Phys. Rev. C* **68**, 041001(R) (2003).
- [39] R. Machleidt and D. R. Entem, *Phys. Rep.* **503**, 1 (2011).
- [40] D. R. Entem, R. Machleidt, and Y. Nosyk, *Phys. Rev. C* **96**, 024004 (2017).
- [41] E. Epelbaum, A. Nogga, W. Glockle, H. Kamada, Ulf-G. Meissner, and H. Witala, *Phys. Rev. C* **66**, 064001 (2002).
- [42] P. Navrátil, *Few-Body Syst.* **41**, 117 (2007).
- [43] A. Gardestig and D. R. Phillips, *Phys. Rev. Lett.* **96**, 232301 (2006).
- [44] D. Gazit, S. Quaglioni, and P. Navrátil, *Phys. Rev. Lett.* **103**, 102502 (2009).
- [45] L. E. Marcucci, A. Kievsky, S. Rosati, R. Schiavilla, and M. Viviani, *Phys. Rev. Lett.* **108**, 052502 (2012); **121**, 049901(E) (2018).
- [46] A. Baroni *et al.*, *Phys. Rev. C* **98**, 044003 (2018).
- [47] L. E. Marcucci, F. Sammarruca, M. Viviani, and R. Machleidt, *Phys. Rev. C* **99**, 034003 (2019).
- [48] R. Schiavilla (private communication).
- [49] V. Bernard, E. Epelbaum, H. Krebs, and Ulf-G. Meissner, *Phys. Rev. C* **77**, 064004 (2008).
- [50] H. Krebs, A. Gasparyan, and E. Epelbaum, *Phys. Rev. C* **85**, 054006 (2012); **87**, 054007 (2013).
- [51] K. Hebel, H. Krebs, E. Epelbaum, J. Golak, and R. Skibinski, *Phys. Rev. C* **91**, 044001 (2015).
- [52] B. S. Pudliner, V. R. Pandharipande, J. Carlson, and R. B. Wiringa, *Phys. Rev. Lett.* **74**, 4396 (1995).
- [53] S. C. Pieper, *AIP Conf. Proc.* **1011**, 143 (2008).
- [54] A. C. Fonseca, *Phys. Rev. Lett.* **83**, 4021 (1999).
- [55] T. W. Phillips, B. L. Berman, and J. D. Seagrave, *Phys. Rev. C* **22**, 384 (1980).
- [56] K. F. Famularo *et al.*, *Phys. Rev.* **93**, 928 (1954) [Minutes of the 1953 Thanksgiving Meeting Held at Chicago, November 27-28, 1953, edited by K. K. Darrow, *Phys. Rev.* **93**, 909 (1954)].
- [57] D. G. McDonald, W. Haberli, and L. W. Morrow, *Phys. Rev.* **133**, B1178 (1964).
- [58] B. M. Fisher, C. R. Brune, H. J. Karwowski, D. S. Leonard, E. J. Ludwig, T. C. Black, M. Viviani, A. Kievsky, and S. Rosati, *Phys. Rev. C* **74**, 034001 (2006).
- [59] M. T. Alley and L. D. Knutson, *Phys. Rev. C* **48**, 1890 (1993).
- [60] Y. Koike and J. Haidenbauer, *Nucl. Phys. A* **463**, 365 (1987).
- [61] H. Witala, W. Glöckle, and T. Cornelius, *Nucl. Phys. A* **491**, 157 (1988).
- [62] A. Kievsky *et al.*, *Nucl. Phys. A* **607**, 402 (1996).
- [63] L. Girlanda, A. Kievsky, and M. Viviani, *Phys. Rev. C* **84**, 014001 (2011).
- [64] L. Girlanda, A. Kievsky, M. Viviani, and L. E. Marcucci, *Phys. Rev. C* **99**, 054003 (2019).
- [65] T. V. Daniels, C. W. Arnold, J. M. Cesaratto, T. B. Clegg, A. H. Couture, H. J. Karwowski, and T. Katabuchi, *Phys. Rev. C* **82**, 034002 (2010).

- [66] M. Viviani, L. Girlanda, A. Kievsky, and L. E. Marcucci, *Phys. Rev. Lett.* **111**, 172302 (2013).
- [67] A. Hemmendinger *et al.*, *Phys. Rev.* **76**, 1137 (1949).
- [68] R. S. Claassen, R. J. S. Brown, G. D. Freier, and W. R. Stratton, *Phys. Rev.* **82**, 589 (1951).
- [69] Y. G. Balashko, I. Y. Barit, L. S. Dulkova, and A. B. Kurepin, *Bull. Russ. Acad. Sci. Phys.* **28**, 1028 (1965).
- [70] N. Jarmie and R. C. Allen, *Phys. Rev.* **114**, 176 (1959).
- [71] J. E. Brolley Jr., T. M. Putnam, L. Rosen, and L. Stewart, *Phys. Rev.* **117**, 1307 (1960).
- [72] C. Manduchi, G. Moschini, G. Tornielli, and G. Zannoni, *Nuovo Cim. B* **57**, 340 (1968).
- [73] M. Ivanovich, P. G. Young, and G. G. Ohlsen, *Nucl. Phys. A* **110**, 441 (1968).
- [74] R. Kankowsky, J. C. Fritz, K. Kilian, A. Neufert, and D. Fick, *Nucl. Phys. A* **263**, 29 (1976).
- [75] J. D. Seagrave, L. Cranberg, and J. E. Simmons, *Phys. Rev.* **119**, 1981 (1960).
- [76] A. R. Sayres, K. W. Jones, and C. S. Wu, *Phys. Rev.* **122**, 1853 (1961).
- [77] V. P. Alfimenkov *et al.*, *Yad. Fiz.* **33**, 891 (1981).
- [78] B. Haesner, W. Heeringa, H. O. Klages, H. Dobiash, G. Schmalz, P. Schwarz, J. Wilczynski, B. Zeitnitz, and F. Kappeler, *Phys. Rev. C* **28**, 995 (1983).
- [79] C. E. Hollandsworth, M. Gilpatrick, and W. P. Bucher, *Phys. Rev. C* **5**, 395 (1972).
- [80] K. Sinram, F. W. Buesser, and F. Niebergall, in *Proceedings of the International Conference on Interactions of Neutrons with Nuclei*, edited by E. Sheldon (Technical Information Center, Energy Research and Development Administration, Oak Ridge, 1976), p. 1363.
- [81] H. O. Klages *et al.*, *Nucl. Phys. A* **443**, 237 (1985).
- [82] P. Jany, W. Heeringa, H. O. Klages, B. Zeitnitz, and R. Garrett, *Nucl. Phys. A* **483**, 269 (1988).
- [83] J. Esterline, W. Tornow, A. Deltuva, and A. C. Fonseca, *Phys. Rev. Lett.* **110**, 152503 (2013).
- [84] J. H. Coon, *Phys. Rev.* **80**, 488 (1950).
- [85] R. Batchelor, R. Aves, and T. H. R. Skyrme, *Rev. Sci. Instrum.* **26**, 1037 (1955).
- [86] J. H. Gibbons and R. L. Macklin, *Phys. Rev.* **114**, 571 (1954).
- [87] J. Als-Nielsen and O. Dietrich, *Phys. Rev.* **133**, B925 (1964).
- [88] R. L. Macklin and J. H. Gibbons, in *Proceedings of the Nuclear Structure Conference* (Norr-Holland, Antwerp, The Netherlands, 1965), p. 13.
- [89] D. G. Costello, S. J. Friesenhahn, and W. M. Lopez, *Nucl. Sci. Eng.* **39**, 409 (1970).
- [90] S. B. Borzakov, K. Maletski, L. B. Pikelner, M. Stempinski, and E. I. Sharapov, *Yad. Fiz.* **35**, 532 (1982).
- [91] G. A. Jarvis, A. Hemmendinger, H. V. Argo, and R. F. Taschek, *Phys. Rev.* **79**, 929 (1950).
- [92] H. B. Willard, J. K. Bair, and J. D. Kington, *Phys. Rev.* **90**, 865 (1953).
- [93] G. A. Jarvis, Los Alamos Scientific Report No. 2014, p. 35 (1956).
- [94] M. Drosig, Los Alamos Scientific Report No. 8215 (1980).
- [95] D. S. Cramer and L. Cranberg, *Nucl. Phys. A* **171**, 59 (1971).
- [96] M. A. Doyle Sr., H. W. Clark, L. J. Dries, J. L. Regner, T. R. Donoghue, and G. M. Hale, *Nucl. Phys. A* **371**, 225 (1981).
- [97] W. Tornow, R. C. Byrd, P. W. Lisowski, R. L. Walter, and T. R. Donoghue, *Nucl. Phys. A* **371**, 235 (1981).
- [98] J. R. Walston *et al.*, *Phys. Rev. C* **58**, 1314 (1998).
- [99] W. S. Wilburn *et al.*, *Few-Body Syst.* **24**, 27 (1998).
- [100] Th. Walcher, *Phys. Lett. B* **31**, 442 (1970).
- [101] R. F. Frosch *et al.*, *Nucl. Phys. A* **110**, 657 (1968).
- [102] G. Kobschall *et al.*, *Nucl. Phys. A* **405**, 648 (1983).
- [103] E. Hiyama, B. F. Gibson, and M. Kamimura, *Phys. Rev. C* **70**, 031001(R) (2004).
- [104] S. Bacca, N. Barnea, W. Leidemann, and G. Orlandini, *Phys. Rev. Lett.* **110**, 042503 (2013).
- [105] S. Bacca, N. Barnea, W. Leidemann, and G. Orlandini, *Phys. Rev. C* **91**, 024303 (2015).
- [106] M. Abramowitz and I. Stegun, *Handbook of Mathematical Functions* (Dover, New York, 1970).
- [107] F. Zernike and H. C. Brinkman, *Proc. Kon. Ned. Acad. Wensch.* **33**, 3 (1935).
- [108] M. Fabre de la Ripelle, *Ann. Phys. (NY)*. **147**, 281 (1983).
- [109] W. Kohn, *Phys. Rev.* **74**, 1763 (1948).
- [110] L. M. Delves, *Advances in Nuclear Physics*, edited by M. Baranger and E. Vogt (Plenum Press, New York, 1972), Vol. 5, p. 126.
- [111] A. Kievsky, *Nucl. Phys. A* **624**, 125 (1997).
- [112] M. Viviani, *Few-Body Syst.* **25**, 177 (1998).
- [113] J. Blatt and L. Biedenharn, *Phys. Rev.* **86**, 399 (1952).
- [114] D. R. Tilley, H. R. Weller, and G. M. Hale, *Nucl. Phys. A* **541**, 1 (1992).
- [115] M. Viviani, L. Girlanda, A. Kievsky, and L. E. Marcucci (unpublished).
- [116] S. Hammerschmied, H. Rauch, H. Clerc, and U. Kischko, *Z. Phys. A* **302**, 323 (1981).
- [117] H. Rauch, D. Tuppinger, H. Woelwitsch, and T. Wroblewski, *Phys. Lett. B* **165**, 39 (1985).
- [118] G. M. Hale, D. C. Dodder, J. D. Seagrave, B. L. Berman, and T. W. Phillips, *Phys. Rev. C* **42**, 438 (1990).
- [119] A. Kievsky, *Phys. Rev. C* **60**, 034001 (1999).
- [120] D. R. Thompson, M. LeMere, and Y. C. Tang, *Nucl. Phys. A* **286**, 53 (1977).
- [121] S. Aoyama, K. Arai, Y. Suzuki, P. Descouvemont, and D. Baye, *Few-Body Syst.* **52**, 97 (2012).
- [122] S. Aoyama, *Prog. Theor. Exp. Phys.* **2016**, 123D01 (2016).
- [123] I. J. Thompson and F. Nunes, in *Nuclear Reactions for Astrophysics* (Cambridge University Press, Cambridge, UK, 2009), p. 301.
- [124] S. A. Rakityansky, S. A. Sofianos, and N. Elander, *J. Phys. A: Math. Theor.* **40**, 14857 (2007).
- [125] W. H. Press, S. A. Teukolsky, W. T. Vetterling, and B. P. Flannery, *Numerical Recipes: The Art of Scientific Computing* (Cambridge University Press, Cambridge, UK, 2007).
- [126] E. Epelbaum, H. Krebs and U.-G. Meissner, *Phys. Rev. Lett.* **115**, 122301 (2015).
- [127] M. Piarulli, L. Girlanda, R. Schiavilla, A. Kievsky, A. Lovato, L. E. Marcucci, S. C. Pieper, M. Viviani, and R. B. Wiringa, *Phys. Rev. C* **94**, 054007 (2016).
- [128] M. Piarulli *et al.*, *Phys. Rev. Lett.* **120**, 052503 (2018).